

**The role of FOXO1 and K_{ATP} channel signalling
in Sim1 expressing neurons for the regulation
of energy homeostasis and stress response**

Inaugural-Dissertation
zur
Erlangung des Doktorgrades
der Mathematisch-Naturwissenschaftlichen Fakultät
der Universität zu Köln

vorgelegt von

Nora Redemann
aus Frechen
Köln, 2010

Berichterstatter: Prof. Dr. Jens C. Brüning
Prof. Dr. Mats Paulsson
Tag der mündlichen Prüfung: 03.02.2010

Table of contents

Table of contents	I
Figure index.....	IV
Table index.....	VI
Abbreviations	VII
1 INTRODUCTION.....	1
1.1 Obesity as an increasing socio-economic health problem.....	1
1.2 Energy Homeostasis: insulin and leptin action.....	2
1.2.1 The role of insulin in energy homeostasis	2
1.2.2 The role of leptin in energy homeostasis.....	5
1.3 The hypothalamic control of energy homeostasis	5
1.3.1 The arcuate nucleus of the hypothalamus	6
1.3.2 The paraventricular nucleus of the hypothalamus.....	7
1.4 K_{ATP} channels as neuronal glucose and insulin sensors	13
1.5 FOXO1 as a transcription factor in insulin signalling	15
1.5.1 The regulation of FOXO1 by posttranslational modification.....	15
1.5.2 The genetic modifications of FOXO genes in mice.....	17
1.5.3 The role of FOXO1 in the periphery and the CNS.....	18
1.6 Objectives	19
2 MATERIALS AND METHODS.....	20
2.1 Chemicals.....	20
2.2 Mouse experiments	21
2.2.1 Animal care	21
2.2.2 Generation of FOXO1DN ^{Sim1} and FOXO1DN/DN ^{Sim1} mice.....	22
2.2.3 Generation of $KATP\Delta N^{Sim1}$ mice and $KATP\Delta N/\Delta N^{Sim1}$	22
2.2.4 Generation of DsRed- $KATP\Delta N^{Sim1}$ mice and Z/EG- $KATP\Delta N^{Sim1}$	23
2.2.5 Determination of the mouse genotype.....	23
2.2.6 Body weight, fat composition and body length.....	24

Table of contents

2.2.7	Food intake, melanotan II sensitivity and indirect calorimetry.....	24
2.2.8	Blood glucose and serum protein concentrations.....	25
2.2.9	Glucose and Insulin Tolerance Tests	25
2.2.10	Ovariectomy.....	26
2.3	Immunocytochemistry	26
2.4	Electrophysiology.....	27
2.5	Molecular biology	28
2.5.1	RNA isolation and expression studies	28
2.5.2	Cloning of promoter fragments or genes	29
2.5.3	Preparation of plasmid-DNA and ligation into expression vectors.....	30
2.5.4	Sequencing.....	31
2.6	Cell culture	31
2.6.1	Preparation of collagen-coated plates	31
2.6.2	Maintenance of PC12 and SK-N-SH cells.....	31
2.6.3	Transfection of PC12 and SK-N-SH cells.....	32
2.6.4	Luciferase assay	32
2.6.5	Electromobility shift assay (EMSA).....	33
2.7	Statistical methods.....	34
3	RESULTS	35
3.1	The K_{ATP} channel in the Sim1 neuron dependent regulation of energy metabolism	35
3.1.1	K_{ATP} channel expression in Sim1 neurons.....	35
3.1.2	Generation and functionality of the $K_{ATP}\Delta N$ overexpression in Sim1 neurons.....	36
3.1.3	Unaltered energy metabolism in $K_{ATP}\Delta N^{Sim1}$ and $K_{ATP}\Delta N/\Delta N^{Sim1}$ mice.....	40
3.1.4	Glucose tolerance and insulin sensitivity of $K_{ATP}\Delta N^{Sim1}$ and $K_{ATP}\Delta N/\Delta N^{Sim1}$ mice.....	47
3.2	FOXO1 in the Sim1 neuron dependent regulation of energy homeostasis.....	50
3.2.1	Generation of the FOXO1DN overexpression in Sim1 neurons	51
3.2.2	Unaltered energy metabolism in FOXO1DN/DN ^{Sim1} mice	53
3.2.3	Unaltered food intake and MTII sensitivity of FOXO1DN/DN ^{Sim1} mice.....	55
3.2.4	Glucose tolerance and insulin sensitivity of FOXO1DN/DN ^{Sim1} mice	59
3.3	FOXO1 in the Sim1 neuron dependent regulation of the stress response.....	62
3.3.1	Impaired HPA axis by Sim1 neuron specific FOXO1DN expression.....	63
3.3.2	Inhibition of CRH and AVP by FOXO1DN expression <i>in vitro</i>	70
3.3.3	The estrogen dependent regulation of argenine vasopressin.....	76

4 DISCUSSION.....	79
4.1 Unaltered energy homeostasis by the K_{ATP} channel and FOXO1 overexpression in Sim1 neurons	80
4.2 Reduced stress response by Foxo1DN overexpression in Sim1 neurons of female mice	81
4.3 The gender specific effect of FOXO1DN on the HPA axis	84
4.4 Perspectives	88
5 SUMMARY.....	89
6 ZUSAMMENFASSUNG.....	90
7 REFERENCES.....	91
8 ACKNOWLEDGEMENTS.....	101
9 ERKÄRUNG	102
10 LEBENSLAUF.....	103

Figure index

Figure 1: Insulin receptor signal transduction (Adapted from [27])	4
Figure 2: Distinct nuclei within the hypothalamus in the regulation of energy homeostasis	6
Figure 3: The hypothalamic pituitary adrenal axis (HPA)	12
Figure 4: FOXO1 shuttling between the nucleus and the cytosol	16
Figure 5: A subset of Sim1-cre neurons of the PVN were tolbutamide responsive	36
Figure 6: The constitutive active $K_{ATP}\Delta N$ targeted to the Rosa26 locus and Sim1-cre mice	37
Figure 7: The $K_{ATP}\Delta N$ /IRES-GFP construct expressed in the hypothalamic Sim1 sites	39
Figure 8: Enhanced change in membrane resistance and reduction of mean membrane potential in the PVN of $K_{ATP}\Delta N^{Sim1}$ mice.....	40
Figure 9: Unaltered body weight and body length of $K_{ATP}\Delta N^{Sim1}$ and $K_{ATP}\Delta N/\Delta N^{Sim1}$ males	41
Figure 10: Unaltered body weight and body length of $K_{ATP}\Delta N^{Sim1}$ and $K_{ATP}\Delta N/\Delta N^{Sim1}$ females..	42
Figure 11: Unaltered body composition of $K_{ATP}\Delta N^{Sim1}$ and $K_{ATP}\Delta N/\Delta N^{Sim1}$ males	43
Figure 12: No difference in food intake of $K_{ATP}\Delta N^{Sim1}$ and $K_{ATP}\Delta N/\Delta N^{Sim1}$ males	44
Figure 13: Melanotan II (MTII) sensitivity of $K_{ATP}\Delta N/\Delta N^{Sim1}$ mice (NCD).....	45
Figure 14: Melanotan II (MTII) sensitivity of $K_{ATP}\Delta N/\Delta N^{Sim1}$ mice (HFD)	46
Figure 15: Unaltered blood glucose levels of $K_{ATP}\Delta N^{Sim1}$ and $K_{ATP}\Delta N/\Delta N^{Sim1}$ mice	48
Figure 16: Glucose tolerance and insulin sensitivity of $K_{ATP}\Delta N^{Sim1}$ and $K_{ATP}\Delta N/\Delta N^{Sim1}$ mice	49
Figure 17: Expression of the FOXO1DN/IRES-GFP construct in the hypothalamic Sim1 sites .	53
Figure 18: Unaltered body weight and body length of FOXO1DN/DN ^{Sim1} mice	54
Figure 19: Unaltered body composition of FOXO1DN ^{Sim1} mice	55
Figure 20: Unaltered random fed and fasted induced food intake of FOXO1DN/DN ^{Sim1} females	56
Figure 21: Unaltered random fed and fasted induced food intake of FOXO1DN/DN ^{Sim1} males .	57
Figure 22: Melanotan II (MTII) sensitivity of FOXO1DN/DN ^{Sim1} females.....	58
Figure 23: Melanotan II (MTII) sensitivity of FOXO1DN/DN ^{Sim1} males	59
Figure 24: Unaltered blood glucose levels of FOXO1DN/DN ^{Sim1} mice	60
Figure 25: Unaltered glucose tolerance and insulin sensitivity of FOXO1DN/DN ^{Sim1} mice	61
Figure 26: Putative forkhead binding sites encoded by the CRH promoter	63
Figure 27: Putative forkhead binding sites encoded by the AVP promoter	64
Figure 28: Neuropeptide levels in the hypothalamus of FOXO1DN/DN ^{Sim1} females	65
Figure 29: Neuropeptide levels in the hypothalamus of FOXO1DN/DN ^{Sim1} males	65
Figure 30: Blunted corticosterone response to restraint stress of FOXO1DN/DN ^{Sim1} females ...	66
Figure 31: No ectopic expression of Sim1-cre in the pituitary or adrenal glands.....	68
Figure 32: Neuropeptide levels in the amygdala in FOXO1DN/DN ^{Sim1} mice.....	69
Figure 33: CRH promoter elements regulating the firefly luciferase reporter.....	71
Figure 34: Reduced forskolin stimulation of the CRH promoter by FOXO1DN overexpression in PC12 cells	72
Figure 35: Inhibition of AVP transcription by FOXO1DN overexpression in PC12 cells	73

Figure 36: Electro mobility shift assay (EMSA) of FOXO1DN transfected SK-N-SH cells.....	74
Figure 37: Specific binding of FOXO1DN to the AVP promoter.....	75
Figure 38: Inhibition of AVP transcription by FOXO1DN overexpression in SK-N-SH cells.....	77
Figure 39: Reduced 17 β -estradiol stimulation of the AVP promoter by FOXO1DN overexpression.....	78
Figure 40: Models of FOXO and ER dependent promoter interaction.....	86

Table index

Table 1: Phenotypes of FOXO knockout mice [110] 17

Table 2: List of chemicals 20

Table 3: Oligonucleotides for the analysis of mouse genotypes 24

Table 4: Realtime probes 29

Table 5: Oligonucleotides for cloning of promoter fragments 30

Table 6: Sequences of EMSA probes 34

Abbreviations

°C	degrees Celsius
3'	three prime end of DNA sequences
5'	five prime end of DNA sequences
A	adenosine
ACTH	adrenocorticotrophin
AgRP	agouti-related peptide
AKT	protein kinase B
ARC	arcuate nucleus
Avertin	tribromoethyl alcohol and <i>tert</i> -amyl alcohol
AVP	arginine vasopressin
AVPR1B	arginine vasopressin receptor 1B
BMI	body mass index
bp	base pairs
C	cytosine
c	DNA concentration
CaCl ₂	calcium chloride
cAMP	cyclic adenosine monophosphate
CBP	CREB binding protein
cDNA	complementary DNA
Ci	Curie
CK	casein kinase
CNS	central nervous system
Cre	site specific recombinase from phage P1 (causes recombination)
CREB	cAMP response element binding protein
CRH	corticotropin releasing hormone
CRHR1	corticotropin releasing hormone receptor 1
d	deci
Da	Dalton
DAPI	4',6-diamidino-2-phenylindole
ddH ₂ O	double distilled water
DMH	dorsomedial hypothalamic nucleus
DMSO	dimethylsulfoxide
DNA	deoxyribonucleic acid
DNase	deoxyribonuclease
dNTP	deoxyribonucleotide-triphosphate
dpm	disintegrations per minute
DTT	1,4-Dithio-DL-threitol
e.g.	exempli gratia
EDTA	ethylenediamine tetraacetate
EGFP	enhanced green fluorescent protein
ELISA	enzyme-linked immunosorbent assay
EtBr	ethidium bromide
EtOH	ethanol
FOXO1	forkheadbox class O1
g	gram
G	guanine

Abbreviations

G6Pase	glucose-6-phosphatase
Gab	growth factor receptor binding protein associated binder
GABA	γ -aminobutyric acid
GFP	green fluorescent protein
GLUT-4	glucose transporter 4
Grb2	growth factor receptor binding protein 2
GTT	glucose tolerance test
Gusb	glucuronidase beta
h	hour
H ₂ O ₂	hydrogen peroxide
HCl	hydrochloric acid
HEPES	N-2-hydroxyethylpiperazine-N'-2-ethansulfonic acid
HFD	high fat diet
hnRNA	heteronuclear RNA (pre-splicing)
HPA axis	hypothalamic pituitary adrenal axis
Hz	Hertz
IGF-1	insulin-like growth factor-1
ip	intraperitoneal
IR	insulin receptor
IRES	internal ribosome entry site
IRS	insulin receptor substrate
ITT	insulin tolerance test
JAK	Janus kinase
JNK	c-Jun N-terminal kinase
k	kilo
K _{ATP} channel	ATP sensitive potassium channel
kb	kilobase pairs
KCl	potassium chloride
kDa	kilodalton
KOH	potassium hydroxide
l	liter
lacZ	gene encoding the enzyme β -galactosidase
LH	lateral hypothalamic area
loxP	recognition sequence for Cre (locus of x-ing over phage P1)
m	milli
M	molar
MAPK	mitogen-activated protein kinase
MCR	melanocortin receptor
MgCl ₂	magnesium chloride
min	minute
mRNA	messenger RNA
MSH	melanocyte-stimulating hormone
n	nano
NaCl	sodium chloride
NaOH	sodium hydroxide
NCD	normal chow diet

NES	nuclear export sequence
NLS	nuclear localization sequence
NMR	nuclear magnetic resonance
NPY	neuropeptide Y
ObRb	long isoform of the leptin receptor
OD	optical density
PAGE	polyacrylamid gel electrophoresis
PBS	phosphate buffered saline
PCR	polymerase chain reaction
PDK1	phosphoinositide-dependent protein kinase 1
PFA	paraformaldehyde
PH	pleckstrin homology
PI3K	phosphatidylinositol 3 kinase
PIP2	phosphatidylinositol (4,5) bisphosphate
PIP3	phosphatidylinositol (3,4,5) trisphosphate
POMC	proopiomelanocortin
PTB	phosphotyrosine binding
PTEN	phosphatase and tensin homolog
PVN	paraventricular nucleus
Raf	proto-oncogene serine/threonine protein kinase
Ras	Ras small GTPase
RNA	ribonucleic acid
RNAi	RNA interference
RNase	ribonuclease
RT	room temperature
SDS	sodiumdodecylsulfate
sec	second
SEM	standard error of the mean
SH	src homology
Shp-2	tyrosine phosphatase-2
Sim1	single minded1
Sirt	sirtuin
SGK	Serine/threonine-protein kinase
SN	substantia nigra
SOCS	suppressor of cytokine signaling
SON	supraoptic nucleus
STAT	signal transducer and activator of transcription
TAE	Tris-acetic acid-EDTA buffer
TBS	Tris buffered saline
TE	Tris-EDTA buffer
Tris	2-amino-2-(hydroxymethyl)-1,3-propandiole
Trp	tryptophan
TRH	tryrotropin releasing hormone
TWEEN	polyoxethylene-sorbitan-monolaureate
Tyr	tyrosine
U	units
UV	ultraviolet
V	Volt
v/v	volume per volume
VMH	ventromedial nucleus of the hypothalamus

Abbreviations

VO ₂	volume of consumed oxygen
w/v	weight per volume
WAT	white adipose tissue
WHO	World Health Organization
β-gal	β-galactosidase
μ	micro

1 Introduction

1.1 Obesity as an increasing socio-economic health problem

During the last decades the prevalence of obesity has increased drastically worldwide to a proportion of a global epidemic with serious health and economic consequences. Global studies in obesity use the body mass index (BMI), which is a measurement of body weight in relation to the body height (body weight/height²), as a parameter to analyze the differences in an entire population in a time dependent manner. The world health organisation (WHO) considers overweight a BMI of 25 to 29.9, and obesity a BMI of 30 or higher. According to this classification, 51 % of the adults in Germany are currently considered overweight, whereas 16 % of the population is classified as obese [1]. This trend of a dramatic increase in the rate of obesity in an entire population has been described in many countries and, particularly for the USA, it has been monitored in detail over the last decades. Thus, whereas in 1990 less than 15% of the US population had a BMI higher than 30, today this value has increased severely to more than 30% of the people in most states of the country being obese [2, 3].

Overweight and obesity lead to serious health problems and the risk of developing associated diseases, such as type 2 diabetes mellitus, high blood pressure, high cholesterol, asthma or arthritis, becomes progressively higher as the BMI increases [4]. Consequently, at least 6% of the total health costs of industrial countries are associated with overweight and obesity according to the WHO, with cardiovascular diseases being the world's primary cause of death [5]. Also type 2 diabetes, a combination of hyperglycemia going along with hyperinsulinemia that is reflected by an increasing insulin resistance, is rapidly evolving into a global epidemic [6-8]. The WHO has predicted 360 million people to be suffering from type 2 diabetes by the year 2030, which would mean a two-fold increase in comparison to the figures today [9].

1.2 Energy Homeostasis: insulin and leptin action

Bodyweight is dependent on age, ethnicity and gender and is determined by a combination of environmental and genetic factors. Moreover, body mass and composition are determined by the balance between calorie intake and energy expenditure. Thus, a positive energy balance results in an increased body weight arising from a high calorie intake that is not balanced by increased energy expenditure [10]; whereas a negative energy balance is the consequence of low energy intake and/or high physical activity resulting in a reduction of body weight (reviewed in [11, 12]). Importantly, the lifestyle in industrialised countries allows unlimited access to calories and a reduction in physical activity, favouring a positive balance.

Importantly, a certain body weight is defended in healthy humans and animal models, which react to artificial overfeeding with a subsequent reduction in food intake and an increase in energy expenditure [13]. Thus, most people are able to keep their body weight steady even in an “obesogenic” environment, while an increasing proportion of the population suffer from chronic positive energy homeostasis, pointing to a genetic contribution in weight gain. Research of the underlying mechanisms in control of energy homeostasis and its defects in obese patients has revealed that multiple hormones such as insulin, leptin and metabolites, e.g. glucose, act in the central nervous system (CNS) regulating food intake, energy expenditure, and glucose homeostasis (reviewed in [14, 15]).

1.2.1 The role of insulin in energy homeostasis

The 51 amino acid hormone insulin is secreted by β -cells of the pancreatic islets of Langerhans in response to rising blood glucose levels. Insulin release from secretory granules into the circulation allows the hormone to reach its target tissues, where it binds to its receptor and induces a cascade of intracellular signalling. Insulin controls a diversity of processes in the periphery through its action on muscle, liver and adipose tissue, promoting glucose uptake and anabolic processes, such as the stimulation of amino acid uptake

and gluconeogenesis, and inhibiting catabolic processes, such as glycogenolysis and hepatic glucose production (reviewed in [16, 17]).

In addition to its role in the periphery, insulin also reaches the CNS by crossing the blood-brain barrier in a receptor-mediated mechanism [18, 19]. It has been shown that insulin signalling in the CNS is crucial for the maintenance of the energy balance. This is reflected by the observation that the neuronal insulin receptor deficient mice exhibit a diet-sensitive obesity and insulin resistance [13]. Moreover, insulin infusion into the brain decreases food intake and body weight, and it has been proposed that insulin action in the CNS acts as an adiposity signal, transferring information about the amount of body fat stores and causing a tendency towards a negative energy balance [20].

Molecular mechanisms of insulin receptor signalling

Insulin mediates its pleiotropic effects by binding to and activating its membrane-bound tyrosine kinase receptor. Insulin binding to the insulin receptor (IR) results in conformational changes that activate the intrinsic tyrosine kinase activity going along with a receptor autophosphorylation of multiple tyrosine residues [21, 22]. This enables the intracellular insulin receptor substrate (IRS) proteins to bind via a phosphotyrosine-binding (PTB) domain [23] (fig. 1). Moreover, the tyrosine kinase activity of the receptor phosphorylates specific tyrosines of the IRS, which allow src-homology-2 (SH2) domain containing proteins to bind to the receptor bound IRS molecule [24, 25]. The IRS proteins can, thereby, serve as central nodes regulating different signalling pathways as a docking platform for SH2 containing proteins.

Two important pathways, involving the mitogen-activated protein kinase (MAPK) [26] or the phosphatidylinositol 3-kinase (PI3K), induce a variety of biological effects of insulin signalling in different tissues (for review see [27]). In the case of the MAPK pathway, the growth factor receptor binding (Grb)2 protein binds through its SH2 domain to phosphorylated IRS proteins, eventually leading to activation of MAPK pathway, which mediates insulin's effect on proliferation [26]. In the case of the PI3K pathway, phosphorylated IRS activates the PI3K by the interaction with the SH domain-containing p85-regulatory subunit, leading to release of the catalytic PI3K subunit (p110), and generation of phosphatidylinositol (3,4,5)-trisphosphate (PIP3) from

phosphatidylinositol (4,5)-bisphosphate (PIP₂) [28]. Subsequently, the pleckstrin homology (PH) domain of the phosphoinositide dependent protein kinase-1 (PDK1) binds to PIP₃, recruiting PDK1 to the membrane, which is crucial for the phosphorylation and activation of another kinase, AKT (also called protein kinases B /PKB) [29]. Finally, the effect of insulin signalling through this pathway can be inhibited by the PTEN phosphatase (phosphatase and tensin homolog), which generates PIP₂ from PIP₃. The PI3K-AKT signalling pathway mediates several effects of insulin, including the glucose transporter translocation and the regulation of gene transcription by phosphorylation of transcription factors, such as FOXO proteins. (for review see [27, 30])

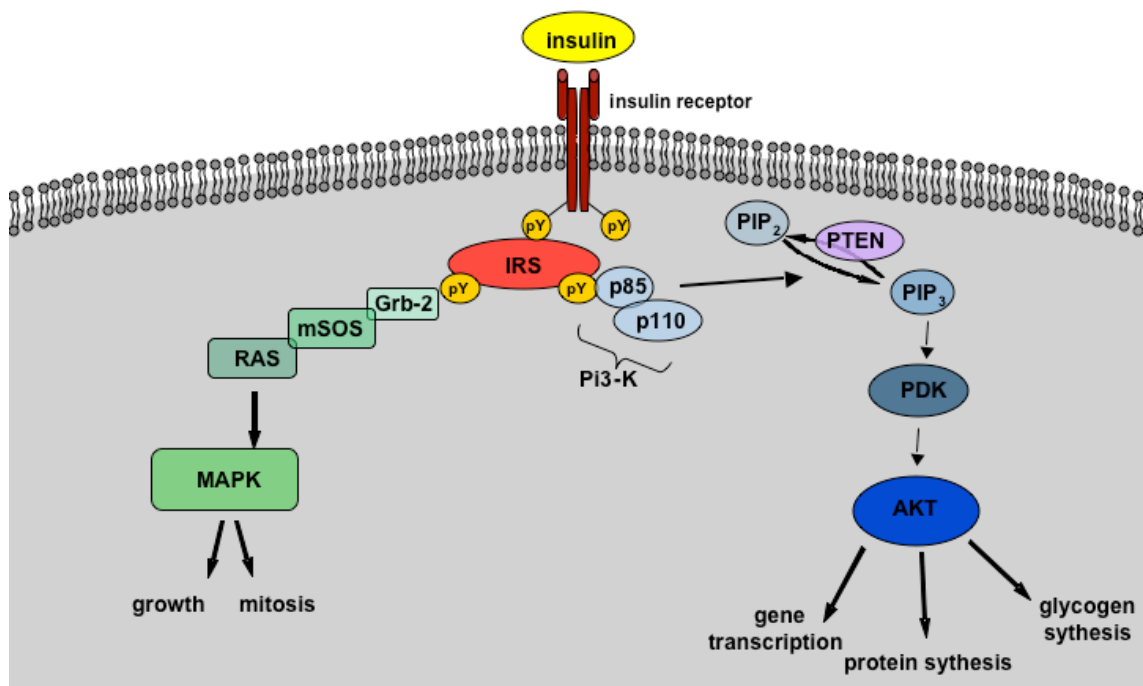


Figure 1: Insulin receptor signal transduction (Adapted from [27])

Upon insulin binding to the extracellular subunits of the insulin receptor, the receptor undergoes a conformational change, activating the intracellular tyrosine kinase activity, resulting in receptor autophosphorylation and subsequently in the phosphorylation of intracellular insulin receptor substrate (IRS) 1 proteins on tyrosine residues. These phosphorylation sites are located in domains that characterize them as binding sites for src-homology 2 (SH2) domain-containing proteins such as the p85-regulatory subunit of phosphatidylinositol 3 kinase (PI3 kinase) and the growth factor receptor binding protein-2 (Grb-2). Binding of these proteins to tyrosine

phosphorylated IRS 1 proteins results in their activation, initiating downstream signals as the activation of the Ras-MAPK cascade or the activation of serine/threonine kinases downstream of PIP3. These signals finally result in the diverse biological effects of insulin signaling. Abbreviations: MAPK, mitogen-activated protein kinase; mSOS, son of sevenless; Ras, Ras small GTPase; p110, catalytic subunit of PI3 kinase; PIP2, phosphatidylinositol (4,5) biphosphate; PIP3, phosphatidylinositol (3,4,5) trisphosphate; PTEN, phosphatase and tensin homolog; PDK1, protein-dependent kinase 1; Akt, protein kinase B

1.2.2 The role of leptin in energy homeostasis

The hormone leptin, secreted by adipose tissue, has been only recently identified as a main regulator in energy homeostasis [31]. In mice, leptin deficiency (*ob/ob* mice) results in hyperphagia, obesity and insulin resistance [31, 32]. In addition, mice with the loss-of-function mutation of the leptin receptor have been characterised as diabetic mice (*db/db*) [33]. In humans, a leptin mutation resulting in hyperphagia and obesity could be rescued by the treatment with the leptin hormone [34, 35]. Importantly, leptin is released from adipose tissue into the circulation in correlation to fat mass and is therefore considered as an adiposity signal, especially for the brain. However, increased circulating levels of leptin in obese patients go along with a reduced sensitivity to its appetite-reducing effect [36].

1.3 The hypothalamic control of energy homeostasis

Since an important role for the CNS in energy homeostasis had been recognized more than 100 years ago, the specific brain nuclei in the CNS regulating food intake and energy expenditure were defined. These studies led to the finding that the hypothalamus integrates both appetite and energy expenditure by sensing the input from nutrients and peripheral hormones, such as insulin and leptin, and coordinating the adequate responses [37]. The hypothalamus is situated below the thalamus and includes a complex network of neurons that are involved in feeding and glucose metabolism. Distinct regions and neuron subpopulations within the hypothalamus have been identified by lesion and electrical stimulation studies as key nuclei for the control of feeding and satiety. Major sites of this network are the ventromedial hypothalamus (VMH), the paraventricular nucleus (PVN), the dorsomedial hypothalamic nucleus (DMH) and the arcuate nucleus (ARC) [38] (fig.2).

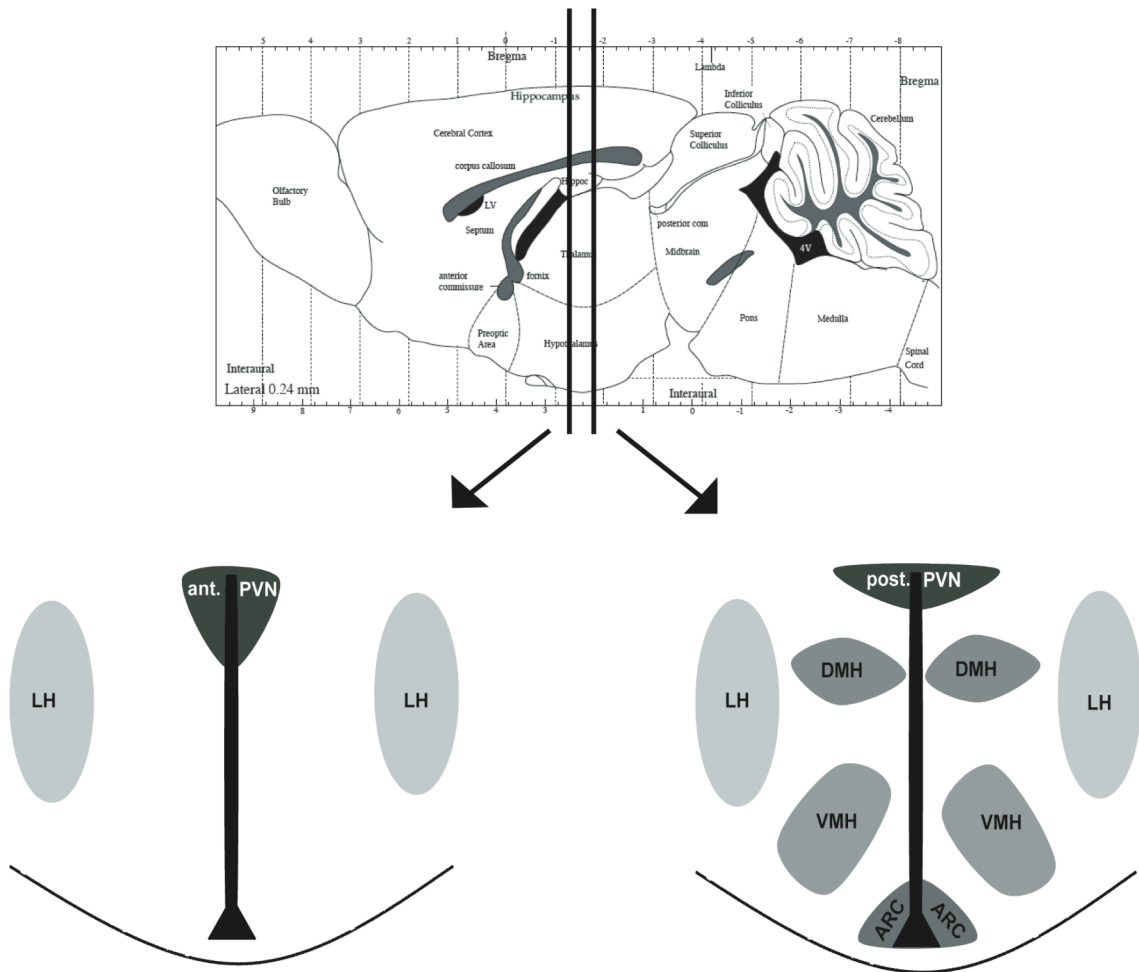


Figure 2: Distinct nuclei within the hypothalamus in the regulation of energy homeostasis

Populations of 1st order neurons in the arcuate nucleus (ARC) are regulated by leptin/insulin and project to 2nd order neurons; coronal sections of the brain at two levels (indicated by vertical lines in sagittal brain from “The Mouse Brain” [39]) are shown at the left and right. ant.PVN: anterior paraventricular nucleus; post.PVN: posterior paraventricular nucleus LH: lateral hypothalamus; VMH: ventromedial nucleus of the hypothalamus; DMH: dorsomedial hypothalamic nucleus

1.3.1 The arcuate nucleus of the hypothalamus

Studies on the hypothalamic effects on energy homeostasis have been focused on the mediobasal hypothalamus. Particularly, in the arcuate nucleus (ARC) two neuron populations, expressing insulin and leptin receptors, exert potent effects on food intake, energy expenditure and glucose homeostasis. The anorexigenic Proopiomelanocortin (POMC) expressing neurons and the orexigenic agouti-related peptide/ neuropeptide Y (AgRP/NPY) expressing neurons are essential for regulation of energy homeostasis by the arcuate nucleus [40-42].

POMC is a 241 amino acid peptide that is further processed to several small peptides: the melanocyte stimulating hormones (MSHs), adrenocorticotropin (ACTH) and β -endorphin [43]. This process is dependent on the cell type-specific expression pattern of prohormone convertases [44]. Alpha-MSH, one of the active products of POMC processing, inhibits food intake and thus is seen as an anorexigenic neuropeptide [45]. Alpha-MSH is released at the nerve terminals of POMC neurons, where it stimulates the melanocortin receptors type 3 and 4 (MC3R/MC4R) on postsynaptic cells [46, 47]. Opposite to the POMC function, NPY and AgRP stimulate food intake and reduce energy expenditure [48]. AgRP functions as an antagonist and/or inverse agonist of the neuronal melanocortin receptors MC3R and MC4R, whereas NPY activates its own receptor on downstream neurons [49, 50].

The anorexigenic or orexigenic nature of these neuropeptides is reflected by the mRNA expression patterns upon fasting. While POMC levels are significantly reduced, AgRP mRNA levels are increased upon fasting [51]. Supporting evidence for the orexigenic role AgRP/NPY neurons was generated by the selective toxin-mediated neuron ablation in adult mice, which results in a drastic reduction of food intake along with a decrease in body weight [52, 53]. Importantly, insulin and leptin affect the energy homeostasis by an alteration of neuropeptide expression levels in the arcuate nucleus, as shown by central insulin and leptin administration. Whereas insulin induces POMC and inhibits NPY expression in the respective populations [54, 55] an administration of leptin stimulates expression of POMC [41, 56] and inhibits expression of AgRP and NPY [57].

Taken together, POMC and AgRP/NPY neurons are considered first order sensors of the energy status of the organism with clearly distinct and opposing effects on energy metabolism. Importantly, these neurons project to second order neurons, including the neurons of the paraventricular nucleus (PVN) of the hypothalamus (fig2) [58-60].

1.3.2 The paraventricular nucleus of the hypothalamus

The paraventricular nucleus (PVN) of the hypothalamus is located in the anterior-medial region of the hypothalamus and it has been proposed to have a

critical role in the regulation of food intake, behaviour and neuroendocrine functions. Classical neuropeptides expressed in the PVN are the corticotropin releasing hormone (CRH), thyrotropin releasing hormone (TRH), arginine vasopressin (AVP) and oxytocin [61].

The diversity of PVN functions is also reflected by the presence of different populations of neurons (magnocellular and parvocellular neurons) within this region, which can be either distinguished by electrophysiological properties [62] or by genetic expression patterns [63]. On one hand, the magnocellular neurosecretory neurons at the posterior magnocellular subdivision of the PVN synthesize and release AVP and oxytocin from their nerve terminals at the posterior pituitary [64]. Magnocellular AVP regulates the organism's water balance enabling the kidneys to conserve water in the case of dehydration [65], whereas oxytocin has originally been known to be released in large amounts at the end of pregnancy and thereafter, to facilitate birth and breastfeeding (see [61] for review). On the other hand, the parvocellular neurons project to the external lamina of the median eminence, where the released peptides are transported via the hypothalamic pituitary portal system to the anterior pituitary [64]. Parvocellular neurons of the PVN either express TRH or coexpress CRH and AVP to initiate the stress response. CRH, originally named corticotropin releasing factor (CRF), is primarily involved in the organisms stress response (see below). Thyrotropin-releasing hormone (TRH), also named thyrotropin releasing factor (TRF), stimulates the release of thyroid-stimulating hormone and prolactin by the anterior pituitary. Both CRH and TRH are anorexigenic neuropeptides (see [61, 66] for review). Interestingly, hypothalamic CRH and TRH are mediators of the anorexigenic effect of leptin and activated by the melanocortin system in the PVN [67, 68].

In summary, the PVN has been implicated in regulating a diversity of processes, such as the stress response and energy homeostasis. However, it remains unclear how the different inputs from other neurons or hormones are integrated to mediate the effects on neuropeptides, as CRH and AVP that are involved in several pathways. For instance, CRH has been characterized as an anorexigenic neuropeptide, but it is also involved in the initiation of the stress response.

1.3.2.1 The transcription factor Sim1 and the melanocortin system

Within the few forms of monogenetic disorders known to result in obesity in humans, two of these, Sim1 (mammalian homologue to the drosophila single minded1 gene) [69] and the MC4R [70, 71] are characteristically expressed in the paraventricular nucleus among other regions that have been described as second order neurons.

Sim1, belonging to the Per-Arnt-Sim (PAS) family of basic helix-loop-helix (bHLH) transcription factors, is essential for the formation of the paraventricular and supraoptic nuclei in the hypothalamus in a dosage dependent manner. Homozygous Sim1 knockout (Sim1^{-/-}) mice die shortly after birth [72]. However, Sim1 haploinsufficient (Sim1^{+/-}) mice are viable and develop early onset obesity resulting from hyperphagia. This is accompanied with an increased linear growth, hyperinsulinemia and hyperleptinemia [73]. Along this line, the overexpression of Sim1 via an adenovirus or a transgene leads to the opposite effects: The calorie consumption is reduced and the mice are resistant to diet-induced obesity [74, 75]. Interestingly, administration of leptin leads to a higher expression of the Sim1 protein [73], but the underlying mechanism is unknown. Recently, it has been shown, that the MC4R, Sim1 and oxytocin are coexpressed in the PVN and that oxytocin might be a mediator of Sim1 signalling, as it partially rescues Sim1 haploinsufficiency [76].

The MC4R is a 7-transmembrane, G-protein-coupled receptor [77] that has an essential role in the regulation of the energy balance. Aforementioned, POMC neurons project to the PVN, where they release α -MSH, which binds to the MC4R and decreases food intake. Moreover, the disruption of the gene leads to severe obesity both in mice and humans [78, 79]. The obesity of MC4R deficient mice is caused by a massive hyperphagia going along with a decrease in energy expenditure [80]. MC4R deficient mice are unresponsive to anorexigenic stimuli, like leptin or the MC4R agonist melanotan II (MTII), while NPY can still stimulate food intake in MC4R deficient mice [81]. The downstream signalling of the MC4R in response to metabolic stimuli is only poorly understood, nevertheless CRH seems to be activated by MTII induced MC4R signalling linking the metabolic pathways with the initiation of the stress

response (see below) [68]. Interestingly, restoration of the MC4R selectively in Sim1 neurons of MC4R deficient mice leads to a 60% reduction of the obesity. This partial rescue of the obese phenotype is due to a reduction in caloric intake while the reduced energy expenditure as seen in MC4R disrupted animals remains unaffected [82]. This suggests that separate populations of neurons receiving input from POMC or AgRP neurons determine food intake and energy expenditure.

Besides their function as second order neurons, getting input from the arcuate nucleus, neurons of the PVN are also capable in directly sensing of metabolic parameters, as leptin and insulin receptors are expressed on PVN neurons [73, 83]. Taken together, the paraventricular nucleus is an important site of second order neurons in response to metabolic signals. However, it is still unclear which precise mechanisms act in response to signals like α -MSH, originating in the arcuate nucleus, and how these mechanisms interact with direct signals, as insulin or metabolites as glucose.

1.3.2.2 The regulation of stress response by the PVN

The mammalian stress response has evolved under conditions that necessitate a sudden change from regular feeding behaviour to an effective escape from natural enemies. In situation of danger, the body has to use its energy in the most effective way and prioritise. This involves a rapid energy use, which is achieved by stimulating gluconeogenesis, glycogenolysis, lipolysis and hepatic glucose secretion to elevate blood glucose levels. Along with this, increased heart rate and blood pressure enables the lungs and muscles to take up more oxygen. Most importantly, the secretion of stress hormones, such as adrenaline and corticosterone, along with endorphins to reduce pain, initiates pathways that are responsible for the effects of stress response (reviewed in [84]).

In response to stress, the parvocellular PVN initiates the hypothalamic pituitary adrenal (HPA) axis, which results in the release of corticosterone (in mice) and cortisol (in humans) from the adrenal glands. It has been shown that calcium/calmodulin and cAMP/CREB dependent pathways in the parvocellular

subset of the PVN induce CRH and AVP [85]. These neuropeptides are released at the nerve terminals of the median eminence into the hypothalamic pituitary portal system to be transported to the anterior pituitary, where the specific receptors (CRHR1/AVPR1B) are expressed on pituitary corticotropes (fig. 3). These G protein-coupled receptors induce the release of ACTH in a calcium/calmodulin and cAMP/CREB dependent manner. Subsequently, ACTH, transported via the blood stream, initiates the corticosterone release in the adrenal cortex. Corticosterone, along with other stress mediators as adrenaline, acts on different brain areas to mediate the effects of acute stress. The target areas include the executive, cognitive, the fear/anger and reward systems as well as the wake sleep centres of the brain (see [84, 86] for review).

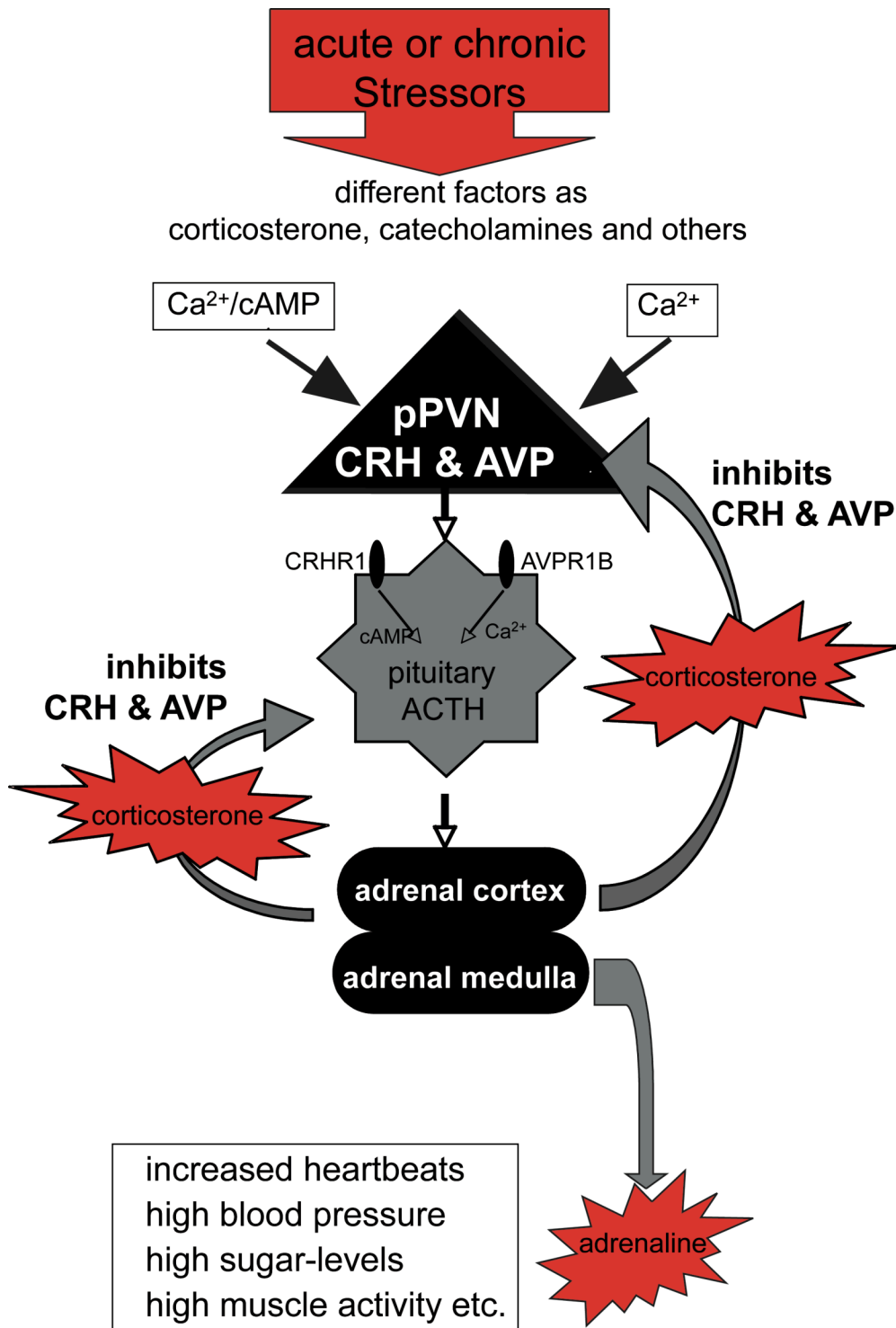


Figure 3: The hypothalamic pituitary adrenal axis (HPA)

Calcium/calmodulin and cAMP/CREB dependent pathways in the parvocellular PVN induce CRH and AVP, which are released into the hypothalamic pituitary portal system to be transported to the anterior pituitary, where the specific receptors (CRHR1/AVPR1B) are expressed on pituitary corticotropes that induce the release of adrenocorticotropin (ACTH). ACTH initiates the corticosterone release in the adrenal cortex. Corticosterone mediates a negative feedback mechanism on CRH, AVP and ACTH. The body reacts to stress by different adjustments as increasing heartbeats, high blood pressure, high glucose-levels and muscle

activity. Ca²⁺, Calcium; cAMP, cyclic adenosine monophosphate; CRH, corticotropin releasing hormone; AVP, arginine vasopressin

Corticosterone binds to its nuclear receptors, whereby high affinity type I mineralocorticoid receptors expressed in the brain maintain a diurnal rhythm of corticosterone [87]. Otherwise, the low affinity glucocorticoid type II receptor (GR) in the hypothalamus mediates a negative feedback mechanism on CRH and AVP. This enables the organism to reduce the HPA response after an acute stress phase [88, 89]. The balance between CRH and AVP expression is dependent on the kind of stress that is administered to the organism, as restraint stress results in a different response than osmotic or immune stress [90]. Interestingly, acute and chronic stress have been shown to differ in their response, favouring an AVP induction in the case of chronic stress [90-93]. Typical symptoms of acute stress are asthma, eczema or migraines, whereas chronic stress may go along with anxiety, depression or metabolic disorders, such as obesity and type II diabetes [84].

An additional activator of CRH and AVP expression in the parvocellular PVN is estrogen, which reflects the different response of females and males to stress [94-98]. The role for estrogen in stress response is supported by the finding that estrogen can impair the glucocorticoid-mediated feedback on the HPA axis [97].

1.4 K_{ATP} channels as neuronal glucose and insulin sensors

Insulin is able to regulate neuronal activity by the modulation of ATP-sensitive potassium (K_{ATP}) channels [99]. K_{ATP} channels are expressed in tissues like skeletal and smooth muscle, heart, pancreatic β -cells, pituitary and brain including the substantia nigra, neocortex, hippocampus and hypothalamus [100]. The octameric K_{ATP} channel is constituted of different subunits that are expressed in a tissue-specific manner. Four inward rectifying potassium channel subunits (Kir6.1 or Kir 6.2) form a pore and are regulated by four sulfonylurea receptor subunits (SUR1 or SUR2) [101].

The activity of the K_{ATP} channel is linked to the energy status of the cell so that a high intracellular ADP-level activates and opens the channel, while a high level of ATP reduces its activity and initiates depolarisation [101]. Hence, increasing glucose concentrations lead to elevated intracellular ATP

concentrations, closure of K_{ATP} channels and enhanced neuronal firing. The finding that intracellular ATP controls firing of several neuronal populations led to the discovery that K_{ATP} channel expression enables neurons to act as glucose sensors, although the relative importance of glucose sensing in different neuronal populations with regards to energy homeostasis is still unknown [102].

Insulin is able to regulate neuronal activity and the phosphatidylinositol 3-kinase (PI3K) pathway has, recently, been associated with the modulation of K_{ATP} channels by insulin [99]. Especially, the analysis of the POMC-neuron specific PTEN deficient mice revealed the newly discovered link between PIP3 levels, which increase upon insulin stimulation, and the K_{ATP} channel. PTEN converts PIP3 into PIP2, thus inhibiting PI3K signalling. POMC-specific PTEN deficient mice exhibit hyperpolarized POMC neurons due to an increased K_{ATP} channel activity that goes along with a reduction of basal firing frequency [99, 103].

To analyse K_{ATP} channel signalling in more detail, a constitutive active variant of the K_{ATP} channel subunit Kir6.2 ($K_{ATP}\Delta N$) was generated. The $K_{ATP}\Delta N$ variant has a N-terminal deletion of 30 aminoacids and an overexpression of the variant leads to an ion channel that is 250 times less sensitive to ATP mediated closure and is therefore constitutively opened. An open K_{ATP} channel results in a constant outflow of the positively charged potassium, which can reduce the firing frequency and hyperpolarize the cell [104, 105]. In pancreatic β -islets, where the K_{ATP} -dependent depolarization leads to insulin secretion, this variant has been shown to cause impaired glucose induced insulin secretion and diabetes [106].

These findings indicate that K_{ATP} channel function in POMC neurons is crucial for the physiological regulation of food intake and body weight [107] and that the constitutive active $K_{ATP}\Delta N$ variant of the K_{ATP} channel is a good model to study the function of this channel in the regulation of membrane excitability.

1.5 FOXO1 as a transcription factor in insulin signalling

Insulin signalling regulates systemic gene expression by acting on several important transcription factors. One of them, FOXO1 was cloned from a human rhabdomyosarcoma and used to be named forkhead found in human rhabdomyosarcoma (FKHR). In the year 2000, the nomenclature of the large family of transcription factors was standardized and the term forkheadbox (FOX) proteins was established. The FOX gene family can be subdivided in 15 classes and until now about 100 FOX proteins have been identified in humans. All FOX proteins have a characteristic forkhead box domain of 100 amino acids, which enables the proteins to bind to the DNA by a helix-turn-helix motive consisting of three α helices and two characteristic large loops (see [108] for review).

One Subclass, the FOXO family, consists of four members: FOXO1, FOXO3A, FOXO4 and FOXO6. FOXO1, FOXO3A and FOXO4 are negatively regulated by the AKT phosphorylation and bind to the same DNA consensus sequence, possibly regulating a similar set of target genes [109].

1.5.1 The regulation of FOXO1 by posttranslational modification

By binding to its tyrosin kinase receptors, insulin, IGF and other growth factors activate AKT by phosphorylation via the IRS/PI3 kinase pathway (see section 4). In absence of signals from AKT or other inactivating kinases, FOXO1 is located in the nucleus, where it activates or suppresses transcription by binding to its consensus sequence on promoters. Upon growth factor stimulation, activated AKT phosphorylates FOXO1 on serine 253, threonine 24 and serine 316, leading to nuclear export of FOXO1 and its ubiquitination-mediated degradation. This export is supported by the chaperone 14-3-3, which masks the nuclear localization sequence (NLS), and a nuclear export sequence (NES), which interacts with the Exportin/Crm1 system. Other kinases as SGK, the Casein kinase 1 (CK1) and dual tyrosine phosphorylated regulated kinase 1 (DYRK1) have also been described to negatively regulate the activity of FOXO1 (for review see [110]).

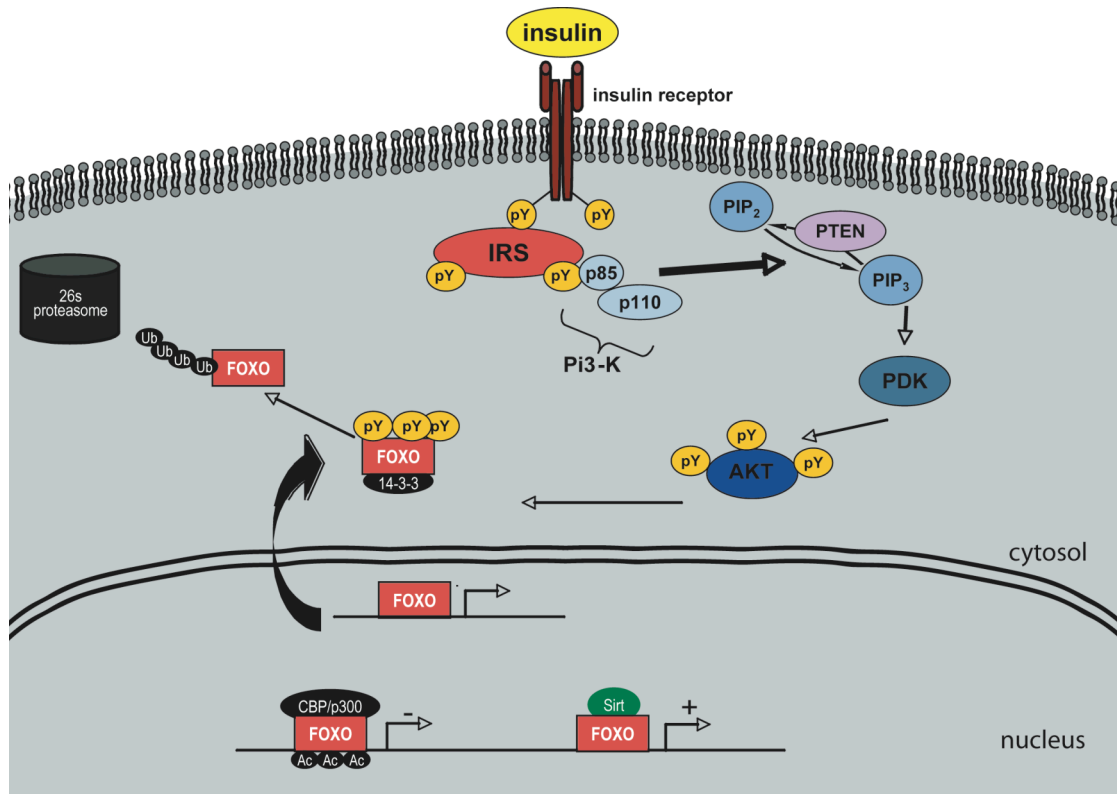


Figure 4: FOXO1 shuttling between the nucleus and the cytosol

Insulin binding to the insulin receptor (IR) results in receptor autophosphorylation, which enables insulin receptor substrate (IRS) proteins to bind. The tyrosine kinase activity of the receptor phosphorylates specific tyrosines of IRS. Phosphorylated IRS activates phosphatidylinositol 3-kinase (PI3K). Phosphatidylinositol (3,4,5)-trisphosphate (PIP3) is generated from phosphatidylinositol (4,5)-bisphosphate (PIP2). This can be reversed by the PTEN phosphatase. The pleckstrin homology (PH) domain of the phosphoinositide dependent protein kinase-1 (PDK1) binds to PIP3, which activates PDK1 to phosphorylate AKT (protein kinase B). AKT inactivates the transcription factor FOXO1 by phosphorylation. In absence of signals from AKT or other inactivating kinases, FOXO1 is located in the nucleus, where it activates or suppresses transcription by binding to its consensus sequence on promoters. Upon growth factor stimulation and AKT-phosphorylation, FOXO1 is exported out of the nucleus resulting in an ubiquitination-mediated degradation, supported by the chaperone 14-3-3. FOXO1 can be activated by Sirt-deacetylation (sirtuin) and suppressed by CBP-acetylation (CREB binding protein)

So far, only few FOXO1 activating kinases have been described. For instance in *Drosophila*, oxidative stress induces the FOXO1 phosphorylation by c-Jun N-terminal kinase (JNK). This has been shown to play a role in aging regulation, as JNK requires FOXO to extend life span of flies [111]. Besides phosphorylation, also the acetylation status of FOXO1 has an effect on its activity. Whereas Sirt1 (sirtuin), involved in insulin secretion and oxidative stress in pancreatic β -cells, has been shown to activate FOXO1 by

deacetylation [112], an acetylation by CBP (CREB binding protein) can suppress the activity of FOXO proteins. [110, 112]

1.5.2 The genetic modifications of FOXO genes in mice

Complete conventional knockout mice of FOXO1, 3A and 4 have been generated. The FOXO1 knockout mice die on embryonic day 10.5, whereas the mice deficient for FOXO3a and 4 are viable but have a diversity of defects including tumors in different tissues of the body (table1). Moreover, the analysis of FOXO1 haploinsufficient mice revealed some important functions of FOXO1 in the adult liver, as insulin receptor haploinsufficient mice are insulin insensitive and this can be rescued by FOXO1 haploinsufficiency [113]. The FOXO genes are expressed in an overlapping manner in different tissues and FOXO1, FOXO3A and FOXO4 have been shown to bind to the same consensus sequence. Hence, different FOXO proteins could regulate the same target genes (reviewed in [109]).

Table 1: Phenotypes of FOXO knockout mice [110]

<i>Knockout mice</i>	<i>Phenotypes</i>	<i>References</i>
FOXO1 <i>-/-</i>	Embryonic lethal day 10.5; defects of vascular development in embryo and yolk sac	[114, 115]
FOXO3a <i>-/-</i>	Viable; abnormal ovarian development; haematological abnormalities; pituitary adenoma	[114, 116, 117]
FOXO4 <i>-/-</i>	Viable; Impaired neointima formation lung adenoma; adenocarcinoma; pituitary adenoma	[117, 118]

The conventional FOXO knockout mice have specific defects in the indicated organs.

To circumvent the problem of redundancy, alternative strategies have been developed by the generation of FOXO1 constitutive active and dominant negative variants. In the case of the constitutive active FOXO1, two or three phosphorylation sites important for inactivation were mutated, so that AKT and other kinases cannot phosphorylate the resulting protein. As a result, unphosphorylated FOXO1 variant remains in the nucleus and the target genes are activated independently of a stimulation of the cell by factors, such as insulin [119, 120].

For the generation of the dominant negative form of FOXO1, the C-terminal region of the protein was eliminated, which results in a truncated protein

consisting only of the N-terminal 253 amino acids (FOXO1DN). Thus, the AKT phosphorylation sites at serine residues 253 and 319, the nuclear export sequence (NES) and the transactivation domain are absent. Similar to the constitutive active FOXO1 variant, this truncated protein can neither be phosphorylated nor exported from the nucleus so that it stays bound to FOXO target sequences via its forkhead domain. Importantly, the lack of the transactivation domain, results in a dominant negative function of the protein [121, 122]. Finally, FOXO1DN can block the DNA binding of endogenous FOXO1, FOXO3a and FOXO4, since the known consensus sequences are identical for all them [123].

1.5.3 The role of FOXO1 in the periphery and the CNS

FOXO proteins are vital integrators of a diversity of pathways and are essential for different tissues and processes, as metabolism, tumor suppression, cell cycle arrest, cellular differentiation, apoptosis and protection from oxidative stress. The overexpression of the constitutive active or dominant negative variant of FOXO1 via adenoviral administration has helped to elucidate the role of FOXO1 in different tissues, such as liver, adipose tissue and the hypothalamus [119, 120, 122, 124].

Hepatic FOXO1 is a positive regulator of glucose production, since FOXO1 positively regulates expression of gluconeogenic enzymes such as G6Pase and PEPCK, and inhibition of hepatic FOXO1 can ameliorate the diabetic phenotype of obese mice [113]. FOXO proteins are also known to be intimately involved in cell cycle control and development. Hence, in adipose tissue, a constitutive active FOXO1 variant increases the cell cycle inhibitor p21 resulting in adipocyte differentiation [113, 125]. Furthermore, FOXO1 action increases expression of pro-apoptotic proteins, in line with FOXO1 activation and growth factor stimulation being inversely linked [126].

Hypothalamic FOXO1 has been shown to be an important player in the metabolic control. FOXO1 competes with the leptin-stimulated transcription factor STAT3 for binding to the promoters of POMC and AgRP, as analysed by the injection of a constitutive active FOXO1 expressing adenovirus into the ARC

[120, 124]. This was further underscored by the use of mice deficient for FOXO1 specifically in POMC expressing neurons. These mice show a decreased food intake but normal energy expenditure. In line with this, POMC-expressing neuron specific FOXO1 deficient mice produce increased levels of the POMC processing products α -MSH and β -endorphin. The latter is a consequence of the upregulation of the Carboxypeptidase E (Cpe), an enzyme involved in POMC processing [127].

Aforementioned, FOXO1 has first been cloned from a human rhabdomyosarcoma. To date, FOXO1, as a central signalling molecule, links the balance between cell cycle and differentiation with the stabilisation of the energy balance of the organism [128], thereby being associated with diseases like cancer and diabetes. The role in peripheral organs has intensively been studied. Nonetheless, in the hypothalamus, where a high FOXO1 expression can be monitored in different areas including the PVN, the role of FOXO1 has only been analysed in the arcuate nucleus [124].

1.6 Objectives

Nutrient and hormone signals, such as insulin, leptin and glucose reflect the nutritional status of the organism and modulate energy homeostasis. How these signals are integrated in the hypothalamus and how the distinct hypothalamic nuclei translate these signals is only started to be elucidated on the molecular level. Research has been mainly focused on the response of first order neurons in the arcuate nucleus of the hypothalamus. However, The integrative function of the paraventricular nucleus (PVN) in stress response and the regulation of energy homeostasis is only poorly understood. The transcription factor FOXO1 and the ATP sensitive potassium (KATP) channel are involved in several important metabolic pathways in different tissues including the arcuate nucleus. Thus, the aim of this thesis was to elucidate if these central molecules are also involved in the diversity of pathways regulated by the PVN.

2 Materials and methods

2.1 Chemicals

Table 2: List of chemicals

<i>Chemicals</i>	<i>Supplier, origin</i>
Agarose	Peqlab, Erlangen, Germany
Agarose Ultra Pure	Invitrogen, Karlsruhe, Germany
Ampicillin	Applichem, Darmstadt, Germany
Bromphenol-blue	Merck, Darmstadt, Germany
Calcium chloride	Merck, Darmstadt, Germany
Chloroform	Applichem, Darmstadt, Germany
DAPI	Vector Laboratories, Burlingham, USA
Diethylpyrocarbonat (DEPC)	Applichem, Darmstadt, Germany
Dimethylsulfoxide (DMSO)	Sigma, Steinheim, Germany
Di-sodium hydrogen phosphate	Merck, Darmstadt, Germany
Deoxyribonucleotide triphosphate (dNTPs)	Amersham, Freiburg, Germany
Dulbecco's Modified Eagle Medium (DMEM)	Gibco, Paisley, UK
Developer G 153	Agfa, Mortsel, Belgium
Ethanol, absolute	Roth, Karlsruhe, Germany
Ethidium bromide	Applichem, Darmstadt, Germany
Ethylendiamine tetraacetate (EDTA)	Applichem, Darmstadt, Germany
Fetal calf serum (FCS)	Invitrogen, Karlsruhe, Germany
Fixing solution G 354	Agfa, Mortsel, Belgium
Formaldehyde	Merck, Darmstadt, Germany
Formamide	Applichem, Darmstadt, Germany
Gene Ruler DNA Ladder Mix	Fermentas, St. Leon-Rot, Germany
Glucose, 20 %	DeltaSelect, Dreieich, Germany
Glycerol	Applichem, Darmstadt, Germany
Hydrochloric acid (37 %)	KMF Laborchemie, Lohmar, Germany
Hydrogen peroxide	Sigma, Steinheim, Germany
Isopropanol (2-Propanol)	Roth, Karlsruhe, Germany
Isopropyl-b-D-thiogalactopyranosid (IPTG)	Sigma, Deisenhofen
Kanamycin	Applichem, Darmstadt
Lipofectamin 2000	Invitrogen, Karlsruhe
Luria-Bertani (LB) Agar	Sigma, Steinheim, Germany
Luria-Bertani (LB) Media	Applichem, Darmstadt, Germany
Methanol	Roth, Karlsruhe, Germany

<i>Chemicals</i>	<i>Supplier, orgin</i>
Morpholinopropansulfonsäure (MOPS)	Applichem, Darmstadt, Germany
N,N,N',N'- Tetramethylethylendiamin (TEMED)	Sigma, Deisenhofen, Germany
Nitrogen (liquid)	Linde, Pullach, Germany
NuSieve (low-melt) Agarose	Biozym, Hess Oldendorf, Germany
Opti-MEM	Gibco, Paisley, UK
Paraformaldehyde (PFA)	Sigma, Steinheim, Germany
1x PBS	Gibco, Karlsruhe, Germany
Penicillin/Streptomycin	Gibco, Paisley, UK
Phenol	Sigma, Deisenhofen, Germany
Phenol/Chloroform/Isoamylalkohol	Applichem, Darmstadt, Germany
Potassium chloride	Merck, Darmstadt, Germany
Bovine serum albumin (BSA)	Applichem, Darmstadt, Germany
Sodium chloride	Applichem, Darmstadt, Germany
Sodium cholide solution, 0.9 %	Berlin-Chemie, Berlin, Germany
Sodium citrate	Merck, Darmstadt, Germany
Sodium di-hydrogen phosphate	Merck, Darmstadt, Germany
Sodiumdodecylsulfate (SDS)	Applichem, Darmstadt, Germany
Sucrose	Sigma, Steinheim, Germany
TRIfast	PeqLab, Erlangen, Germany
Trishydroxymethylaminomethan (Tris)	Applichem, Darmstadt, Germany
Triton X-100	Sigma, Steinheim, Germany
Trypsin	Gibco, Paisley, UK
Tween	Applichem, Darmstadt, Germany
X-Gal (5-bromo-4-chloro-3-indolyl-beta-D-galactopyranoside)	Sigma, Deisenhofen, Germany

2.2 Mouse experiments

2.2.1 Animal care

Care of all animals was within institutional animal care committee guidelines. All animal procedures were conducted in compliance with protocols, approved by local government authorities (Bezirksregierung Köln, Cologne, Germany) and were in accordance with NIH guidelines. Mice were housed in groups of 3–5 at 22–24°C using a 12-hour light / 12-hour dark cycle. Animals were either fed normal chow diet (Teklad Global Rodent 2018; Harlan) containing 53.5% carbohydrates, 18.5% protein, and 5.5% fat (12% of calories from fat) or a high

fat diet (HFD; C1057; Altromin) containing 32.7% carbohydrates, 20% protein, and 35.5% fat (55.2% of calories from fat). Animals had ad libitum access to water at all times, and food was only withdrawn if required for an experiment. Mice were sacrificed using CO₂ or cervical dislocation.

2.2.2 Generation of FOXO1DN^{Sim1} and FOXO1DN/DN^{Sim1} mice

FOXO1DN^{stoplox/lox} mice were previously generated as described in Belgardt et.al. [129]. FOXO1DN^{stoplox/lox} mice were backcrossed six times onto a C57BL/6 background before crossing to Sim1-Cre animals [82]. Sim1-Cre mice were crossed to FOXO1DN^{stoplox/lox} for the generation of heterozygous FOXO1DN^{Sim1} mice, whereas to generate homozygous FOXO1DN/DN^{Sim1} mice FOXO1DN^{stoplox/lox} mice were first bred to heterozygous FOXO1DN^{Sim1} and then to homozygous FOXO1DN/DN^{Sim1}. The background was unchanged throughout all experiments. Littermates were used for analysis at all times. Mice were genotyped by PCR using genomic DNA isolated from tail tips as described in section 2.6.

2.2.3 Generation of KATPΔN^{Sim1} mice and KATPΔN/ΔN^{Sim1}

KATPΔN^{stoplox/lox} mice were previously generated [130] and a C57BL/6 background was ensured by backcrossing KATPΔN^{stoplox/lox} mice six times before crossing them to Sim1-Cre animals [82]. First, heterozygous KATPΔN^{Sim1} mice were generated by crossing Sim1-Cre mice to KATPΔN^{stoplox/lox}, and in a second step KATPΔN^{stoplox/lox} mice were first bred to heterozygous KATPΔN^{Sim1} and then to homozygous KATPΔN/ΔN^{Sim1} to establish littermate groups that consist of homozygous KATPΔN/ΔN^{Sim1} mice and KATPΔN^{stoplox/lox} mice as controls. The background was unchanged throughout all experiments. Littermates were used for analysis at all times. Mice were genotyped by PCR using genomic DNA isolated from tail tips as described in section 2.6.

2.2.4 Generation of DsRed-KATP Δ N^{Sim1} mice and Z/EG-KATP Δ N^{Sim1}

To generate Z/EG-KATP Δ N^{Sim1} mice or DsRed-KATP Δ N^{Sim1} for electrophysiological experiments “lacZ/EGFP” (Z/EG) [131] or “B6.Cg-Tg(CAG-DsRed*MST)1Nagy/J” (DsRed) [132] mice were bred to heterozygous KATP Δ N^{Sim1}. The background was unchanged throughout all experiments. Littermates with the genotype Z/EG^{Sim1} or DsRed^{Sim1} were used for analysis as controls at all times.

2.2.5 Determination of the mouse genotype

For isolation of genomic DNA, mouse tail biopsies were incubated in lysis buffer (10 mM Tris/HCl [pH 8]; 10 mM EDTA; 150 mM NaCl; 0.2 % (w/v) SDS; 400 mg/ml proteinase K) at 55 °C for 3-12 hours. DNA was precipitated by adding an equal volume of isopropanol, mixed and pelleted by centrifugation. After washing with 70 % (v/v) Ethanol, the pellet was dried at room temperature and resuspended in TEbuffer (10 mM Tris/HCl [pH 8]; 1 mM EDTA)[133].

The polymerase chain reaction was performed to amplify a DNA fragment *in vitro* to detect targeted alleles or transgenes by size of amplified fragment for genotyping of mice[134, 135]. This was performed with 500 ng DNA isolated from tail biopsies in a total volume of 25 μ l containing 25 pmol of each primer (listed in table 3), 25 μ mol dNTPs, 2 to 6 % (v/v) DMSO, 1 to 1.2 U REDTaq ® DNA Polymerase and 1 x REDTaq ® PCR Reaction Buffer (Sigma, Steinheim, Germany). Thereby, the different PCRs started with an initial denaturation step at 95°C for 5 min, followed by 34 to 45 cycles of denaturation at 95°C for 30 sec, annealing at 54 to 62°C for 30 to 45 sec and elongation at 72°C for 30 to 90 sec. The elongation was finished with a final extension step at 72°C for 10 min. All PCR reactions were carried out either in an iCycler Thermocycler (Bio-Rad, Hercules, CA, USA) or in a PTC-200 Peltier Thermal Cycler (MJ Research, Waltham, MA, USA). Amplified DNA fragments were separated by size using agarose gel electrophoresis (1 to 3 % (w/v) agarose (depending on fragment size); 1 x TAE; 0.5 mg/ml ethidiumbromide; 1 x TAE electrophoresis buffer).

Table 3: Oligonucleotides for the analysis of mouse genotypes.

<i>Name</i>	<i>Sequence</i>
CAGS_forw	AAAGTCGCTCTGAGTTGTTATC
CAGS_rev_wt	GATATGAAGTACTGGGCTCTT
CAGS_rev	TGTCGCAAATTA ACTGTGAATC
SIM1-Cre 1	CACGACCGGCAAACGGACAGAA
SIM1-Cre 2	TTTTGGTTTTGGATGAGTCTGTGGAG
SIM1-Cre 3	TGGGATTAGCGTGTTTCAACTGAGC
lacZ 1	ATC CTC TGC ATG GTC AGG TC
lacZ 2	CGT GGC CTG ATT CAT TCC
DsRed 1	CCC ATG GTC TTC TTC TGC A
DsRed 2	AAG GTG TAC GTG AAG CAC CC
DsRed 3	CTA GGC CAC AGA ATT GAA AGA TCT
DsRed 4	GTA GGT GGA AAT TCT AGC ATC ATC C

2.2.6 Body weight, fat composition and body length

Body weight was measured once a week. Body fat content was measured *in vivo* by nuclear magnetic resonance using the minispec mq 7.5 (Bruker). At the end of the study period of 18 weeks, the animals were sacrificed using CO₂ or cervical dislocation, body length (naso-anal length) was determined, relevant organs were extracted and stored at -80°C until further preparation.

2.2.7 Food intake, melanotan II sensitivity and indirect calorimetry

Mice were acclimated to the food intake settings for at least three days. Food intake was measured over a two-week period, during which mice were housed individually in accustomed cages using food racks. To minimize handling of animals, food racks were weighed weekly and daily food intake was calculated as the average daily intake of chow within the time stated.

To measure the melanotan II (MTII) sensitivity the mice were adjusted to the food intake handling and to a daily injection for four days of 1 x PBS just before the initiation of the dark phase. On the day of the experiment the food was removed for four hours and MTII or 1 x PBS was injected immediately before the beginning of the dark phase. The food intake was measured 2, 4, 14 and 24 hours after injection. The experiment was repeated after a two day washout

period, so that every animal was injected with MTII on one day and 1 x PBS on the other.

Indirect calorimetry was automatically determined by a calorimetry module (Phenomaster). Mice were housed individually for one week in training cages that mimic the conditions during the experiment and the first two hours after initiating the Phenomaster evaluation were used for acclimatization before the parameters were measured twice per hour for at least 48 hours, while food and water were provided *ad libitum*.

2.2.8 Blood glucose and serum protein concentrations

Tail bleeding of mice at an age of 8 or 18 weeks was performed according to Hogan[136] and Silver[137] in the morning to avoid variations by the circadian rhythm. Serum was separated from blood cells and platelets by 30 minutes of centrifugation at a speed of 13000 rpm and stored at -20°C. Blood glucose values were determined from tail whole venous blood using an automatic glucose monitor (GlucoMen^R *GlycO*; A. Menarini Diagnostics).

Mice were handled at least weekly after weaning. Before the restraint of 8 week old mice, blood was taken from the tail vein for determination of basal serum corticosterone levels, which was followed by 60 minutes of restraint stress of the mice in a 50 ml plastic tube with openings for air supply. Immediately after the restraint period, blood was collected from the tail vein to determine stress serum corticosterone levels.

Serum insulin, leptin and corticosterone levels were measured by Enzyme-linked Immunosorbent Assay (ELISA) using mouse standards according to manufacturer's guidelines (Mouse Leptin ELISA, Mouse/Rat Insulin ELISA, Crystal Chem; Corticosterone Enzyme Immunoassay Kit, Assay Designs Inc.).

2.2.9 Glucose and Insulin Tolerance Tests

Glucose tolerance tests (GTT) were performed with 16-17 hours fasted animals in the age of 12 weeks. After determination of fasted blood glucose levels each animal received an intraperitoneal injection of 20% glucose (10 ml/kg body

weight) (DeltaSelect). Blood glucose levels were detected 15, 30, 60 and 120 minutes after the glucose injection.

Whereas, Insulin tolerance tests (ITT) were performed with random fed 13 week old mice. The determination of basal blood glucose levels was followed by an injection of 0.75 U per kilogram body weight of human regular insulin (Novo Nordisk) into the peritoneal cavity. Blood glucose levels were detected 15, 30 and 60 minutes following the insulin injection.

2.2.10 Ovariectomy

Ovariectomy (OVX) was performed as previously described [138]. Animals were anaesthetised by an i.p. injection of a mixture of ketamine/xylazine and OVX or sham operations were performed by bilateral dorsal abdominal incisions so that the ovary and the oviduct could be rapidly removed. In the sham surgery group, the ovary and oviduct were visualized before incisions were sutured.

2.3 Immunocytochemistry

All immunocytochemical procedures were performed as previously described in [103, 129, 139, 140]. Briefly, Sim1-cre mice were mated with RosaArte1 reporter mice [141]. FOXODN/DN^{Sim1} (GFP detection) and LacZ^{Sim1} mice (LacZ detection) (Rosa-ArtE.X-gal) were anesthetized intraperitoneally with Avertin (240 mg/kg) (2,2,2-tribromoethanol, Sigma, Steinheim, Germany) and transcardially perfused with saline, for GFP stainings followed by 4 % (w/v) paraformaldehyde (PFA) in 0.1 M phosphate buffered saline (PBS [pH 7.4]). The brains were dissected and frozen in tissue freezing medium (Jung Tissue Freezing Medium; Leica Microsystems, Wetzlar, Germany) after post-fixation in 4 % (w/v) PFA at 4 °C over night (in the case of GFP) and soaking in 20 % (w/v) sucrose for 6 h (in the case of GFP). 25 µm thick free-floating coronal sections were cut through the ARC using a freezing microtome (Leica Microsystems, Wetzlar, Germany).

For GFP stainings, the sections were washed, pretreated with 0.3% H₂O₂, blocked with PBT/azide containing 3% donkey serum, and incubated overnight with primary antibody (anti-GFP rabbit serum, 1:10.000 in blocking solution;

A6455 from Invitrogen/Molecular Probes). Incubation with secondary antibody (anti-rabbit IgG biotin, 1:500; 711-065-152 from Jackson ImmunoResearch) was followed by an additional incubation with the VECTASTAIN Elite ABC kit (Vector Laboratories) for 1 h and visualization with 0.4% DAB/0.01% H₂O₂. Afterwards the sections were mounted onto gelatin-coated slides and covered with glycerin and processed as previously described [139].

For lacZ stainings, the sections were washed extensively in PBS to remove cryoprotectant. Afterwards, the sections were treated with 0.3 % (v/v) H₂O₂ in PBS for 20 minutes to quench endogenous peroxidase activity. Following pretreatments, the sections were stained using the Renaissance® TSATM Fluorescence Systems Tyramide Signal Amplification Kit (PerkinElmer™, Waltham, MA, USA) according to manufacturer's guidelines (primary antibody: rabbit anti-lacZ; secondary antibody: goat anti-rabbit peroxidase labeled. The stained sections were embedded in Vectashield Mounting Medium containing DAPI (Vector Laboratories Burlingame, CA, USA).

2.4 Electrophysiology

All electrophysiological procedures were performed as previously described in [103, 129]. Briefly, coronal brain slices (250 - 300 μm) containing the ARC were prepared from 6-week old Z/EG^{Sim1} and K_{ATP}ΔN-Z/EG^{Sim1} mice. Brain slices remained at least 15 min at 35°C in artificial cerebrospinal fluid (aCSF; in mM: 125 NaCl, 21 NaHCO₃, 2.5 KCl, 1.2 NaH₂PO₄, 2 CaCl₂, 2 MgCl₂, 10 HEPES (pH 7.4), and 5 glucose.) and were gassed with 95% O₂ and 5% CO₂. Moreover, a Zeiss Axioskop fitted with fluorescence and infrared differential interference contrast (IR-DIC) videomicroscopy was used and fluorescent Sim1-GFP neurons were identified by epifluorescence and patched under IR-DIC optics. For whole-cell current-clamp and voltage-clamp recordings an EPC-9 patch-clamp amplifier was used, as previously described [103]. Patch pipettes had resistances of 3-5 MΩ when filled with internal solution (in mM: 128 K-gluconate, 10 KCl, 10 HEPES, pH 7.3, 0.1 EGTA, 2 MgCl₂, 0.3 Na-GTP, and 3 K₂-ATP). Externally the slices were continuously perfused at 2 - 4 ml/min with gassed aCSF in all experiments. Experiments were carried out at 22 -25°C. Data were filtered, sampled with Pulse/Pulsefit and software (Heka, Elektronik,

Germany, version 8.67) and analyzed with Pulsefit and Origin (Microcal, Northampton, MA) software (version 6.0).

2.5 Molecular biology

Standard methods of molecular biology were performed according to protocols described by J. Sambrook[142], if not stated otherwise.

2.5.1 RNA isolation and expression studies

Measurements of mRNA levels were carried out by quantitative RT-PCR on RNA extracted from dissected tissues. Hypothalamus and amygdala were dissected with the aid of a mouse brain atlas (Franklin and Paxinos, 1997) using a coronal acrylic brain matrix (Braintree Scientific) to identify the hypothalamus and amygdala 0 to 2 mm posterior relative to bregma. The brain areas were then dissected from the coronal sections using a scalpel. Brain and brown adipose tissue were homogenized in TriFast reagent (peqLab) using the Ultra Turrax homogenizer (IKA). Phenol-chloroform extraction and precipitation with Isopropanol were performed according to the manufacturers instruction of the TriFast reagent. This was followed by an DNase digestion (PeqLab) in 1 x buffer and with 3 U DNase and the spectrophotometry quantification of the RNA concentration (NanoDrop; peqLab). An optical density of 1 at a wavelength of 260 nm (OD₂₆₀ of 1) corresponds to 40 µg/ml RNA and a high purity is reflected by the Quotient of OD₂₆₀/OD₂₈₀ at a level of 1.8 to 2.0. Each total RNA (200ng) was reversely transcribed by EuroScript Reverse Transcriptase (Eurogentec) according to the manufactures instructions in a 10 µl reaction including 1 µl 10x buffer, 2 µl 25 mM MgCl₂, 2 µl 2.5 mM dNTP, 0.5 µl random nonamer, 0.2 µl RNase inhibitor and 0.25 µl reverse transcriptase. The reverse transcription was mediated by an initial 10 minutes incubation at 25°C, which was followed by 30 minutes of elongation at 45°C and a 5 minutes reverse transcriptase inactivation step at 95°C. The cDNA was amplified using TaqMan® Universal PCR-Master Mix, NO AmpErase UNG with TaqManR Assay on demand kits (Applied Biosystems). Quantitative PCR was performed on an ABI-PRISM 7700 Sequence Detector (Applied Biosystems) measuring corticotropin

releasing hormone (CRH), arginine vasopressin (AVP) with intronic probes stated in table 4. (Applied Biosystems, Foster City, CA, USA). Samples were adjusted for relative RNA content by glucuronidase beta (Gusb) and hypoxanthine guanine phosphoribosyl transferase (Hprt) (Applied Biosystems, Foster City, CA, USA). Calculations were performed by a comparative method (2-ddCT). Assays were linear over 4 orders of magnitude.

Table 4: Realtime probes

<i>Probe</i>	<i>Sequence</i>
CRH_i3	GCG GTG ACC CTT CTT TGG AGA
CRH_i5	GAT TAG GGT GTG CGA CAG CTT AAA CC
CRH_probe	GAC GTT TGG GAG GTC CTT AGG AAG
AVP_i3	CTA ACT TCG CTT TTT CAA ATC GCC A
AVP_i5	GTA GGC AGC GCC TAG ACG GG
AVP_probe	CTA TGC ATG TAT GTG TGT CGC TAA CTG

2.5.2 Cloning of promoter fragments or genes

Total RNA (200ng) isolated by phenol chloroform extraction using TriFast reagent (PeqLab) was reversely transcribed by EuroScript Reverse Transcriptase (Eurogentec) according to the manufactures instructions. The generated cDNA was used to amplify DNA fragments by the High Fidelity PCR Master Kit (Roche).

To minimize PCR mistakes for molecular cloning strategies, the High Fidelity PCR Master Kit (Roche), a mixture of a regular Taq- and the proofreading *Tgo* DNA-Polymerase, was used according to the manufactures instructions with 500 ng template cDNA and 25 pmol of each primer (table 5). After an initial denaturation step at 94 °C for 3 min, 14 cycles of denaturation at 94 °C for 45 sec, annealing at 54 °C for 45 sec and elongation at 68 °C for 1 to 3 min were followed by another 24 cycles of denaturation at 94 °C for 45 sec, annealing at 54 °C for 45 sec and elongation at 72 °C for 2 to 5 min. The PCR was completed with a final extension step at 72 °C for 10 min.

Amplified or digested DNA fragments were separated by size using agarose gel electrophoresis (1 to 3 % (w/v) agarose (depending on fragment size); 1 x TAE; 0.5 mg/ml ethidiumbromide; 1 x TAE electrophoresis buffer). To Isolate DNA

fragments from a PCR or restriction digest the QIAEX II Gel Extraction Kit (Quiagen) was used according to the manufactures instructions after the separation of the DNA fragments on a 1% agarose gel (Invitrogen). PCR products were subcloned into the pGEM-T Easy Vector (Promega) using 5 µl ligation buffer, 1 µl pGEM-T Easy vector, 3 µl gel extracted PCR product and 1 µl T4 DNA ligase. The ligation was incubated for 1h or over night at room temperature followed by the transformation into chemically competent *Escherichia coli* by the blue and white selection method on ampicillin containing LB agar plates. Competent *Escherichia coli* (E. coli) DH5α cells were prepared according to a standard protocol (Inoue et al., 1990) and used in heat shock transformation of plasmid DNA (30 min on ice; 30 sec at 42°C; 1h at 37°C in 600 µl Luria-Bertani (LB) media).

Table 5: Oligonucleotides for cloning of promoter fragments

<i>Name</i>	<i>Sequence</i>
5XhoCRH1.0kb	CTCGAGTTCC CACTTAGACA TAATCTCC
5XhoCRH300bp	CTCGAGCCGT ATCTGGCCTA TCATAGT
3HindCRH	AAGCTTCACACCAGAG CCTGGAGTG
5XhoAVP1.3	CTCGAGCATAGGCCAACTAATCTGGG
3BgIIAVP	AGATCTGCCTTGGCGGGCTGGGC

2.5.3 Preparation of plasmid-DNA and ligation into expression vectors

The preparation of plasmid DNA from transformed *E.coli* colonies was performed using Maxiprep-Kit (Qiagen) if high concentrations were desired and the Plasmid Miniprep Kit I (PeqLab) for small concentrations of plasmid DNA according to the manufactures instructions. For the isolation of the plasmid DNA a bacteria suspension of 200 ml LB-Media (Maxiprep-Kit) or 3 ml LB-Media (Miniprep Kit) was incubated at 37°C overnight.

The concentration and purity of plasmid DNA was determined by the NanoDrop (PeqLab). An optical density of 1 at a wavelength of 260 nm (OD₂₆₀ of 1) corresponds to 50 µg/ml of dsDNA and a high purity is reflected by the quotient OD₂₆₀/OD₂₈₀ at a level of 1.8 to 2.0.

To analyse the correct insertion into vectors or to isolate fragments for ligation into the expression vectors, 0.5 to 10 µg plasmid DNA were digested with appropriate restriction enzymes (EcoRI, XhoI, BglII, HindIII; Fermentas). Therefore 10 to 20 units were used in 1 X Buffer of the corresponding enzyme according to the manufactures instructions.

The ligation of purified DNA into the expression vectors was mediated by 400 U T4-DNA-Ligase (NEB) at 20°C for 4 hours with a 1:3 to 1:7 relation of insert to vector and the transformation of bacteria was performed as described in section 2.5.2.

2.5.4 Sequencing

DNA-sequencing was performed using Big Dye Termination v3.1 Cycle Sequencing Kits (Applied Biosystems). Therefore 0.5 µl Ready Reaction Premix (2.5x), 1.5 µl BigDye Sequencing Buffer (5x), 1.6 pmol Primer and 150-300 ng dsDNA were adjusted to a final volume of 10 µl and submitted to 90 cycles of the following temperature program: 30 sec at 94°C; 15 sec at 50°C; 4 min at 60°C.

The sequence was automatically determined with the ABI373A und ABI377 Systems.

2.6 Cell culture

2.6.1 Preparation of collagen-coated plates

Plates/wells were covered with 30 µg/ml Collagen G (Biochrom) diluted in PBS and incubated at 4°C overnight. To avoid drying out of the collagen, plates were stored up to 2 months at 4°C.

2.6.2 Maintenance of PC12 and SK-N-SH cells

On uncoated plates PC12 cells grew unattached in growth media [D-MEM GlutaMAX (low Glucose), Gibco/Invitrogen; 1% Penicillin / Streptomycin, PAA; 10% Horse Serum, Invitrogen; 5% FCS, Invitrogen] and media was changed

every 2-3 days by centrifuging the cells down and resuspending in fresh media. Cells were split 1:5 or 1:10 after centrifugation.

SK-N-SH cells grew attached in growth media (E-MEM (low Glucose), PAA; 1% Penicillin / Streptomycin, PAA; 1% glutamine, Invitrogen; 1% non-essential amino acids, PAA; 1% sodium pyruvate, PAA 10% FCS, Invitrogen) and media was changed every 2-3 days by trypsin treatment, centrifugation of the cells and resuspending in fresh media. Cells were split 1:5 or 1:10 after centrifugation.

For experiments involving the estrogen receptor, SK-N-SH cells were kept in phenol red free media supplemented with charcoal stripped fetal calf serum (D-MEM (low Glucose), Gibco/Invitrogen; 10% charcoal stripped FCS, Sigma; 1% Glutamine, Invitrogen; 1% non-essential amino acids, PAA; 1% sodium pyruvate, PAA).

2.6.3 Transfection of PC12 and SK-N-SH cells

To achieve a confluency of 90% on the day of transfection, at the day before transfection, the cells were counted (Neubauer Zählkammer) and plated on collagen-coated 24-well plates at 2.5×10^5 cells per well for PC-12 cells and on regular plates at 0.5×10^5 cells for SK-N-SH cells. Cells were plated in 0.5 ml of their normal growth medium containing serum and without antibiotics.

On the day of transfection, 0.8 µg DNA per well were diluted into 50 µl of OPTI-MEM® I Reduced Serum Medium (Gibco/Invitrogen). This was combined with the dilution of 1.5 µl lipofectamine 2000™ reagent (Invitrogen) (PC12) or 1.0 µl lipofectamine LTX™ reagent (Invitrogen) (SK-N-SH) in 50 µl OPTI-MEM I Medium per well. After 20 minutes of incubation at room temperature to allow DNA-lipofectamine liposome mediated complexes to form, the DNA-lipofectamine reagent complexes were added directly to each well containing 400 µl fresh media.

2.6.4 Luciferase assay

Estrogen (10 nM-1 µM) or Forskolin (100 nM) stimulation was initiated for 15 hours 24 hours after the termination of transfection or six hours 16-18 hours

after the termination of transfection, respectively. To lyse the cells, the media was removed, the cells were washed with PBS and incubated at RT for 15 minutes in 100 μ l 1 x Lysis Buffer (Promega). To evaluate luciferase activity, 20 μ l of the samples were measured automatically (Luminoskan Ascent Type 392, Thermo Labsystems) with 50 μ l LAR II (Promega) to determine the firefly luciferase activity and subsequently with 50 μ l Stop & Glo (Promega) to stop the firefly luminescence and initiate the renilla luciferase reaction.

2.6.5 Electromobility shift assay (EMSA)

The EMSA was performed as previously described in [143]. Briefly, SK-N-SH cells were homogenized in hypotonic solution (10 mM HEPES [pH 7.6]; 10 mM KCl; 2 mM MgCl₂; 0.1 mM EDTA; protease inhibitor cocktail (Roche, Basel, Switzerland)) and, after 10 min incubation on ice, NP-40 was added to 1 % (v/v). After centrifugation, the nuclear pellet was washed in hypotonic buffer, centrifugated again and, subsequently, resuspended in extraction buffer (50 mM HEPES [pH 7.8]; 50 mM KCl; 300 mM NaCl; 0.1 mM EDTA; 10 % (v/v) glycerol). Protein concentration was determined with the Nanodrop (PeqLab) and the “Christian Warburg formula”. Hypothalamic nuclear extracts (4 μ g) were incubated at room temperature for 30 min with 2 μ g poly(dI-dC) (Amersham Pharmacia Biotec, Uppsala, Sweden) and 0.5 ng of ³²P-labeled probe (table 6). Samples were fractionated on a 5 % (w/v) PAGE over night and visualized by autoradiography.

Table 6: Sequences of EMSA probes

<i>Position on promoter</i>	<i>Forward sequence</i>	<i>Reverse sequence</i>
-182 bp CRH	CAAGGAGGCGATAAATATC TGTTGATATAA	TTATATCAACAGATATTTATC GCCTCCTTG
-975 bp AVP	AAAGCTCTTTCCTCTTTACG GCTGTGGGTCT	AGACCCACAGCCGTAAAGA GGAAAGAGCTTT
-1090 bp AVP	TCAGACTGGCTCTGTTTAGC TGGGTCTCCTC	GAGGAGACCCAGCTAAACA GAGCCAGTCTGA
-1148 bp AVP	CTGCCTTAGAAACAAACAAC TGACTTACAG	CTGTAAGTCAGTTGTTTGT TCTAAGGCAG
-1329 bp AVP	TGGGCCCAAACCATAAAG TTTTTCTGGTGC	GCACCAGAAAACTTTATGG TTTGGGGCCCA
FOXO consensus [144]	GGGATAAATACTGTGCTCG GGCAG	CTGCCCGAGCACAGTATTT ATCCC
SP1 [144] (pos. control)	ATTCGATCGGGGCGGGGC GAG	CTCGCCCCGCCCGATCGT AA

2.7 Statistical methods

Data was analyzed for statistical significance using a two-tailed unpaired student's T-Test. All data were normally distributed. Data were analyzed for statistical significance using a two-tailed unpaired student's t-Test. All displayed values are means \pm SEM. * $p \leq 0.05$; ** $p \leq 0.01$; *** $p \leq 0.001$ versus control.

3 Results

The paraventricular nucleus of the hypothalamus (PVN) has been shown to be involved in a diversity of processes including the role as a site of second order neurons in the hypothalamic response to metabolic signals [15]. Moreover, specific neurons within the PVN initiate the stress response of the organism. The transcription factor forkhead box O1 (FOXO1), inhibited by insulin signalling, and the ATP-sensitive potassium (K_{ATP}) channel are widely expressed throughout the brain and one area of high expression is the PVN [124, 145, 146]. However, it is unclear, in which of the diverse mechanisms, controlled by the PVN, FOXO1 transcriptional control and K_{ATP} channel-dependent membrane excitability are involved. Therefore, the aim of this thesis was to compare, contrast and integrate the electrophysiological properties with insulin signalling mediated transcriptional control of Sim1 neurons within the PVN. To this extent, the role of the K_{ATP} channel and the transcription factor FOXO1 was investigated.

3.1 The K_{ATP} channel in the Sim1 neuron dependent regulation of energy metabolism

The PVN has been implicated in a diversity of pathways including energy metabolism. In this context, the PVN mediates insulin's effects on food intake by responding to signals originating in the arcuate nucleus [73, 80, 82]. However, it remains unclear if the PVN, besides its role as second order neuron population, also directly responds to hormone and metabolite input. Since hormones such as insulin and metabolites as glucose regulate neuronal function by opening or closing K_{ATP} channels, the physiologic effect of chronic K_{ATP} channel opening specifically in Sim1-positive PVN neurons on energy homeostasis control was assessed [103].

3.1.1 K_{ATP} channel expression in Sim1 neurons

To analyse whether K_{ATP} channels are expressed on Sim1 neurons within the PVN we analysed the electrophysiological properties of Sim1 expressing

Results

neurons after treatment with tolbutamide, a K_{ATP} channel inverse agonist that leads to depolarization of the neuron. Sim1 expressing neurons were marked by crossing Sim1-cre mice with Z/EG reporter mice, in which transcription of a green fluorescent protein (GFP) gene under control of the ubiquitously expressed Rosa26 promoter is prevented by a floxed β -galactosidase/neomycin-resistance gene. [131].

As seen in figure 5, treatment of a subset of Sim1 expressing neurons with tolbutamide indeed resulted in a clear depolarization after a couple of minutes time lag and the reaction was reversible by washing out the tolbutamide. Approximately two out of three (61.9%; n=21) Sim1 expressing neurons responded to tolbutamide, indicating that at least a subset of the Sim1 expressing neurons co-express the K_{ATP} channel.

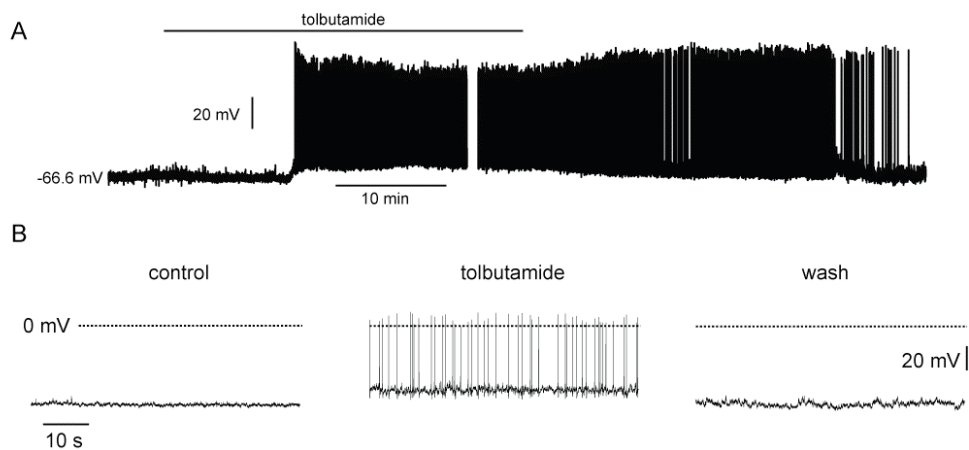


Figure 5: A subset of Sim1-cre neurons of the PVN were tolbutamide responsive

Representative membrane potential recordings of identified Sim1 neurons in PVN slices from Z/EG^{Sim1} mice before and after addition of 200 μ M tolbutamide. A: tolbutamide response of a Sim1-cre PVN neuron; B: tolbutamide induction of firing rate of a Sim1-cre PVN neuron and wash out to basal levels; kindly provided by Moritz Paehler (AG Kloppenburg, Institute for Zoology, University of Cologne)

3.1.2 Generation and functionality of the $K_{ATP}\Delta N$ overexpression in Sim1 neurons

It has been demonstrated that an N-terminal deletion of 14 amino acids in the kir6.2 subunit of the K_{ATP} channel ($K_{ATP}\Delta N$) results in a higher probability of the open confirmation and lower ATP sensitivity of the channel [106]. Since K_{ATP} channels consist of four Kir6.2 subunits, overexpression of this constitutive

active variant of the K_{ATP} channel leads to a competition with the endogenous kir6.2 subunit to form the pore of the K_{ATP} channel. Consequently, $K_{ATP}\Delta N$ overexpressing cells were shown previously to hyperpolarize by a constant potassium outflow [105, 147].

To investigate the effect of overexpression of this constitutive active K_{ATP} channel in Sim1 neurons, the previously generated $K_{ATP}\Delta N$ mice were used, which have been generated by Dr. Thomas Wunderlich in the laboratory of Professor Jens C. Brüning [130]. In these mice, the expression of the transgene is targeted to the Rosa26 locus and is dependent on the CAGGs promoter, which consists of a cytomegalovirus (CMV) enhancer and a chicken beta actin promoter. A locus of X-over P1 (loxP) flanked neomycin resistance followed by a Westphal stop sequence is located upstream of the start codon (fig. 6A). Upon expression of the cre-recombinase, the loxP flanked stop sequence can be removed by recombination, leading to expression of the transgene (fig. 6C). Downstream of the $K_{ATP}\Delta N$ sequence is a flip-recombinase target (FRT) site flanked green fluorescent protein (GFP), which is preceded by an internal ribosomal entry site (IRES). As such, a bicistronic mRNA mediates protein expression of both $K_{ATP}\Delta N$ as well as GFP (fig. 6A&C).

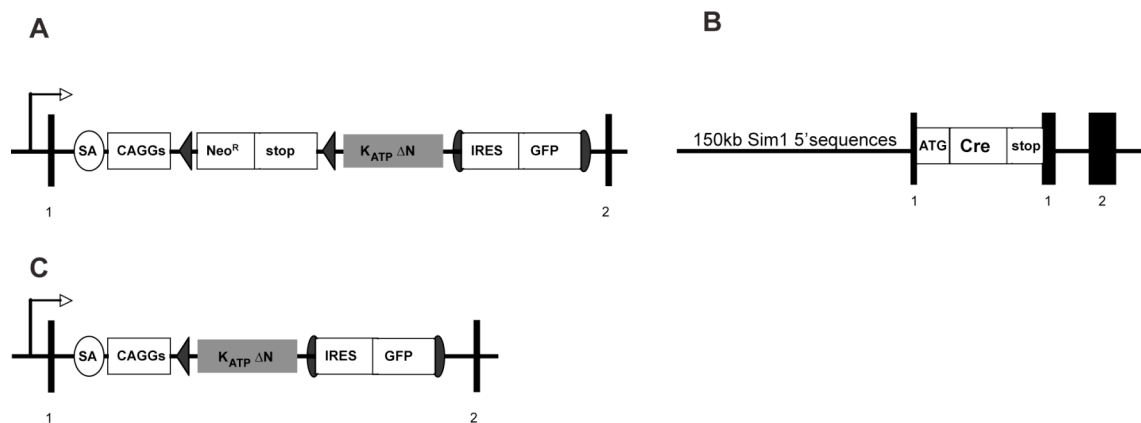


Figure 6: The constitutive active $K_{ATP}\Delta N$ targeted to the Rosa26 locus and Sim1-cre mice

A: A constitutive active $K_{ATP}\Delta N$ construct is homologously recombined into the Rosa26 locus and the transcriptional activation is enhanced by the CAGGs promoter; B: randomly integrated Sim1-cre construct; C: the Rosa26 locus targeted constructs after cre-mediated excision of the neomycin/stop-cassette; exons (vertical bar), splice acceptor (SA), CMV enhancer, chicken beta actin promoter (CAGGs), locus of X-over P1 (loxP/arrow heads), neomycin resistance cassette (Neo^R), Westphal stop sequence (stop), internal ribosomal entry site (IRES), green fluorescent protein (GFP), flip-recombinase targets (FRT/oval)

To generate a mouse line expressing $K_{ATP}\Delta N$ specifically in Sim1 neurons, $K_{ATP}\Delta N$ mice were crossed to Sim1-cre mice (heterozygous: $K_{ATP}\Delta N^{Sim1}$ mice; homozygous: $K_{ATP}\Delta N/\Delta N^{Sim1}$ mice) (fig. 6B). Sim1-cre transgenic mice have been previously generated [82] and were shown to express the cre recombinase in areas as the PVN, the supraoptic nucleus (SON), the nucleus of the lateral olfactory tract (NLOT) of the amygdala and the posterior hypothalamic nucleus (PH). This Sim1 expression pattern was confirmed by immunohistochemical analysis of the brain areas in $K_{ATP}\Delta N/\Delta N^{Sim1}$ mice. As these mice express an mRNA that contains the gene of interest followed by an IRES and the GFP sequence, expression of GFP is a measure for the $K_{ATP}\Delta N$ expression at these sites (fig 7C; strategy). In line with the previously described expression pattern of Sim1 in the hypothalamus, $K_{ATP}\Delta N/\Delta N^{Sim1}$ mice expressed GFP in the classical Sim1 sites in the PVN and SON, whereas no expression was detected in the arcuate nucleus, the brain area where K_{ATP} channels have been described to play a crucial role in insulin signalling in POMC neurons [120, 124]. Taken together, these data indicate that the $K_{ATP}\Delta N$ /IRES-GFP bicistronic cDNA is expressed in Sim1-expressing neurons in $K_{ATP}\Delta N/\Delta N^{Sim1}$ mice.

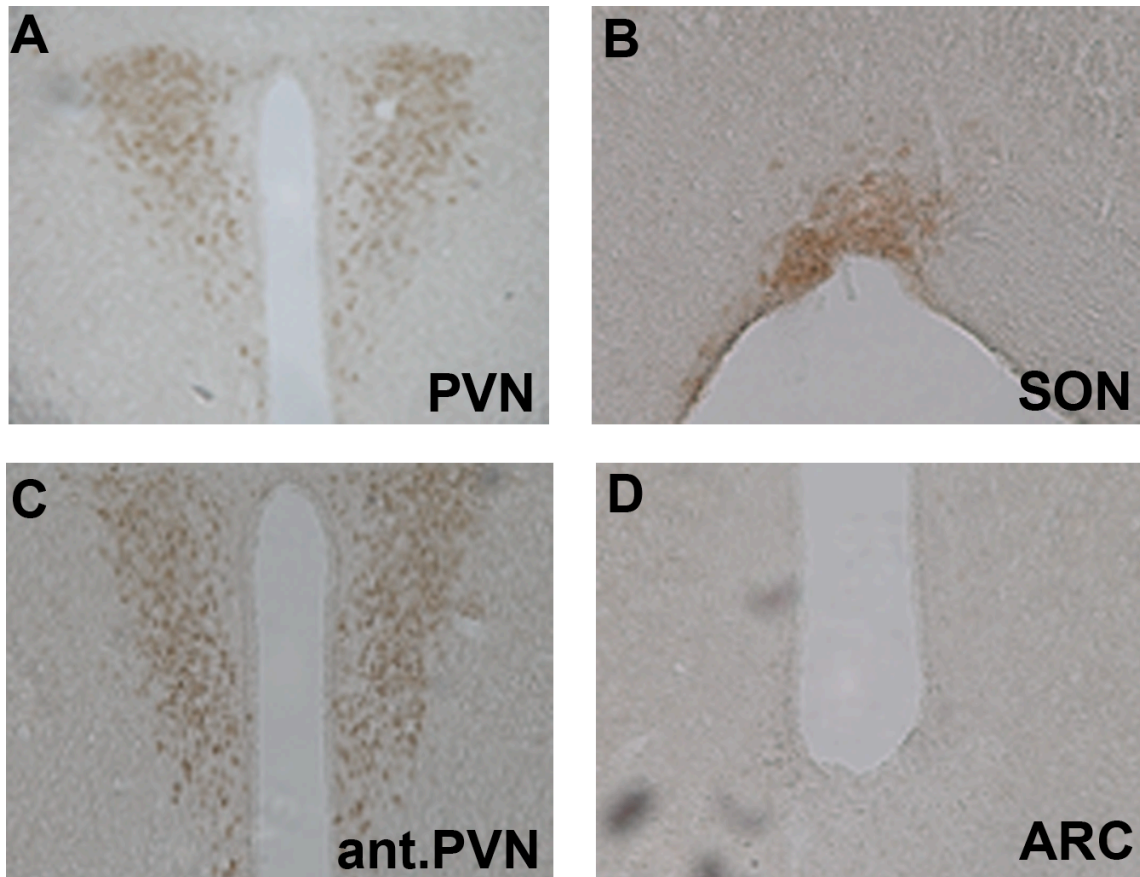


Figure 7: The $K_{ATP}\Delta N/IRES-GFP$ construct expressed in the hypothalamic *Sim1* sites

Homozygous $K_{ATP}\Delta N/\Delta N^{Sim1}$ mice express the $K_{ATP}\Delta N/IRES-GFP$ transgene in *Sim1* areas. GFP staining of brain slides from mice that are heterozygous for *Sim1-cre* and homozygous for $K_{ATP}\Delta N/IRES-GFP$; A: paraventricular nucleus (PVN); B: supraoptic nucleus (SON); C: anterior region of the PVN (ant.PVN); D: arcuate nucleus (ARC)

To analyse whether overexpression of constitutive active K_{ATP} channels affects the electrophysiological properties of *Sim1* neurons, $K_{ATP}\Delta N^{Sim1}$ and *Sim1-cre* control mice were inter-crossed with *Z/EG* mice ($K_{ATP}\Delta N-Z/EG^{Sim1}$, Z/EG^{Sim1} mice, respectively). A comparable amount of *Sim1-cre* neurons reacted to tolbutamide in $K_{ATP}\Delta N-Z/EG^{Sim1}$ mice (59.26 %; n=27) and control Z/EG^{Sim1} (61.9%; n=21). In the subset of tolbutamide responsive neurons, additional electrophysiological properties were determined. Identified *Sim1* neurons of $K_{ATP}\Delta N-Z/EG^{Sim1}$ mice showed increased input resistance, reduced mean membrane potential, whereas the cell capacitance and K_{ATP} conductance appeared to be unaltered in these neurons. Conclusively, the closure of K_{ATP} channels in response to tolbutamide was impaired in GFP and thereby *Sim1* positive neurons of $K_{ATP}\Delta N-Z/EG^{Sim1}$ mice, which designated these mice as functional models to study the role of the K_{ATP} channel dependent alteration of

Results

the membrane potential in Sim1 expressing neurons of the PVN. However, as this effect in heterozygous $K_{ATP}\Delta N^{Sim1}$ mice was not as pronounced as expected, the homozygous $K_{ATP}\Delta N/\Delta N^{Sim1}$ mice with their respective control groups were included in the further analysis.

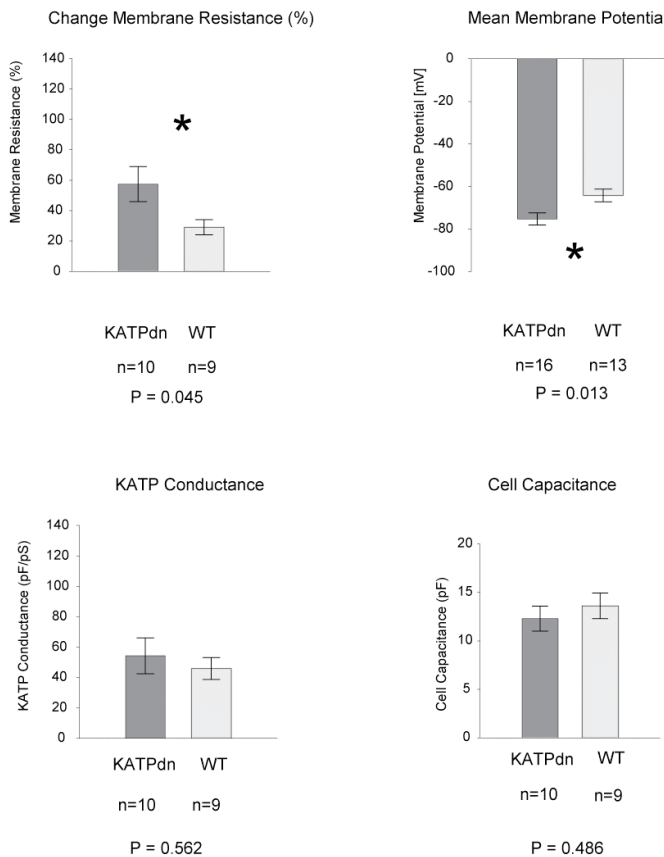


Figure 8: Enhanced change in membrane resistance and reduction of mean membrane potential in the PVN of $K_{ATP}\Delta N^{Sim1}$ mice

From the subset of tolbutamide responsive neurons the change in membrane resistance, the mean membrane potential, the K_{ATP} conductance and the cell capacitance were determined. The number of neurons analysed and the p values are indicated on each diagram. Displayed values are means \pm S.E.M.; *, $p < 0.05$. Kindly provided by Moritz Paehler (AG Kloppenburg, Institute for Zoology, University of Cologne)

3.1.3 Unaltered energy metabolism in $K_{ATP}\Delta N^{Sim1}$ and $K_{ATP}\Delta N/\Delta N^{Sim1}$ mice

As K_{ATP} channels were shown to be involved in the insulin and leptin mediated effect on food intake and energy metabolism in the arcuate nucleus, a similar function in Sim1 neurons was addressed. Therefore, the body parameters of

$K_{ATP}\Delta N^{Sim1}$ and $K_{ATP}\Delta N/\Delta N^{Sim1}$ mice were analysed and compared to control mice ($K_{ATP}\Delta N^{stoplox/+}$ and $K_{ATP}\Delta N^{stoplox/lox}$ mice that do not express Sim1-cre).

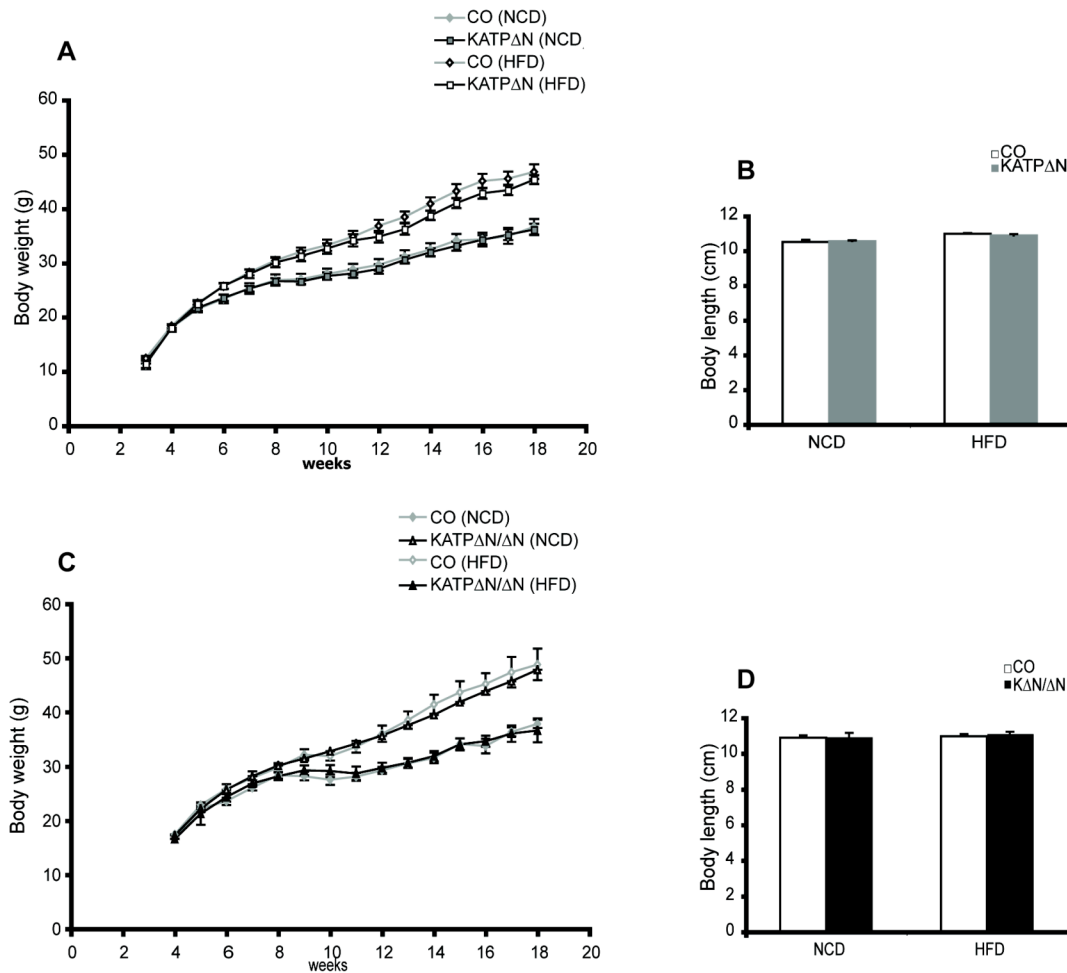


Figure 9: Unaltered body weight and body length of $K_{ATP}\Delta N^{Sim1}$ and $K_{ATP}\Delta N/\Delta N^{Sim1}$ males

$K_{ATP}\Delta N^{Sim1}$ (A) and $K_{ATP}\Delta N/\Delta N^{Sim1}$ (C) males displayed increased body weight during the analysed period of 18 weeks but this was unaltered in comparison to the respective control groups. HFD feeding of the mice resulted in significantly increased body weights from the age of 8 weeks (A) or 12 weeks (C); ttest; $p < 0.001$; The body length of $K_{ATP}\Delta N^{Sim1}$ (B) and $K_{ATP}\Delta N/\Delta N^{Sim1}$ (D) males was similar to control groups. A (NCD): CO, $n=13$; $K_{ATP}\Delta N$, $n=13$; A (HFD): CO, $n=34-35$; $K_{ATP}\Delta N$, $n=17-21$; B (NCD): CO, $n=12$; $K_{ATP}\Delta N$, $n=13$; B (HFD): CO, $n=32$; $K_{ATP}\Delta N$, $n=16$; C (NCD): CO, $n=8-13$; $K_{ATP}\Delta N/\Delta N$, $n=8-13$; C (HFD): CO, $n=15-16$; $K_{ATP}\Delta N/\Delta N$, $n=20-27$; D (NCD): CO, $n=6$; $K_{ATP}\Delta N/\Delta N$, $n=5$; D (HFD): CO, $n=8$; $K_{ATP}\Delta N/\Delta N$, $n=15$

The body weight of both $K_{ATP}\Delta N^{Sim1}$ and $K_{ATP}\Delta N/\Delta N^{Sim1}$ mice increased with the age during the analysed period of 18 weeks and was unaltered compared to sex- and age-matched control animals. To study the Sim1 neuron specific expression of a constitutive open K_{ATP} channel in an insulin resistant state, a subset of the mice were fed a high fat diet (HFD), which results in diet induced

Results

obesity (DIO). The expected enhanced body weight gain by the feeding of HFD in comparison to a normal chow diet (NCD) was significant in relation to NCD groups from week 8 ($K_{ATP\Delta N}^{Sim1}$) or week 12 ($K_{ATP\Delta N/\Delta N}^{Sim1}$). However, $K_{ATP\Delta N}^{Sim1}$ and $K_{ATP\Delta N/\Delta N}^{Sim1}$ mice did not differ from their respective control littermates regarding their body weight gain. Moreover, this age-dependent weight gain was similar in males (fig. 9A&C) and females (fig. 10A&C).

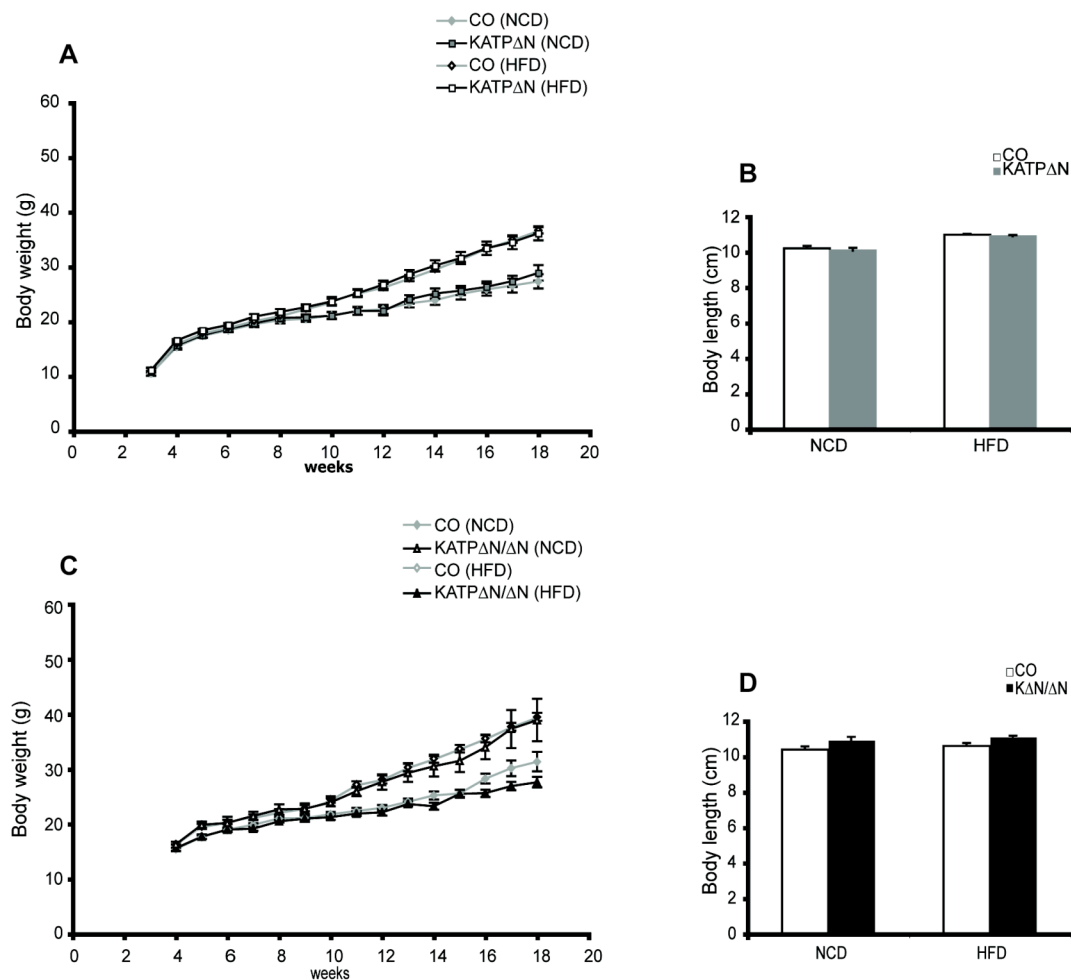


Figure 10: Unaltered body weight and body length of $K_{ATP\Delta N}^{Sim1}$ and $K_{ATP\Delta N/\Delta N}^{Sim1}$ females

$K_{ATP\Delta N}^{Sim1}$ (A) and $K_{ATP\Delta N/\Delta N}^{Sim1}$ (C) females displayed increased body weight during the analysed period of 18 weeks but this was unaltered in comparison to respective control groups. HFD feeding of the mice resulted in significantly increased body weights from the age of 8 weeks (A) or 12 weeks (C); ttest; $p < 0.001$; The body length of $K_{ATP\Delta N}^{Sim1}$ (B) and $K_{ATP\Delta N/\Delta N}^{Sim1}$ (D) females was similar to control groups. A (NCD): CO, $n=15$; $K_{ATP\Delta N}$, $n=8-10$; A (HFD): CO, $n=20-21$; $K_{ATP\Delta N}$, $n=23$; B (NCD): CO, $n=12$; $K_{ATP\Delta N}$, $n=8$; B (HFD): CO, $n=19$; $K_{ATP\Delta N}$, $n=20$; C (NCD): CO, $n=8-17$; $K_{ATP\Delta N/\Delta N}$, $n=9-26$; C (HFD): CO, $n=10$; $K_{ATP\Delta N/\Delta N}$, $n=11$; D (NCD): CO, $n=5$; $K_{ATP\Delta N/\Delta N}$, $n=5$; D (HFD): CO, $n=7$; $K_{ATP\Delta N/\Delta N}$, $n=6$

As the PVN has been associated with an alteration of the body length, somatic growth of $K_{ATP}\Delta N^{Sim1}$, $K_{ATP}\Delta N/\Delta N^{Sim1}$ and control mice was determined [82, 148]. Going along with the unaltered body weight, the body length of both $K_{ATP}\Delta N^{Sim1}$ and $K_{ATP}\Delta N/\Delta N^{Sim1}$ mice was unaltered in relation to respective control littermates. As female and male mice showed similar results regarding body parameters, further analysis will only address the role of the K_{ATP} channel in *Sim1* neurons in male mice.

The unaltered body weight gain in $K_{ATP}\Delta N^{Sim1}$ and $K_{ATP}\Delta N/\Delta N^{Sim1}$ compared to control mice was further confirmed by measuring the epigonadal fat pad weight or the whole body fat percentage via nuclear magnetic resonance spectroscopy (NMR) (fig. 11). In line with the aforementioned results, $K_{ATP}\Delta N^{Sim1}$ and $K_{ATP}\Delta N/\Delta N^{Sim1}$ mice and their respective control groups had similar fat percentages and epigonadal fat pad weights (fig x).

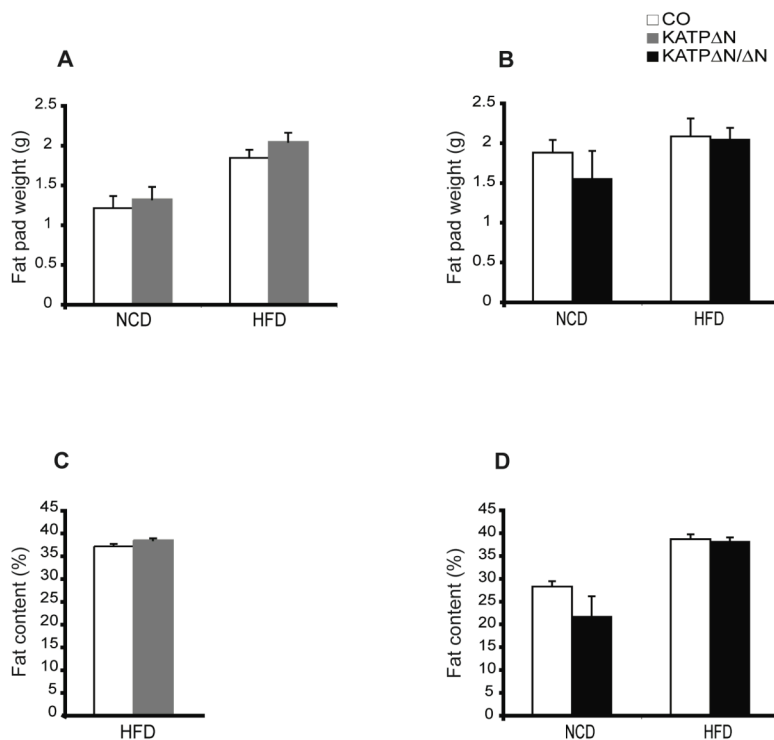


Figure 11: Unaltered body composition of $K_{ATP}\Delta N^{Sim1}$ and $K_{ATP}\Delta N/\Delta N^{Sim1}$ males

The fat deposition of $K_{ATP}\Delta N^{Sim1}$ and $K_{ATP}\Delta N/\Delta N^{Sim1}$ males was unaltered. A: epigonadal fat pad weight of $K_{ATP}\Delta N^{Sim1}$ males and controls; B: epigonadal fat pad weight of $K_{ATP}\Delta N/\Delta N^{Sim1}$ males and controls; C: NMR determined fat content (%) of $K_{ATP}\Delta N^{Sim1}$ males and controls; D: NMR determined fat content (%) of $K_{ATP}\Delta N/\Delta N^{Sim1}$ males and controls; A/C (NCD): CO, n=12; $K_{ATP}\Delta N$, n=8; A/C (HFD): CO, n=19; $K_{ATP}\Delta N$, n=20; B/D (NCD): CO, n=5; $K_{ATP}\Delta N/\Delta N$, n=5; B/D (HFD): CO, n=7; $K_{ATP}\Delta N/\Delta N$, n=6

Results

As mentioned before, genetic modifications of key PVN molecules as melanocortin receptor 4 (MC4R) and Sim1 leads to hyperphagia, indicating the association of this specific neuronal population with the control of food intake. However, a possible contribution of K_{ATP} channel mediated changes to membrane excitability of Sim1 neurons in the control of food intake has not been analysed yet. The absolute random food intake of all mice was measured under conditions of ad libitum food accessibility. Absolute food intake levels of $K_{ATP}\Delta N^{Sim1}$ and $K_{ATP}\Delta N/\Delta N^{Sim1}$ mice were unaltered in comparison to control groups, independent of the consumed diet (fig. 12). Together these results indicate that overexpression of a constitutive active K_{ATP} channel on Sim1 neurons does not affect the basic energy metabolism of these mice, as is reflected on their normal body weight gain and food intake.

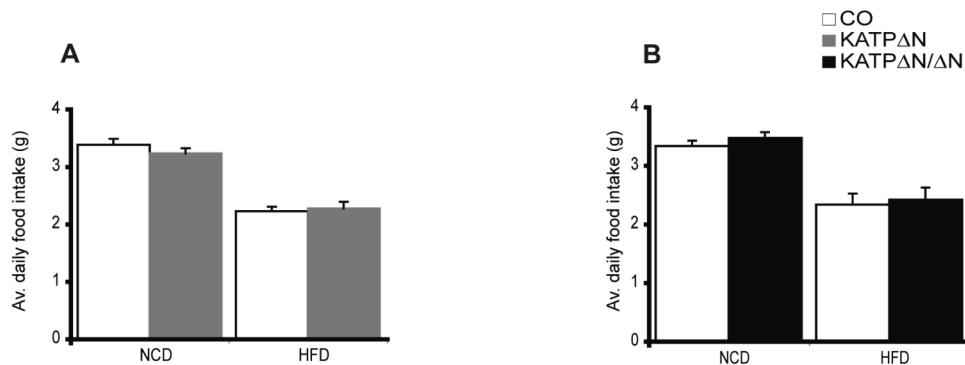


Figure 12: No difference in food intake of $K_{ATP}\Delta N^{Sim1}$ and $K_{ATP}\Delta N/\Delta N^{Sim1}$ males

A: The average daily food intake of homozygous $K_{ATP}\Delta N/\Delta N^{Sim1}$ males at the age of 9-10 weeks; B: The average daily food intake of homozygous $K_{ATP}\Delta N/\Delta N^{Sim1}$ males at the age of 9-10 weeks; A (NCD): CO, n=12; $K_{ATP}\Delta N$, n=17; A (HFD): CO, n=10; $K_{ATP}\Delta N$, n=11; B (N CD) $K_{ATP}\Delta N/\Delta N$, n=17

One processing product of POMC, alpha melanocyte stimulating hormone (α -MSH), binds to the MC4R on PVN neurons to inhibit food intake. Melanotan II (MTII), a MC4R agonist, mimics α -MSH induction and reduces food intake temporarily [73, 80, 82, 149]. However, the exact signalling mechanism of the MC4R has not been unravelled yet. To evaluate if a K_{ATP} channel dependent change in membrane potential is crucial for MC4R signalling, the response to MTII was analysed for $K_{ATP}\Delta N^{Sim1}$ and $K_{ATP}\Delta N/\Delta N^{Sim1}$ mice. This can only be detected, if the mice receive a strong stimulus for the initiation of food intake.

Therefore, the food was removed 4 hours before the onset of the dark phase. In this context, the short period of absence of the food and the onset of the dark phase induced the food intake, which is normally highest in the first hours of night. Subsequently, mice were injected with 5 mg/kg MTII just before the onset of the dark phase. As seen in figure 13, MTII significantly reduced the food intake in control animals two to four hours after injection, whereas food intake returned to normal levels after 14 hours, supporting the temporal effect of MTII. However, this MTII mediated response was comparable in $K_{ATP}\Delta N/\Delta N^{Sim1}$ mice and control mice, indicating that the MTII response was not affected by a constitutive opening of the K_{ATP} channel (fig. 13&14).

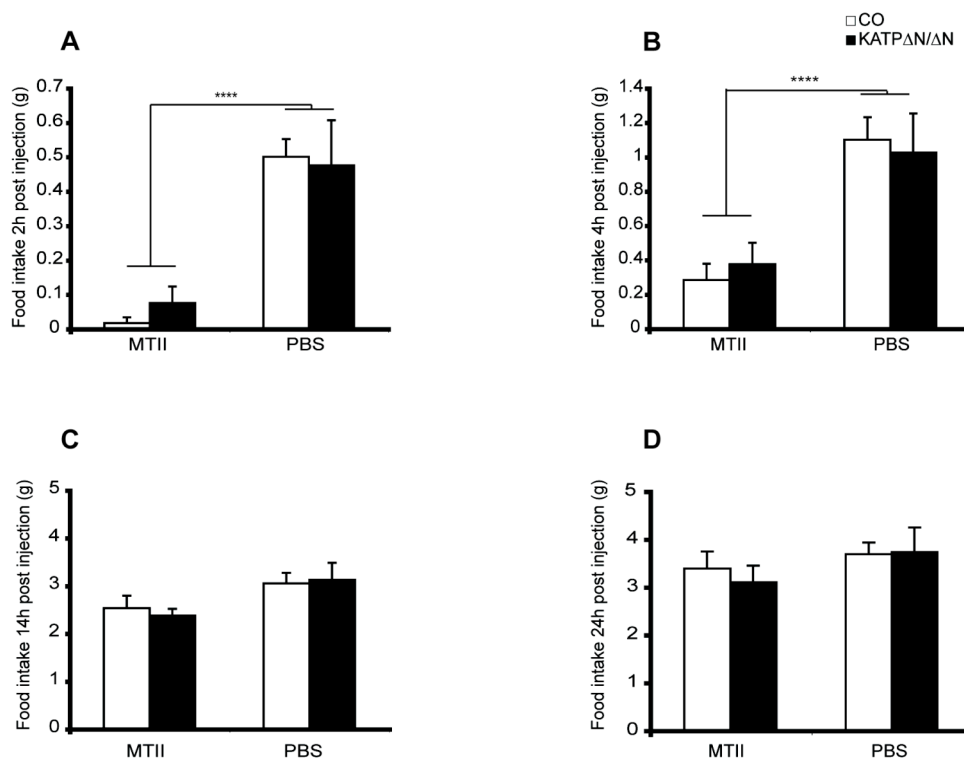


Figure 13: Melanotan II (MTII) sensitivity of $K_{ATP}\Delta N/\Delta N^{Sim1}$ mice (NCD)

After a 4 hours fasting period, NCD males (11 weeks of age) were injected 5 mg/kg melanotan II (MTII) or PBS at the onset of the dark phase. A: Food intake 2 hours post MTII/PBS injection; B: food intake 4 hours post MTII/PBS injection; C: food intake 14 hours post MTII/PBS injection; D: food intake 24 hours post MTII/PBS injection; CO, n=7; $K_{ATP}\Delta N/\Delta N$, n=7

Similarly, the reduction of food intake by MTII injection was also observed in mice fed a HFD. Interestingly, the reduced food intake of HFD fed animals by MTII administration seemed to be more prolonged than in NCD males, as the reduction was still significant after the whole night phase (fig. 14C).

Results

Nevertheless, HFD-fed $K_{ATP}\Delta N^{Sim1}$ and $K_{ATP}\Delta N/\Delta N^{Sim1}$ mice were as sensitive to MTII as their respective control groups.

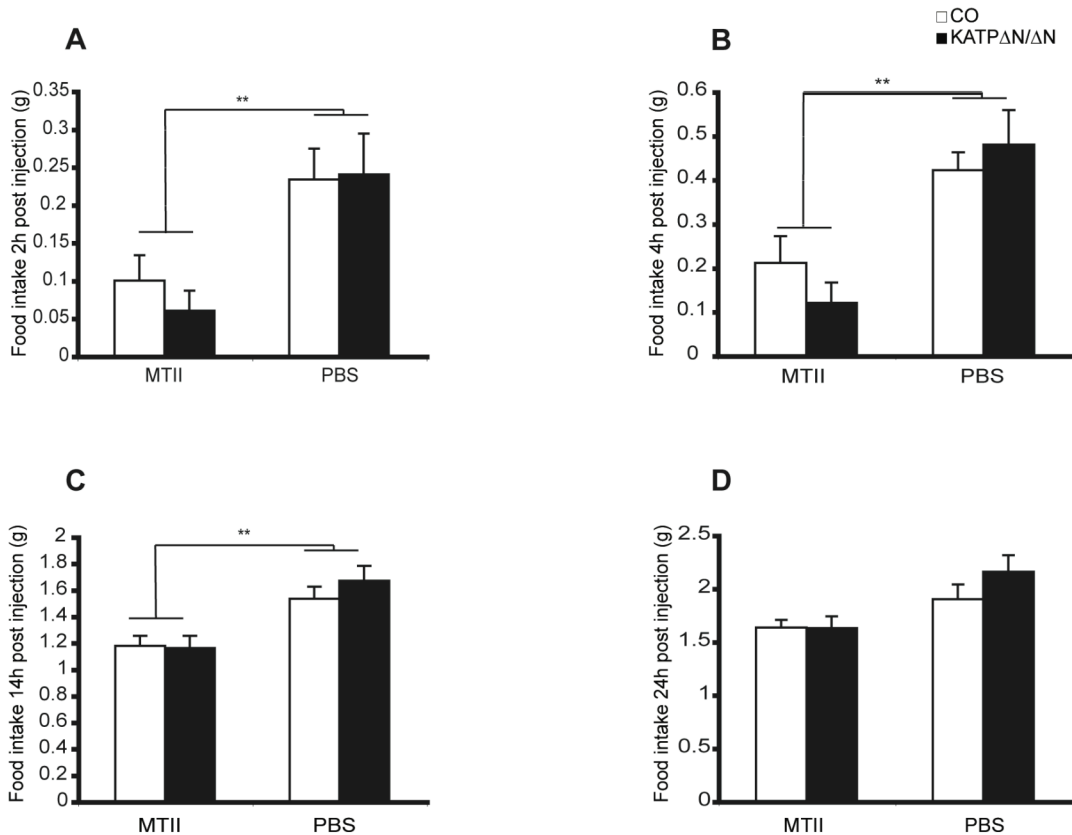


Figure 14: Melanotan II (MTII) sensitivity of $K_{ATP}\Delta N/\Delta N^{Sim1}$ mice (HFD)

After a 4 hours fasting period, HFD males (11 weeks of age) were injected 5 mg/kg melanotan II (MTII) or PBS at the onset of the dark phase. A: Food intake 2 hours post MTII/PBS injection; B: food intake 4 hours post MTII/PBS injection; C: food intake 14 hours post MTII/PBS injection; D: food intake 24 hours post MTII/PBS injection; CO, n=9; $K_{ATP}\Delta N/\Delta N$, n=10

In summary, $K_{ATP}\Delta N^{Sim1}$ and $K_{ATP}\Delta N/\Delta N^{Sim1}$ males fed a NCD or a HFD consumed a similar amount of calories as their respective control littermates, which was also reflected by their sensitivity to MTII. In addition, $K_{ATP}\Delta N^{Sim1}$ and $K_{ATP}\Delta N/\Delta N^{Sim1}$ mice on both diets gained weight as expected over the 18 weeks of experimental period. Moreover, body parameters, as body fat levels and body length, of the analysed groups of mice were unaltered in comparison to their respective control littermates. To conclude, $K_{ATP}\Delta N^{Sim1}$ and $K_{ATP}\Delta N/\Delta N^{Sim1}$ animals fed a NCD or a HFD exhibited an unaltered energy metabolism. Hence, the K_{ATP} channel dependent regulation of the membrane potential in Sim1

expressing neurons is not essential for the regulation of the energy homeostasis.

3.1.4 Glucose tolerance and insulin sensitivity of $K_{ATP}\Delta N^{Sim1}$ and $K_{ATP}\Delta N/\Delta N^{Sim1}$ mice

Hypothalamic insulin signalling has been shown to be involved in peripheral glucose metabolism, as neuronal insulin receptor deficient mice are insulin resistant and AgRP-neuron specific insulin receptor deficient mice display a reduced hepatic glucose production despite of an unaltered body weight [13, 140]. Interestingly, Insulin stimulates the K_{ATP} channel opening in POMC neurons by increasing PIP3 levels, which bind and activate the K_{ATP} channel opening [103] and several hypothalamic neuron populations have been implicated to react directly on rising glucose levels in the brain by glucose sensing via K_{ATP} channels [150, 151]. However, the effect on insulin signalling and glucose-sensing on Sim1 neurons has not been studied with respect to the K_{ATP} channel. Thus, the glucose responsiveness and the insulin tolerance of $K_{ATP}\Delta N^{Sim1}$ and $K_{ATP}\Delta N/\Delta N^{Sim1}$ mice were analysed.

The blood glucose levels of ad libitum fed $K_{ATP}\Delta N^{Sim1}$ and $K_{ATP}\Delta N/\Delta N^{Sim1}$ mice as well as of control littermates were between 130 and 150 mg/dl (fig. 15A&C) whereas the levels of fasted mice varied between 70 and 90 mg/dl (fig. 15B&D). The exposure to HFD resulted in increased blood glucose levels in both the fasted and fed state. Nevertheless, blood glucose levels of $K_{ATP}\Delta N^{Sim1}$ and $K_{ATP}\Delta N/\Delta N^{Sim1}$ were similar to the respective control mice, independent of the diet or the nutritional status of the animal.

Results

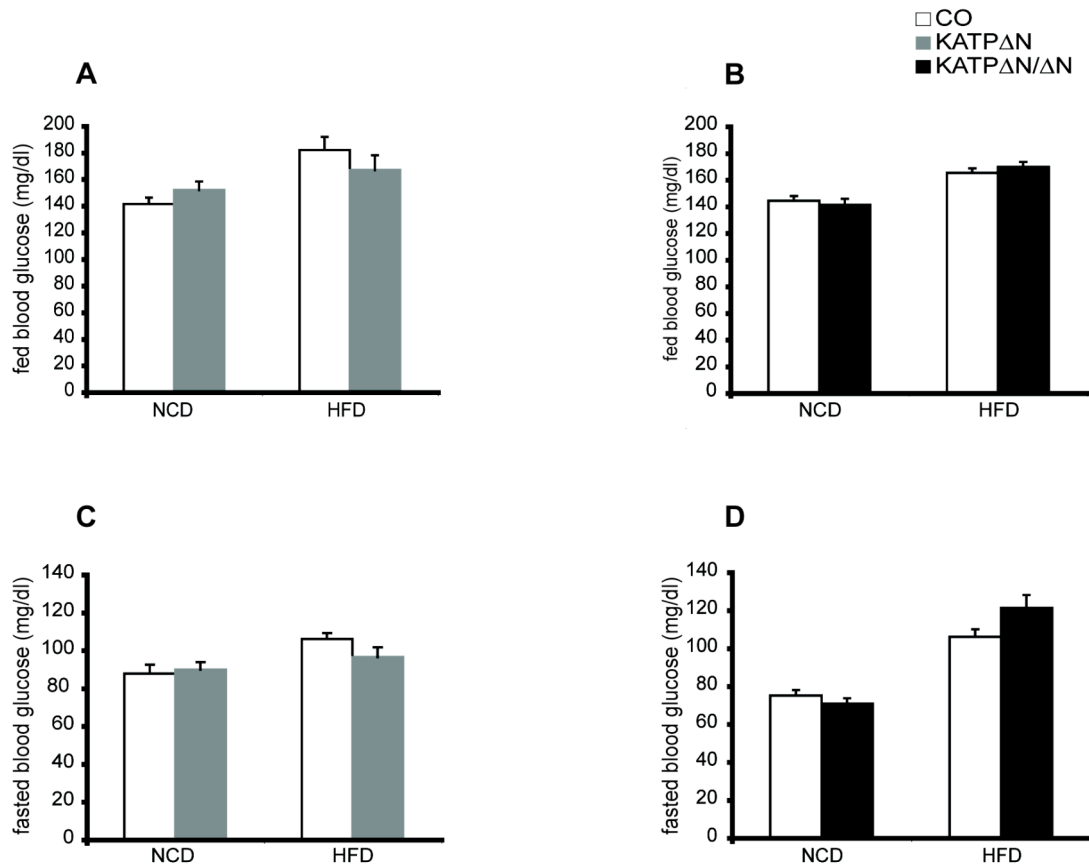


Figure 15: Unaltered blood glucose levels of K_{ATP}ΔN^{Sim1} and K_{ATP}ΔN/ΔN^{Sim1} mice

Blood glucose levels of K_{ATP}ΔN^{Sim1} and K_{ATP}ΔN/ΔN^{Sim1} mice and controls (12-13 weeks) were determined 2 to 3 hours after the onset of the light phase, in the random fed state and after 16 hours of fasting. A: random fed blood glucose levels of K_{ATP}ΔN^{Sim1} males and controls; B: random fed blood glucose levels of K_{ATP}ΔN/ΔN^{Sim1} males and controls; C: 16 hours fasted blood glucose levels of K_{ATP}ΔN^{Sim1} males and controls; D: 16 hours fasted blood glucose levels of K_{ATP}ΔN/ΔN^{Sim1} males and controls; NCD: CO, n=13/ K_{ATP}ΔN, n=13; CO, n=10/ K_{ATP}ΔN/ΔN, n=10; HFD: CO, n=46/ K_{ATP}ΔN, n=27; CO, n=15/ K_{ATP}ΔN/ΔN, n=20

To further investigate whether Sim1-specific K_{ATP}ΔN overexpressing mice have an altered glucose metabolism, glucose tolerance tests (GTT) were performed. Fasting induced a state of low blood glucose resulting in decreased blood insulin levels. After overnight fasting, mice were injected with 20% glucose (10 ml/kg body weight) and subsequently blood glucose levels were determined 15, 30, 60 and 120 minutes after the injection. This experiment mimics the organism's response to a meal, as blood glucose levels rise shortly after a meal. The glucose injection is sensed by pancreatic β-cells, which release insulin in proportion to rising blood glucose levels. Insulin subsequently stimulates different tissues, as muscles, to take up glucose from the blood stream. As seen in figure 16 A&B, blood glucose levels rose shortly after the

injection followed by a stage, in which the blood glucose levels started to fall again until they returned to resting values over the 120 minutes experimental period. The GTT response of $K_{ATP}\Delta N^{Sim1}$ and $K_{ATP}\Delta N/\Delta N^{Sim1}$ mice was unaltered to control animals. In accordance to the expected glucose intolerance of HFD fed animals, blood glucose levels of mice fed a HFD were elevated during the course of the experiment compared to the NCD fed mice, but no difference could be observed among the different genotypes.

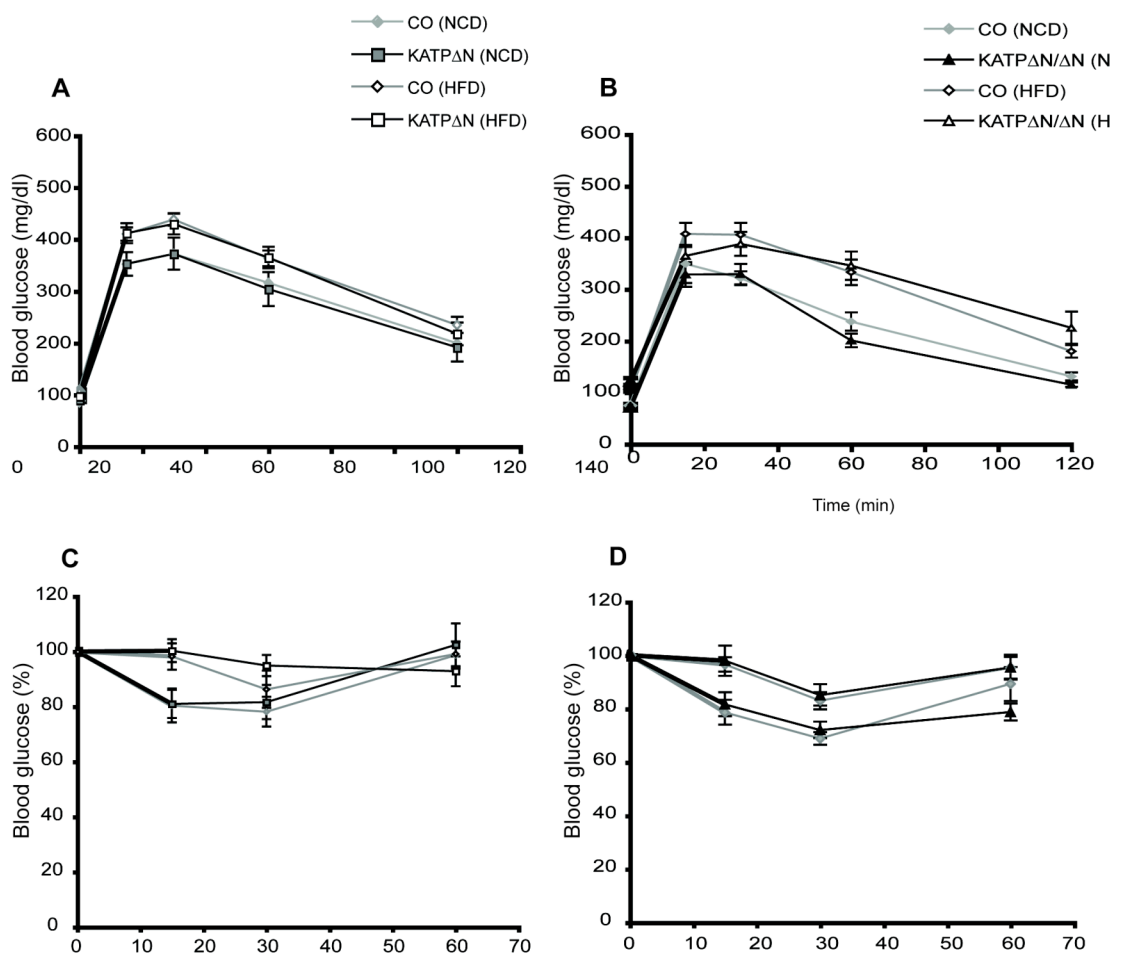


Figure 16: Glucose tolerance and insulin sensitivity of $K_{ATP}\Delta N^{Sim1}$ and $K_{ATP}\Delta N/\Delta N^{Sim1}$ mice

Mice were submitted to glucose tolerance tests (GTT) at an age of 12 weeks after 16 hours of fasting and to insulin tolerance tests (ITT) at an age of 13 weeks. A: GTT of $K_{ATP}\Delta N^{Sim1}$ males and controls; B: GTT of $K_{ATP}\Delta N/\Delta N^{Sim1}$ males and controls; C: ITT of $K_{ATP}\Delta N^{Sim1}$ males and controls; D: ITT of $K_{ATP}\Delta N/\Delta N^{Sim1}$ males and controls; NCD: CO, n=13/ $K_{ATP}\Delta N$, n=13; CO, n=10/ $K_{ATP}\Delta N/\Delta N$, n=10; HFD: CO, n=46/ $K_{ATP}\Delta N$, n=27; CO, n=15/ $K_{ATP}\Delta N/\Delta N$, n=20

To directly address the insulin sensitivity, insulin tolerance tests were performed. To this extent, mice were injected 0.75 units insulin per kilogram

body weight and the blood glucose levels were measured 15, 30 and 60 minutes after the injection. As mentioned before, rising insulin levels stimulate different tissues to take up glucose leading to decreased blood glucose levels. The observation of blood glucose levels after injection of insulin relative to random fed levels before injection, give an idea of the sensitivity of the peripheral organs to insulin. As seen in figure 16, $K_{ATP}\Delta N^{Sim1}$ and $K_{ATP}\Delta N/\Delta N^{Sim1}$ mice fed a NCD were as responsive to insulin as control groups. Mice fed a HFD were insulin resistant, which was reflected by a delayed response to insulin in comparison to NCD (fig. 16C&D). However, no difference could be observed among the different genotypes analysed.

Taken together, the energy and glucose homeostasis of $K_{ATP}\Delta N^{Sim1}$ and $K_{ATP}\Delta N/\Delta N^{Sim1}$ mice were analysed both under normal conditions as well as under the insulin resistant state of diet-induced obesity. These mice displayed an unaltered energy metabolism and were sensitive to stimuli as the α -MSH agonist MTII, glucose and insulin. This leads to the conclusion that a K_{ATP} channel dependent hyperpolarization or depolarization of Sim1 neurons is not essential for the control of energy and glucose homeostasis.

3.2 FOXO1 in the Sim1 neuron dependent regulation of energy homeostasis

The PI3K-Akt-FOXO1 pathway contributes to the actions of insulin and leptin in several cell types, including neurons in the central nervous system [103, 124, 129]. More precise, hypothalamic expression of a constitutive active FOXO1 variant has been shown to affect body weight, food intake and energy expenditure of mice [120]. Although two neuronal cell types of the arcuate nucleus of the hypothalamus, the AgRP and POMC neurons, have been shown to contribute to these FOXO1 mediated effects, it remains to be investigated whether other neuronal populations of the hypothalamus are dependent on FOXO1 signalling in the control of energy homeostasis, as well. Given the fact that the PVN has been shown to be involved in the regulation of energy homeostasis and that insulin receptors as well as downstream insulin receptor signalling molecules such as FOXO1 are expressed in this brain area, an

possible contribution of Sim1 neuron specific FOXO1 signalling in energy metabolism was addressed.

3.2.1 Generation of the FOXO1DN overexpression in Sim1 neurons

Under basal conditions, the transcription factor FOXO1 resides in the nucleus and is bound to specific elements in the promoter of its target genes. Upon phosphorylation, for example by the insulin activated kinase AKT, FOXO1 is exported from the nucleus and degraded. It has been shown that a dominant negative variant of FOXO1 can be attained by a C-terminal deletion of the transactivation domain [122]. This leads to a truncated variant of FOXO1 (FOXO1DN) that can no longer be exported from the nucleus as this C-terminal deletion abrogates the phosphorylation sites that are necessary for the protein's inactivation. Consequently, the FOXO1DN variant still contains the DNA binding forkhead domain, constitutively binds the DNA and blocks the endogenous FOXO1 [152].

To analyse the dominant negative effect FOXO1DN on metabolic signalling in Sim1 neurons, the previously generated FOXO1DN overexpressing mice were used [129]. Briefly, these mice were generated by targeting the FOXO1DN sequence into the ubiquitously expressed Rosa26 locus. Expression of this transgene is dependent on cre-mediated excision of the loxP flanked neomycin and Westphal stop cassette located upstream of the start codon. The transgene sequence is followed by an IRES and GFP sequence. As such, a bicistronic mRNA is transcribed upon cre-mediated recombination, leading to the consequent expression of both FOXO1DN as well as GFP.

As a role of FOXO1DN overexpression in the PVN, and more precisely in Sim1 expressing neurons, was addressed, FOXO1DN overexpressing mice were crossed with mice that express the cre-recombinase in a Sim1 promoter dependent way (homozygous FOXO1DN/DN^{Sim1}). To analyse whether these mice expressed the transgene specifically in previously described Sim1 expressing neurons, GFP expression was analysed by immunohistochemistry. In line with what has previously been described [82], FOXO1DN/DN^{Sim1} mice expressed GFP in the PVN, SON and amygdala NLOT region, whereas no expression was detected in the arcuate nucleus lateral hypothalamic areas

(LHA) or cortex (fig. 17). Importantly, as an expression in the arcuate nucleus could be excluded, the phenotype of FOXO1DN/DN^{Sim1} mice was not influenced by FOXO1's well-characterized functions in neurons of the arcuate nucleus. In summary, a correct expression of the FOXO1DN gene in Sim1 neurons could be confirmed for FOXO1DN/DN^{Sim1} mice, which allows the further characterization of FOXO1 signalling in distinct hypothalamic areas as mainly the PVN and SON.

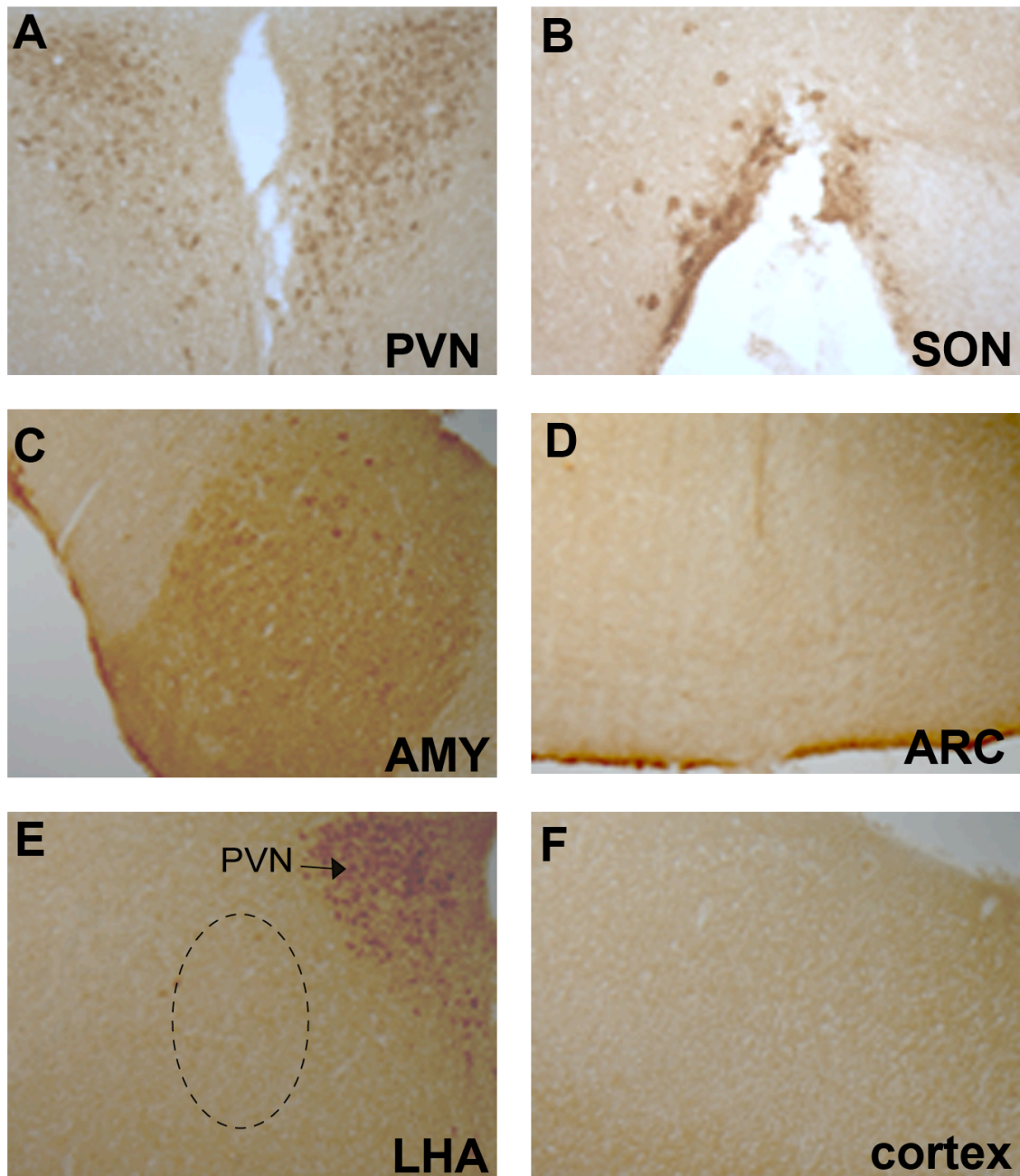


Figure 17: Expression of the FOXO1DN/IRES-GFP construct in the hypothalamic Sim1 sites

Homozygous FOXO1DN/DN^{Sim1} mice express the FOXO1DN/IRES-GFP transgene in Sim1 areas. GFP staining of brain slides from mice that are heterozygous for Sim1-cre and homozygous for FOXO1DN/IRES-GFP; A: paraventricular nucleus (PVN); B: supraoptic nucleus (SON); C: amygdala (AMY); D: arcuate nucleus (ARC); E: lateral hypothalamic areas (LHA); F: cortex

3.2.2 Unaltered energy metabolism in FOXO1DN/DN^{Sim1} mice

To address an involvement of FOXO1 signalling in Sim1 neurons in energy metabolism, the body weight of homozygous FOXO1DN/DN^{Sim1} and control

Results

mice (FOXO1DN^{stoplox/lox} mice that do not express the Sim1-cre) was measured weekly. Both female and male mice increased their body weight steadily during the study period of 18 weeks starting from week 4, whereby male mice reached a maximum weight of about 40 and female mice of about 35 grams. However, the expression of the dominant negative FOXO1 in Sim1 cells did not result in an alteration of body weight in relation to control animals (fig 18).

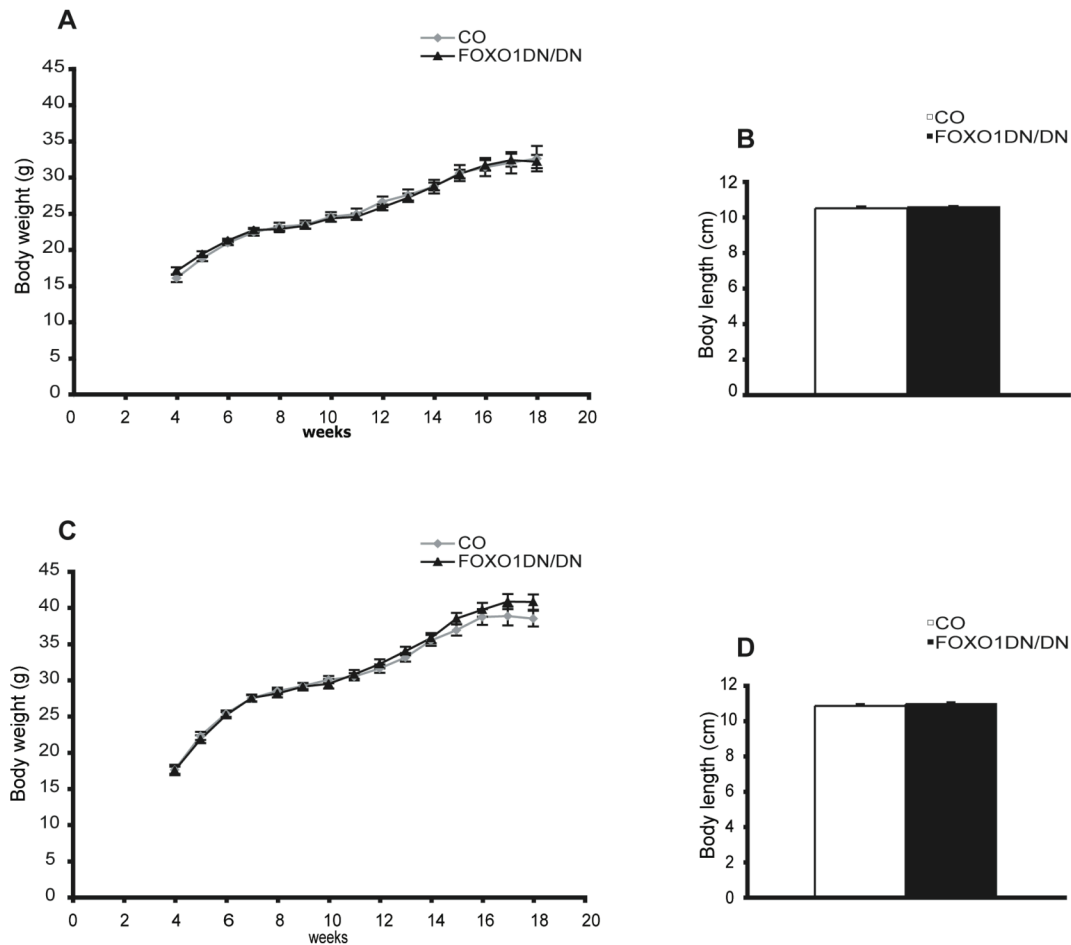


Figure 18: Unaltered body weight and body length of FOXO1DN/DN^{Sim1} mice

FOXO1DN/DN^{Sim1} females (A) and males (C) increased the body weight during the analysed period of 18 weeks but this was unaltered in comparison to control groups. The body length of female (B) and male (D) mice was similar to control groups. A: CO, n=18-38, FOXO1DN/DN, n=22-32; B: CO, n=21; FOXO1DN/DN, n=32; C: CO, n=17-26, FOXO1DN/DN, n=28-36; D: CO, n=16; FOXO1DN/DN, n=28

As MC4R and Sim1 knockout studies [73, 82] demonstrated that the PVN plays a role in the determination of the somatic growth, the total body length of FOXO1DN/DN^{Sim1} mice was compared to control animals. Nevertheless, the

unaltered body weight of FOXO1DN/DN^{Sim1} mice went along with a normal body length (fig 18) of the animals.

A relatively high proportion of the body composition is fat. The amount can either be determined measuring the weight of the epigonadal fat pad or by nuclear magnetic resonance spectroscopy (NMR). In line with the unaltered total body weight, the relative body fat content as well as the absolute fat pad weight of FOXO1DN/DN^{Sim1} mice did not differ from levels seen in control mice (fig 19).

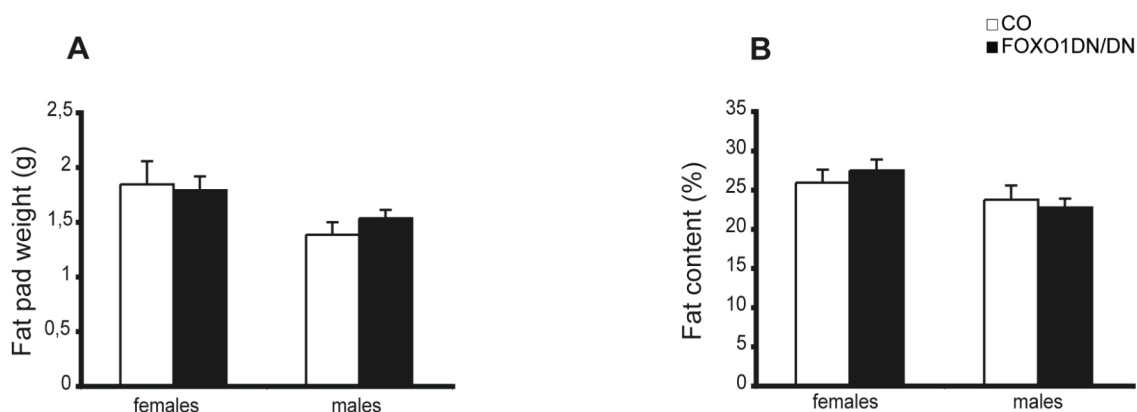


Figure 19: Unaltered body composition of FOXO1DN^{Sim1} mice

The body composition was determined at 18 weeks of age for FOXO1DN/DN^{Sim1} mice and controls. A: epigonadal fat pad; B: nuclear magnetic resonance spectroscopy (NMR); FOXO1DN^{stoplox/lox} mice A: CO, n=21; FOXO1DN/DN, n=32; B: CO, n=16; FOXO1DN/DN, n=28

Taken together, over the analysed period of study FOXO1DN/DN^{Sim1} mice increased body weight and fat mass normally. Conclusively, signalling via FOXO1 in Sim1 neurons is not essential for keeping the body weight in balance.

3.2.3 Unaltered food intake and MTII sensitivity of FOXO1DN/DN^{Sim1} mice

Aforementioned, genetic modifications of key PVN molecules as MC4R and Sim1 lead to a condition of hyperphagia, indicating an important role of this specific neuronal population in the control of food intake [73, 82]. However, a Sim1 neuron-specific role of FOXO1 in the control of food intake has not been

Results

analysed, thus far. Insulin induces α -MSH release from neurons of the arcuate nucleus to stimulate the MC4R on PVN neurons. In a state of fasting, insulin levels in the body are low, resulting in low levels of α -MSH release and MC4R signalling [51]. To compare the conditions of low with regular levels of α -MSH, the food intake of FOXO1DN/DN^{Sim1} mice was measured under random fed and fasting conditions.

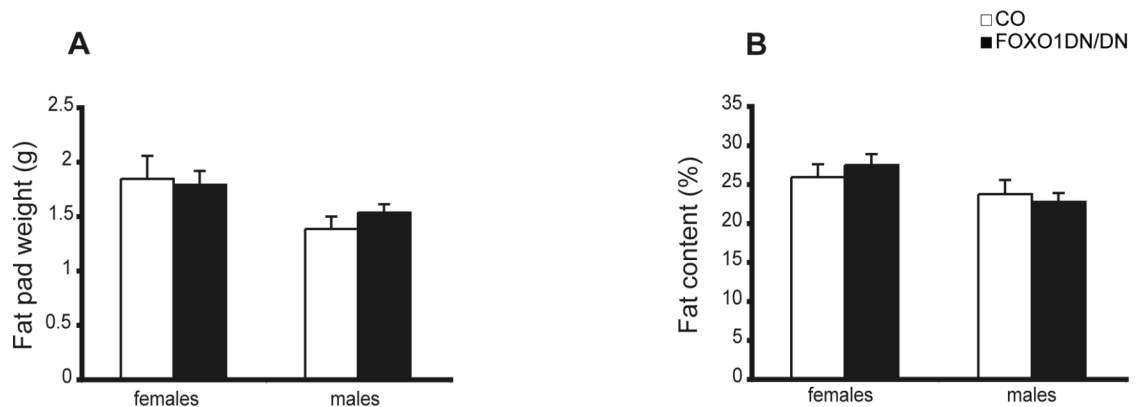


Figure 20: Unaltered random fed and fasted induced food intake of FOXO1DN/DN^{Sim1} females

A: The average daily food intake of homozygous FOXO1DN/DN^{Sim1} females at the age of 9-10 weeks; B: The food intake of 24 hours fasted FOXO1DN/DN^{Sim1} females (11 weeks old) was determined after 4 hours and 24 hours of feeding following the fasting; FOXO1DN^{stoplox/lox} mice; CO, n=10; FOXO1DN/DN, n=19

For the measurement of daily random food intake, mice were provided ad libitum with food. This was compared to the food intake of mice that were fasted for 24 hours, before the addition of standard diet. The food intake of fasted mice was determined 4 and 24 hours after the onset of feeding. Mice exhibited increased food intake following a fasting period, as the 24 hours food intake after a fasting period reached 5 grams in comparison to 3 grams under regular conditions (fig 20). As seen in figure 21, the food intakes of fasted or randomly fed FOXO1DN/DN^{Sim1} mice were unaltered in comparison to the respective littermate control groups, which was independent of gender.

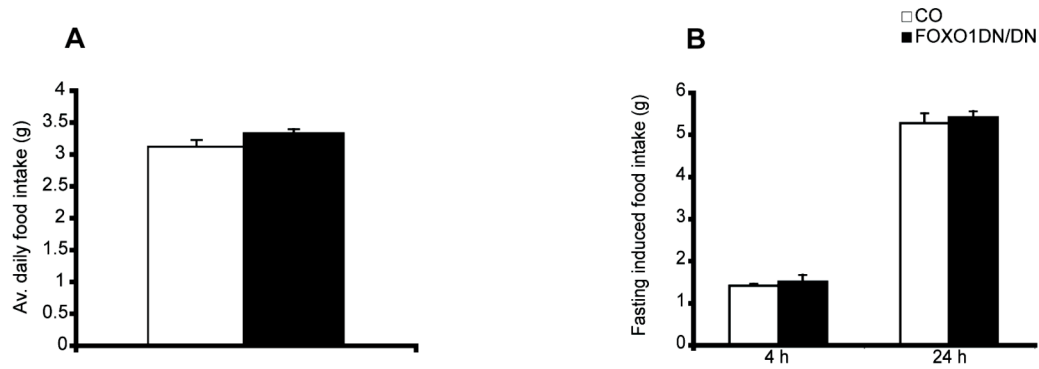


Figure 21: Unaltered random fed and fasted induced food intake of FOXO1DN/DN^{Sim1} males

A: The average daily food intake of homozygous FOXO1DN/DN^{Sim1} males at the age of 9-10 weeks; B: The food intake of 24 hours fasted FOXO1DN/DN^{Sim1} males (11 weeks old) was determined after 4 hours and 24 hours of feeding following the fasting FOXO1DN^{stoplox/lox} mice CO, n=14; FOXO1DN/DN, n=17

To further evaluate the full functionality of the MC4R signalling in FOXO1DN/DN^{Sim1} mice, the opposite condition of the fasted state was analysed by mimicking high levels of α -MSH release. Melanotan II (MTII) has been shown to act as MC4R agonist, which has the ability to activate MC4R signalling thereby mimicking the α -MSH-dependent reduction of food intake *in vivo* [153]. Notably, the MTII induced food intake reduction has been described as being a temporary effect that can only be monitored in the first hours of the dark phase, when the induction of food intake is highest [82].

For this reason, the food was first removed 4 hours before the onset of the dark phase. Then, just before the onset of the dark phase the mice were injected with MTII (5 mg/kg body weight) or PBS and presented to fresh standard diet. Therefore, the mice were eventually induced to begin feeding. Finally, the food intake was measured after 2, 4, 14 and 24 hours after the injection.

Results

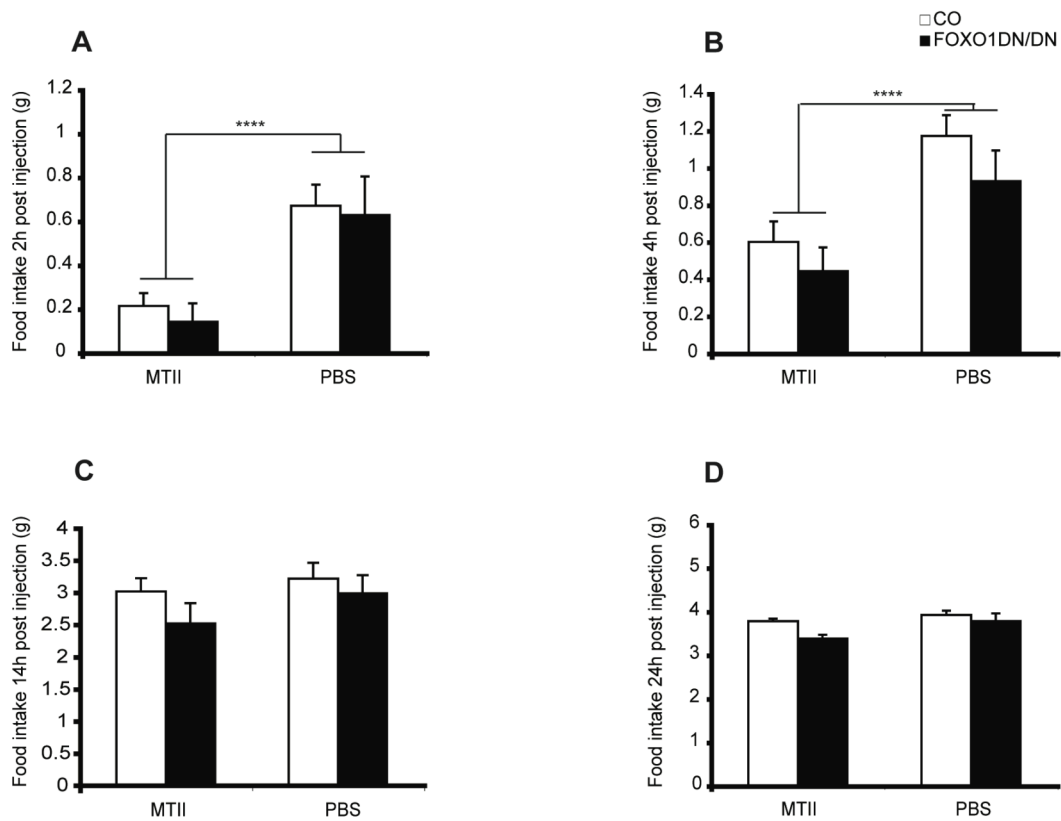


Figure 22: Melanotan II (MTII) sensitivity of FOXO1DN/DN^{Sim1} females

After a 4 hours fasting period, females (11 weeks of age) were injected 5 mg/kg melanotan II (MTII) or PBS at the onset of the dark phase. A: Food intake 2 hours post MTII/PBS injection; B: food intake 4 hours post MTII/PBS injection; C: food intake 14 hours post MTII/PBS injection; D: food intake 24 hours post MTII/PBS injection; FOXO1DN^{stoplox/lox} females (CO/ n=7); FOXO1DN/DN^{Sim1} females (FOXO1DN/DN/ n=7)

All mice clearly consumed less calories 2 and 4 hours after MTII injection compared to PBS injection (fig. 22A&B). The transient effect of MTII injection was reflected by the fact that 14 hours after injection food intake levels returned to the levels seen for PBS injected control mice (fig. 22C&D). However, FOXO1DN/DN^{Sim1} mice responded similar to the injection of MTII as control littermates, independent of their gender (compare fig. 22 to fig. 23).

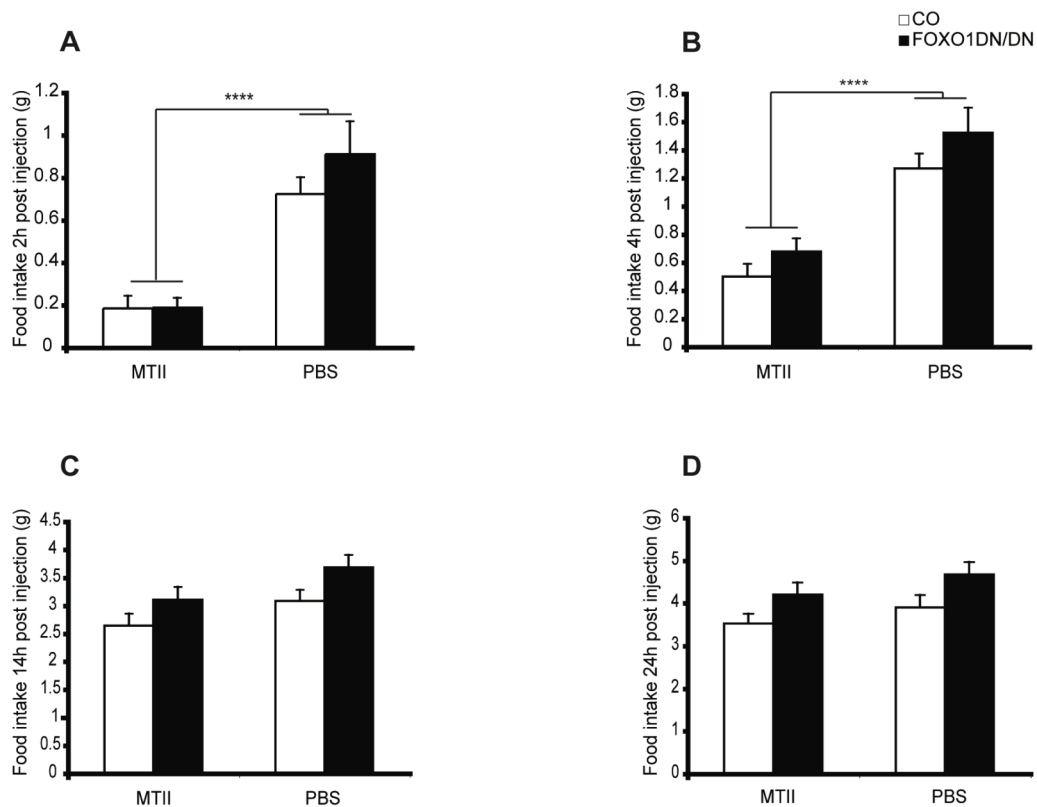


Figure 23: Melanotan II (MTII) sensitivity of FOXO1DN/DN^{Sim1} males

After a 4 hours fasting period, males (11 weeks of age) were injected 5 mg/kg melanotan II (MTII) or PBS at the onset of the dark phase. A: Food intake 2 hours post MTII/PBS injection; B: food intake 4 hours post MTII/PBS injection; C: food intake 14 hours post MTII/PBS injection; D: food intake 24 hours post MTII/PBS injection; FOXO1DN^{stoplox/lox} males (CO/ n=13); FOXO1DN/DN^{Sim1} males (FOXO1DN/DN/ n=9)

Taken together, the Sim1 neurons in FOXO1DN/DN^{Sim1} mice were sensitive to α -MSH, as these mice responded normally to low, random and high levels of α -MSH/MTII, which were represented by fasted, random fed and MTII injected mice, respectively. This suggests that overexpression of FOXO1DN in Sim1 neurons of the PVN does not affect MC4R mediated signalling in these neurons.

3.2.4 Glucose tolerance and insulin sensitivity of FOXO1DN/DN^{Sim1} mice

FOXO1 has been shown to be a central node of various signalling pathways. In the hypothalamus FOXO1 plays an important role in the regulation of POMC

Results

and AgRP expression by insulin and leptin leading to increased POMC and decreased AgRP levels [120, 124]. Moreover, hypothalamic insulin signalling has also been shown to be involved in peripheral glucose metabolism [13, 140]. To investigate whether FOXO1 signalling in Sim1 neurons similarly affects peripheral glucose and insulin metabolism, the response of FOXO1DN/DN^{Sim1} mice to peripheral glucose or insulin injection was analysed. After a 16 hours fasting period, blood glucose levels decreased dramatically from values between 130 and 150 mg/dl for ad libitum fed mice (fig. 24A&C) to values from 70 to 90 mg/dl for fasted mice (fig. 24B&D). Blood glucose levels of FOXO1DN/DN^{Sim1} mice were comparable to the respective control littermates, independent on the nutritional status of the animal.

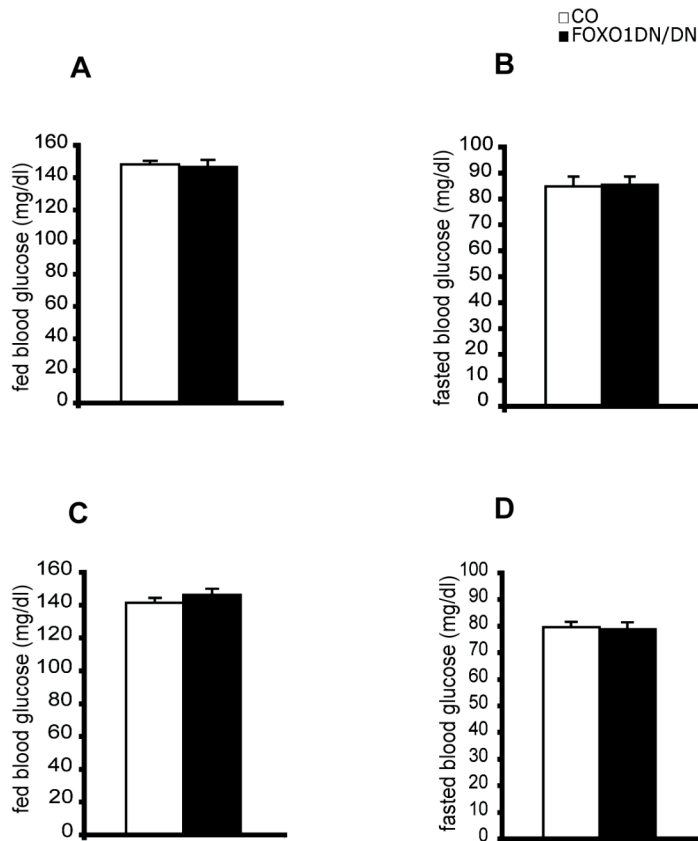


Figure 24: Unaltered blood glucose levels of FOXO1DN/DN^{Sim1} mice

Blood glucose levels of FOXO1DN/DN^{Sim1} mice and controls (12-13 weeks) were determined 2 to 3 hours after the onset of the light phase, in the random fed state and after 16 hours of fasting. A: random fed blood glucose levels of females; B: 16 hours fasted blood glucose levels of females; C: random fed blood glucose levels of males; D: 16 hours fasted blood glucose levels of males; females: CO, n=14; FOXO1DN/DN, n=19-22; males: CO, n=12-19; FOXO1DN/DN, n=20-22

To further analyse the ability of FOXO1DN/DN^{Sim1} and control mice to metabolise glucose, glucose tolerance tests were performed. In brief, overnight fasted mice were injected with 20% glucose (10 ml/kg body weight) and the blood glucose was determined 15, 30, 60 and 120 minutes after the injection. FOXO1DN/DN^{Sim1} mice responded similar to intraperitoneal glucose injection as control animals (fig. 25).

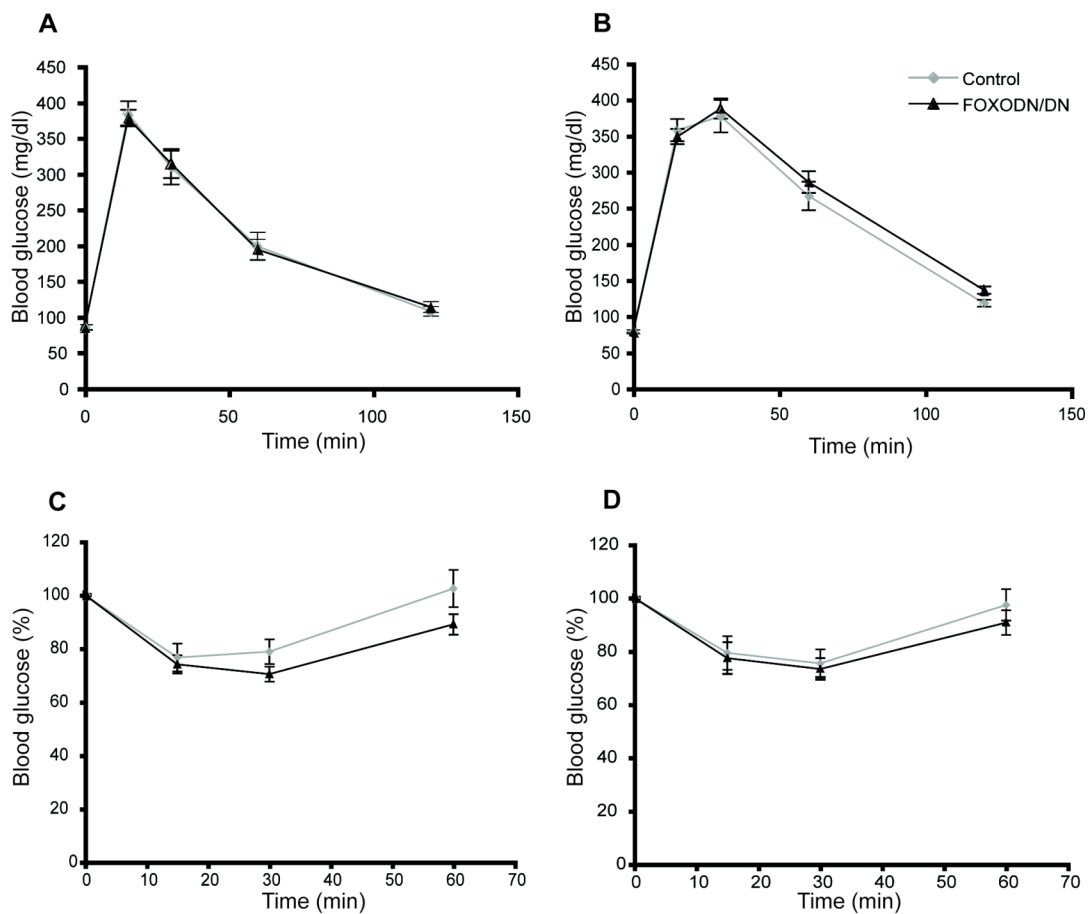


Figure 25: Unaltered glucose tolerance and insulin sensitivity of FOXO1DN/DN^{Sim1} mice

Mice were subjected to glucose tolerance tests (GTT) at an age of 12 weeks after 16 hours of fasting and to insulin tolerance tests (ITT) at an age of 13 weeks in the random fed state.

A: GTT of females; B: GTT of males; C: ITT of females; D: ITT of males; females: CO, n=14; FOXO1DN/DN, n=19-22; males: CO, n=12-19; FOXO1DN/DN, n=20-22

To directly address the insulin sensitivity in these mice, insulin tolerance tests were performed. The insulin tolerance was determined by the injection of 0.75 units insulin per kilogram body weight and the blood glucose levels were measured 15, 30 and 60 minutes after the injection. Notably, rising insulin levels

leads to glucose uptake of different tissues and thereby a decrease in blood glucose levels directly after injection. As seen in figure 25 C-D, insulin injection led to a drop in the relative glucose levels after 15 and 30 minutes after which the glucose levels were restored to pre-injection levels. However, the insulin sensitivity was indistinguishable between control mice and FOXO1DN/DN^{Sim1} mice, irrespective of the gender.

In summary, body weight of FOXO1DN/DN^{Sim1} male and female mice increased normally over the 18 weeks of the experimental period and body parameters, as body fat levels and body length were unaltered in comparison to respective control littermates. This went along with an unchanged food intake and α -MSH/MTII sensitivity of FOXO1DN/DN^{Sim1} female and male mice. In addition, FOXO1DN/DN^{Sim1} mice were glucose tolerant and insulin sensitive. To conclude, FOXO1 shuttling in Sim1 expressing neurons is not essential for the overall energy metabolism studied in this experimental setup.

3.3 FOXO1 in the Sim1 neuron dependent regulation of the stress response

The parts of the hypothalamus that constitutes the PVN and SON are not only indispensable for the regulation of metabolic processes such as food intake and energy expenditure, but they also play a major role in the body's stress response [154]. Two neuropeptides expressed in PVN/SON neurons, the corticotropin releasing hormone (CRH) and arginine vasopressin (AVP), are the initiators of the so-called hypothalamic pituitary adrenal (HPA) axis of stress response (see [84, 86] for review). Importantly, whereas CRH is more involved in the response to an acute stressor, AVP plays a more important role in a state of chronic stress [90, 92, 93].

3.3.1 Impaired HPA axis by Sim1 neuron specific FOXO1DN expression

Although the importance of CRH and AVP in the regulation of stress responses is well established, their transcriptional regulation is largely unknown. Both neuropeptides are known to be activated in a cAMP/ cAMP response element binding protein (CREB) dependent manner and several CREB binding sites (cAMP response elements; CRE) have been experimentally validated [85, 155]. To gain further insight into how these important mediators of stress responses are regulated at the transcriptional level, we performed an *in silico* analysis of the promoter of both genes, using the Genomatix MatInspector software. This software program mathematically predicts the presence of potential transcription factor binding sites based on their consensus sequence. Amongst many potential transcription factor binding sites, both AVP and CRH promoter sequences had several putative binding sites for forkhead transcription factors (fig. 26).



Figure 26: Putative forkhead binding sites encoded by the CRH promoter

The CRH promoter contains several cAMP response elements (CRE), and putative FOXO binding sites (FOXO).

In case of the CRH promoter, two putative forkhead binding sites, which have not been experimentally validated so far, were identified within 1000 base pairs upstream of the transcriptional start site. One site is located in close proximity to known and experimentally validated binding sites for CREB, CRE (fig 26) [85, 156].

Similarly, the AVP promoter contains four putative forkhead binding elements, which are encoded about 1000 base pairs upstream of the transcriptional initiation. Moreover, the AVP promoter contains three estrogen response elements (ERE), which are encoded about 150 bp more proximal than the putative forkhead binding sites to the transcriptional start (fig. 27) [157].

Results



Figure 27: Putative forkhead binding sites encoded by the AVP promoter

The AVP promoter contains several cAMP response elements (CRE), estrogen response elements (ERE) and putative FOXO binding sites (FOXO).

The presence of putative FOXO binding sites in the promoters of CRH and AVP suggests a potential involvement of FOXO proteins in the regulation of the hypothalamic stress response. To this extend, we evaluated the effect of Sim1 neuron specific FOXO1DN overexpression on the hypothalamic expression of CRH and AVP. In this regard, Aguilera et al. have stated: “The use of intronic probes for the analysis of the nascent transcript of heteronuclear RNA (hnRNA) has facilitated studies on the effects of acute stress on CRH and AVP transcription. The level of hnRNA reflects the direct change of transcription in response to stress stimuli and is independent on mRNA stability [154].” Animals were subjected to one hour of restraint stress before decapitation to induce the CRH/AVP transcription. The analysis did not reveal any differences in CRH hnRNA expression levels between FOXO1DN/DN^{Sim1} mice and control mice (fig. 28&29A). However, it has to be noted that CRH levels exhibited a high variation among the groups analysed. In contrast, FOXO1DN/DN^{Sim1} female but not male mice, showed a strong tendency towards decreased AVP levels in the hypothalamus (fig. 28B). Although we observed a 40% reduction in AVP expression levels in the FOXO1DN overexpressing female mice, this inhibition did not reach statistical significance, probably due to the high variability of AVP expression levels between animals.

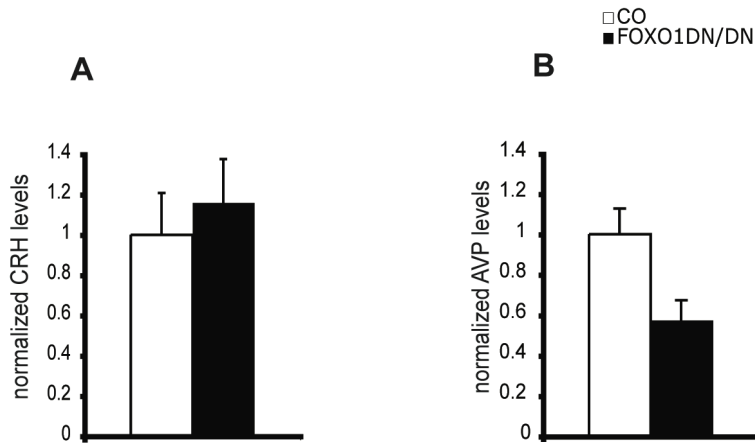


Figure 28: Neuropeptide levels in the hypothalamus of FOXO1DN/DN^{Sim1} females

The hypothalamic and pituitary neuropeptide hnRNA levels of females that were subjected to 1 hour of restraint stress at an age of 10 weeks; A: hypothalamic corticotropin releasing hormone (CRH) levels normalized on control levels; B: hypothalamic arginine vasopressin (AVP) levels normalized on control levels; CO, n=8-9; FOXO1DN/DN, n=9-11

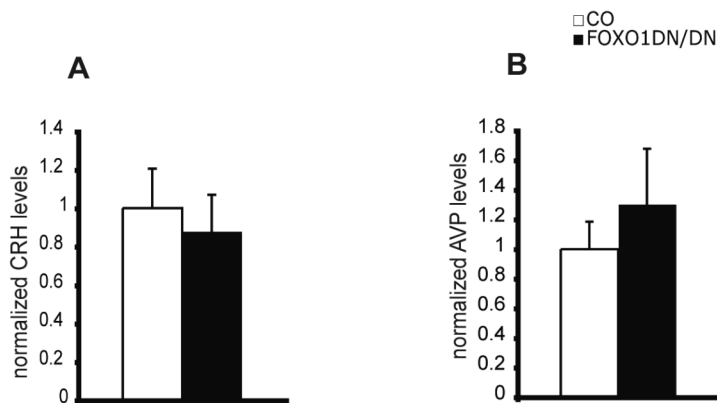


Figure 29: Neuropeptide levels in the hypothalamus of FOXO1DN/DN^{Sim1} males

The hypothalamic and pituitary neuropeptide hnRNA levels of males that were subjected to 1 hour of restraint stress at an age of 10 weeks; A: hypothalamic corticotropin releasing hormone (CRH) levels normalized on control levels; B: hypothalamic arginine vasopressin (AVP) levels normalized on control levels CO, n=8-9; FOXO1DN/DN, n=9-11

AVP expressed in the magnocellular PVN has a role in the control of the kidney water balance, which is independent of the stress response. Otherwise, AVP is one of the initiators of the stress response from the parvocellular PVN, which is a subset of Sim1 neurons [86]. Therefore, it is not unlikely that small but significant differences in gene expression in these neurons were masked by the unchanged levels in the surrounding areas. To circumvent this problem with regard to the AVP expression in FOXO1DN/DN^{Sim1} and control mice, more

Results

downstream targets of AVP were analysed. Upon stress induction, AVP is released from the PVN and in turn induces the release of ACTH in the pituitary, which is transported via the blood stream to the adrenal glands to initiate the corticosterone release. Hence, the potentially altered AVP expression in the hypothalamus of stressed $\text{FOXO1DN/DN}^{\text{Sim1}}$ mice was indirectly analysed by measuring the stress induced serum corticosterone levels released from the adrenal glands. Both female and male control groups significantly increased the serum corticosterone levels upon stress induction. $\text{FOXO1DN/DN}^{\text{Sim1}}$ female mice, however, failed to increase their serum corticosterone levels under stressed conditions. Interestingly, this blunted stress response in $\text{FOXO1DN/DN}^{\text{Sim1}}$ mice was a gender specific effect, since stress induced serum corticosterone levels of $\text{FOXO1DN/DN}^{\text{Sim1}}$ male mice were comparable to wildtype littermate controls (fig. 30).

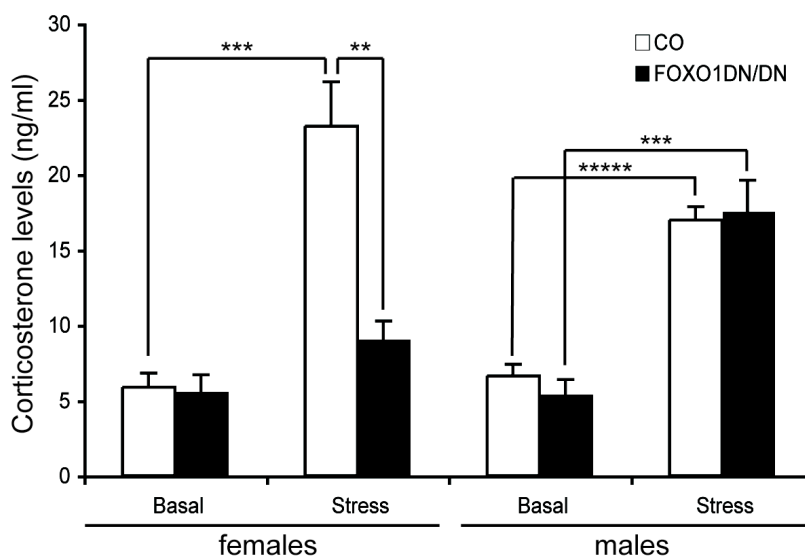


Figure 30: Blunted corticosterone response to restraint stress of $\text{FOXO1DN/DN}^{\text{Sim1}}$ females

Serum corticosterone levels before and after 1 hour of restraint stress of 9 week old mice; females: CO, n=7; FOXO1DN/DN , n=7; males: CO, n=7; FOXO1DN/DN , n=7; statistically significant difference from basal levels (***, $p < 0.001$; *****, $p < 0.00001$); statistically significant difference between stressed $\text{FOXO1DN/DN}^{\text{Sim1}}$ and stressed control females (**, $p < 0.01$)

To exclude that the observed effect on the corticosterone levels of $\text{FOXO1DN/DN}^{\text{Sim1}}$ female mice was mediated by an ectopic expression of the

Sim1-cre and thereby FOXO1DN expression in the adrenal gland or pituitary, the beta-galactosidase activity of lacZ^{Sim1} mice was analysed in these organs (fig. 31). LacZ^{Sim1} mice express β -galactosidase only upon cre-mediated recombination in Sim1 expressing cells. The β -galactosidase expression can either be detected by its enzymatic activity on its substrate, bromo-chloro-indolyl-galactopyranoside (X-Gal), resulting in a blue staining, or immunohistochemically by antibody detection for the β -galactosidase protein. Neither the adrenal glands nor the pituitary of lacZ^{Sim1} mice were positive for β -galactosidase expression (fig. 31), suggesting that the observed effect on the corticosterone levels in FOXO1DN/DN^{Sim1} female mice was due to an alteration originated in hypothalamic Sim1 neurons.

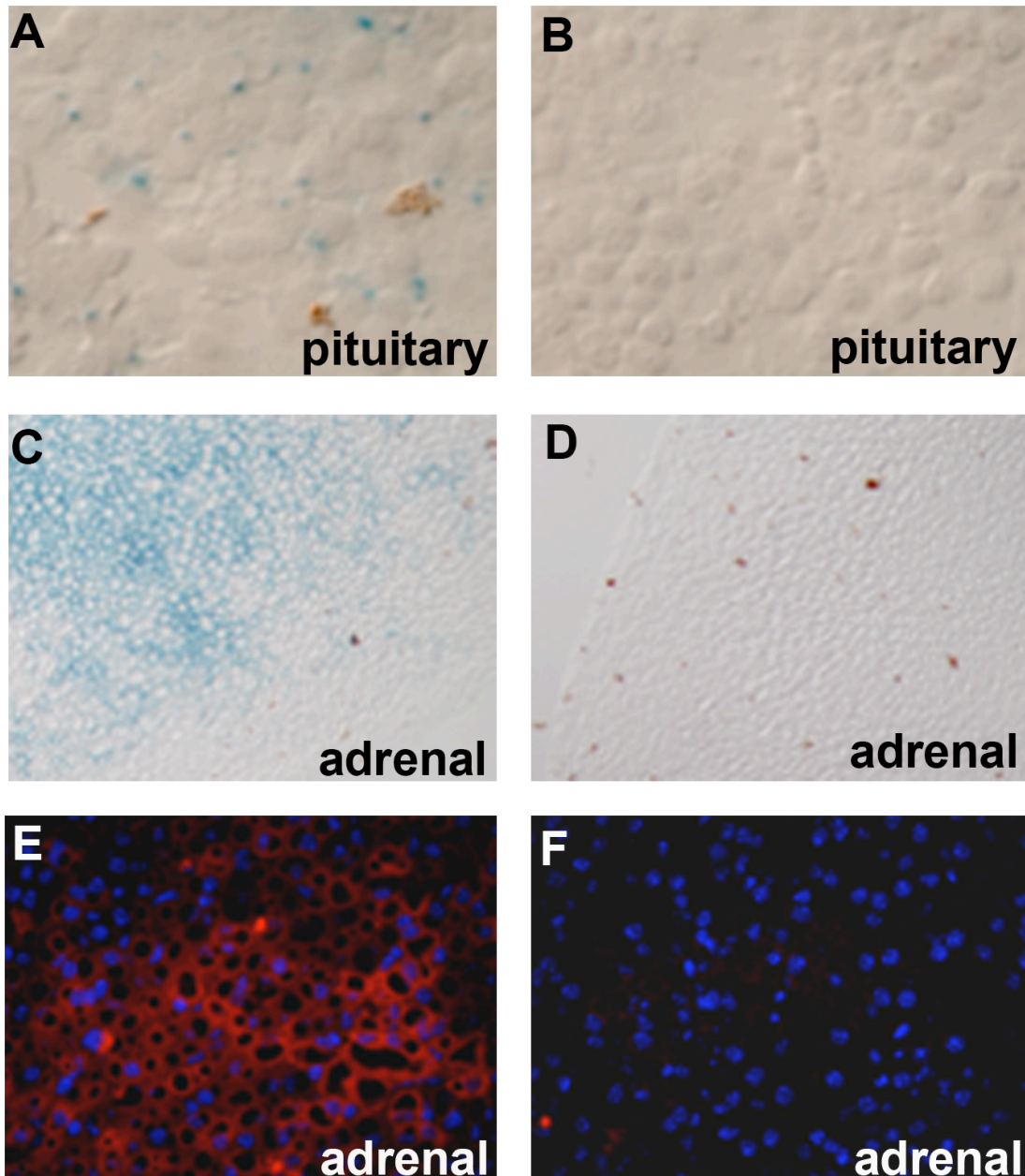


Figure 31: No ectopic expression of Sim1-cre in the pituitary or adrenal glands

Sim1-cre did not recombine loxP flanked DNA in the pituitary or in the adrenal glands, since no β -galactosidase activity could be detected in lacZ^{Sim1} mice in these organs. A,C,E: DsRed mice expressing lacZ in all cells were used as positive controls. B,D,F: lacZ mice crossed to Sim1-cre mice expressed the β -galactosidase in Sim1-cre positive cells. A,B: X-gal / β -galactosidase reaction in the pituitary; C,D, X-gal / β -galactosidase reaction in the adrenal gland; E,F: β -galactosidase immunohistochemistry from the adrenal gland

As aforementioned, Sim1 is also expressed in the amygdala in addition to the classical sites as the PVN. This brain region is involved in the acquisition and consolidation of fear, memory and is known to modulate CRH and AVP expression in response to stress. Moreover, corticosterone administration to the

amygdala modulates anxiety and reinforces CRH/AVP induction in the amygdala [158]. To evaluate a contribution of the amygdala to the altered stress response in $\text{FOXO1DN/DN}^{\text{Sim1}}$ and control mice, these mice were exposed to one hour of restraint stress, after which CRH and AVP hnRNA levels in the amygdala were analysed. Stressed $\text{FOXO1DN/DN}^{\text{Sim1}}$ female mice showed significantly reduced levels of AVP, but not CRH expression in the amygdala compared to control animals (fig. 32). In contrast, we could not observe any significant changes in CRH or AVP levels in male $\text{FOXO1DN/DN}^{\text{Sim1}}$ versus control mice and $\text{FOXO1DN/DN}^{\text{Sim1}}$ male mice even had a tendency towards increased CRH levels. These results were in line with the observations from the hypothalamic AVP levels and blood serum corticosterone levels, pointing towards a gender specific effect of FOXO1DN overexpression in Sim1 neurons on the body's stress response.

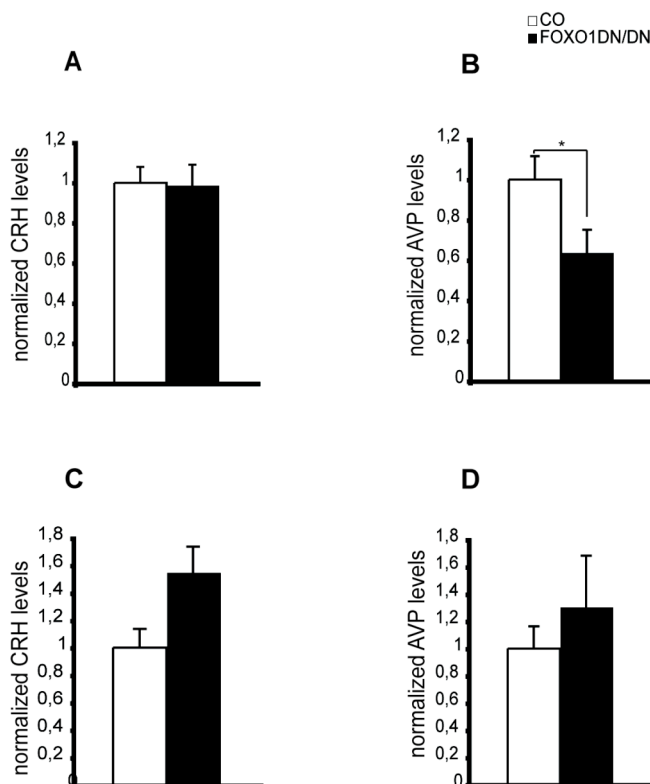


Figure 32: Neuropeptide levels in the amygdala in $\text{FOXO1DN/DN}^{\text{Sim1}}$ mice

The amygdala neuropeptide hnRNA levels of mice that were subjected to 1 hour of restraint stress at an age of 10 weeks; A: corticotropin releasing hormone (CRH) levels of females (normalized on control levels); B: arginine vasopressin (AVP) levels of females (normalized on control levels); C: corticotropin releasing hormone (CRH) levels of males (normalized on control levels); D: arginine vasopressin (AVP) levels of males (normalized on control levels); females: CO, n=8-9; FOXO1DN/DN , n=9-11; males: CO, n=7-8; FOXO1DN/DN , n=10-11

Taken together, these data demonstrate that FOXO1DN overexpression in Sim1 neurons impaired the initiation of the stress response in the PVN and/or SON. This was reflected by a massive alteration of corticosterone on the peripheral level of the HPA axis. Interestingly, this was a gender specific effect, as the reduced stress response in FOXO1DN/DN^{Sim1} mice was only observable in female mice. Additionally, AVP levels in the amygdala were reduced in FOXO1DN/DN^{Sim1} female mice, suggesting an involvement of FOXO1DN not only in the stress response, but also in the regulation of anxiety. Finally, the limitation of the phenotype to female mice suggests an involvement of estrogen on the HPA axis.

3.3.2 Inhibition of CRH and AVP by FOXO1DN expression *in vitro*

The *in vivo* data of CRH and AVP hnRNA levels in the Sim1 neurons can not fully explain the observed blunted corticosterone release in FOXO1DN/DN^{Sim1} female mice. However, the presence of putative binding sites in CRH and AVP promoter sequences suggests a direct involvement of FOXO1 on the transcriptional control of the CRH and AVP genes.

To investigate whether FOXO1DN overexpression directly influences the expression of AVP and CRH, an *in vitro* approach was used. For this purpose, firefly luciferase reporter constructs were generated containing promoter fragments of the AVP or CRH genes. These were cloned into the regulatory area of the luciferase gene in the pGL4.17 vector (Promega). The first promoter fragment of CRH of 1000 base pairs contained 2 putative forkhead binding sites along with 3 cAMP response elements (CRE). The second CRH promoter fragment was truncated to 300 base pairs including one putative forkhead site and 3 CRE sites (fig. 33).

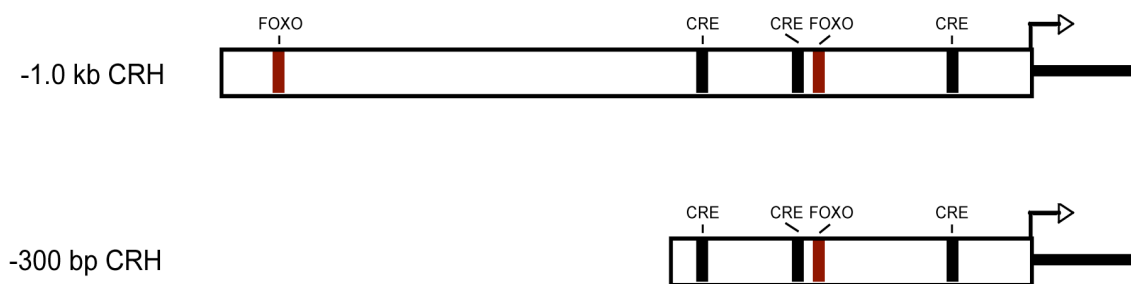


Figure 33: CRH promoter elements regulating the firefly luciferase reporter

The CRH promoter regulating the firefly luciferase reporter contained several cAMP response elements (CRE), and putative forkhead binding sites (FOXO).

The pGL4.17 vector, generated for the analysis of the AVP promoter, encoded 1.3 kilobases (-1.3 kb AVP) of the AVP promoter to drive the transcription of the firefly luciferase (fig. 27). The promoter fragment included the 4 predicted forkhead binding sites, 4 CREs and 3 estrogen response elements (EREs).

The reporter constructs were transiently transfected along with a FOXO1DN overexpressing vector or an empty control vector into the rat neuronal cell line PC12. The pGL4.17 empty vector encoded a minimal promoter and was used as a control. The drug forskolin results in a cAMP production and therefore has been shown to activate the CRH promoter [85]. The minimal promoter of pGL4.17 was not sensitive to forskolin induction and a cotransfection of the FOXO1DN expression vector did not result in an alteration of the promoter activity. As can be expected from the presence of cAMP response elements in the promoter fragment, forskolin clearly enhanced luciferase expression from both CRH promoter constructs (fig. 34A, white bars). Interestingly, the 300 bp promoter fragment was induced to a higher extent than the 1 kb promoter, which could be explained by the absence of potential inhibitory elements. However, cotransfection of the FOXO1DN expression vector significantly reduced luciferase expression in the case of both promoter constructs. This clearly indicates that FOXO1DN overexpression had an inhibitory effect on CRH promoter activity. However, the FOXO1DN overexpression could mediate these effects by a direct transcriptional regulation of the CRH promoter or by the regulation of a different gene that acts on the CRH promoter.

Results

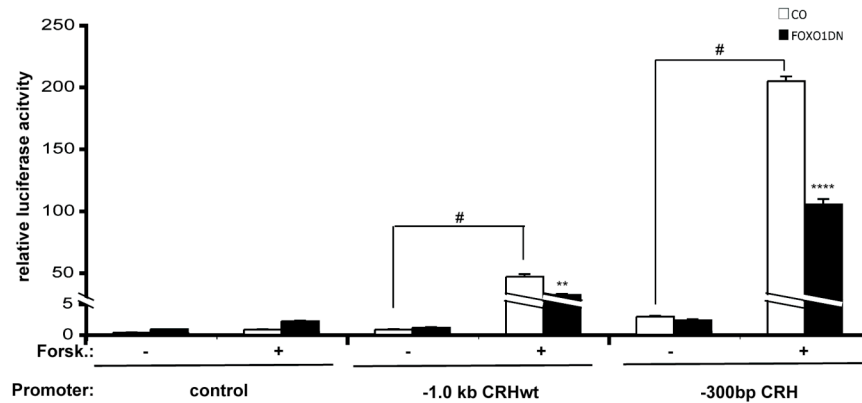


Figure 34: Reduced forskolin stimulation of the CRH promoter by FOXO1DN overexpression in PC12 cells

PC-12 cells were transfected as described with the indicated promoter constructs and the empty pCDNA control vector (open) or the pCDNA FOXO1DN expression vector (solid). Cells were treated with vehicle (-) or forskolin (+) to stimulate cAMP signalling. A: Transfected were the empty pGL4.17 vector with a minimal promoter (control), pGL4.17 with a 1kb wildtype CRH promoter fragment (-1,0 kb CRHwt) or with a 300bp wildtype CRH promoter fragment (-300bp CRH) upstream of the firefly luciferase; All transfections were done in triplicates and all assays were repeated 3 times. The pRL-0 vector was co-transfected and all firefly expression levels were standardized by the renilla values. Statistically significant difference between forskolin simulated and unstimulated levels (#, $p < 0.0001$); statistically significant difference between FOXO1DN and control pCDNA co-transfected luciferase levels (**, $p < 0.01$); (****, $p < 0.0001$)

Similarly, to the CRH promoter experiment, the AVP promoter luciferase reporter was transiently transfected along with the FOXO1DN overexpression vector or an empty control vector into the neuronal cell line PC12. The activity of the AVP promoter construct was increased by the induction with forskolin (fig. 35, white bars), although this induction was not as strong as for the CRH promoter. However, the cotransfection of the FOXO1DN expression vector significantly reduced the expression of luciferase from the AVP promoter. As the luciferase activity was reduced upon FOXO1DN cotransfection at basal and forskolin induced conditions, this reduction of the promoter activity seemed to be independent of cAMP signalling.

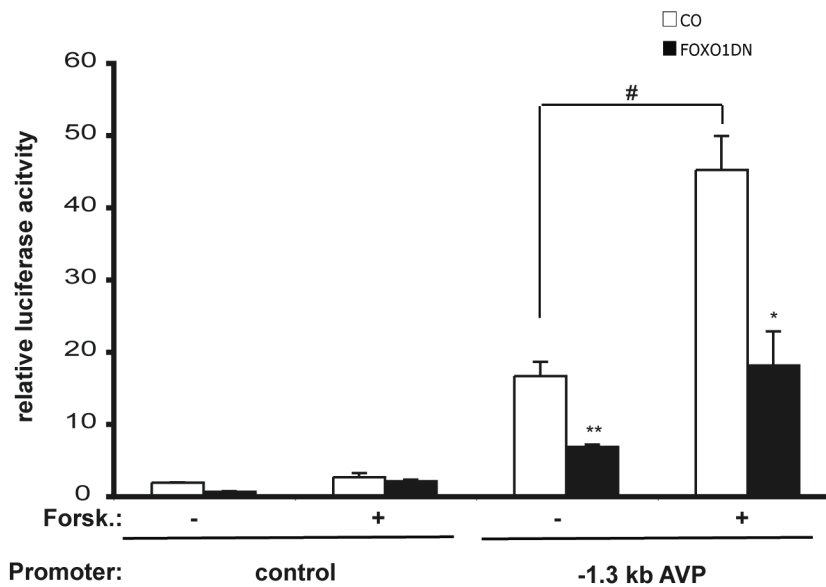


Figure 35: Inhibition of AVP transcription by FOXO1DN overexpression in PC12 cells

PC12 cells were transfected as described with the indicated promoter construct, the empty pGL4.17 vector with a minimal promoter (control), pGL4.17 with a 1.3kb wildtype AVP promoter fragment upstream of the firefly luciferase (-1,3 kb AVPwt). Co-transfected were the empty pCDNA control vector (open) or the pCDNA FOXO1DN expression vector (solid). Cells were treated with vehicle (-) or forskolin (+) to stimulate cAMP signalling. All transfections were done in triplicates and all assays were repeated 3 times. The pRL-0 vector was co-transfected and all firefly expression levels were standardized by the renilla values. Statistically significant difference between forskolin simulated and unstimulated levels (#, $p < 0.001$); statistically significant difference between FOXO1DN and control co-transfected luciferase levels (**, $p < 0.01$; *, $p < 0.05$)

The effect of a reduction of the promoter activity by FOXO1DN overexpression can arise from a direct binding of FOXO1DN to putative forkhead binding sites or from the inhibitory effect of FOXO1DN on other genes or signalling molecules that indirectly modulate the AVP or CRH transcription. Therefore, a direct binding of FOXO1DN to the putative forkhead binding sites was analysed by electro mobility shift assays (EMSA). DNA probes of about 30 base pairs were generated encoding the consensus forkhead response element (EMSA probe published in [144]) and the predicted forkhead binding sites along with surrounding CRH/AVP promoter sequences. SK-N-SH neuroblastoma cells were transiently transfected with a wildtype FOXO1 (FOXO1wt) or a FOXO1DN expression vector, nuclear extracts were isolated and incubated with the EMSA probes. In addition, the FOXO1DN transfected nuclear extracts were incubated

Results

with an antibody against the N-terminus of FOXO1 to confirm a specific binding of FOXO1 to the promoter.

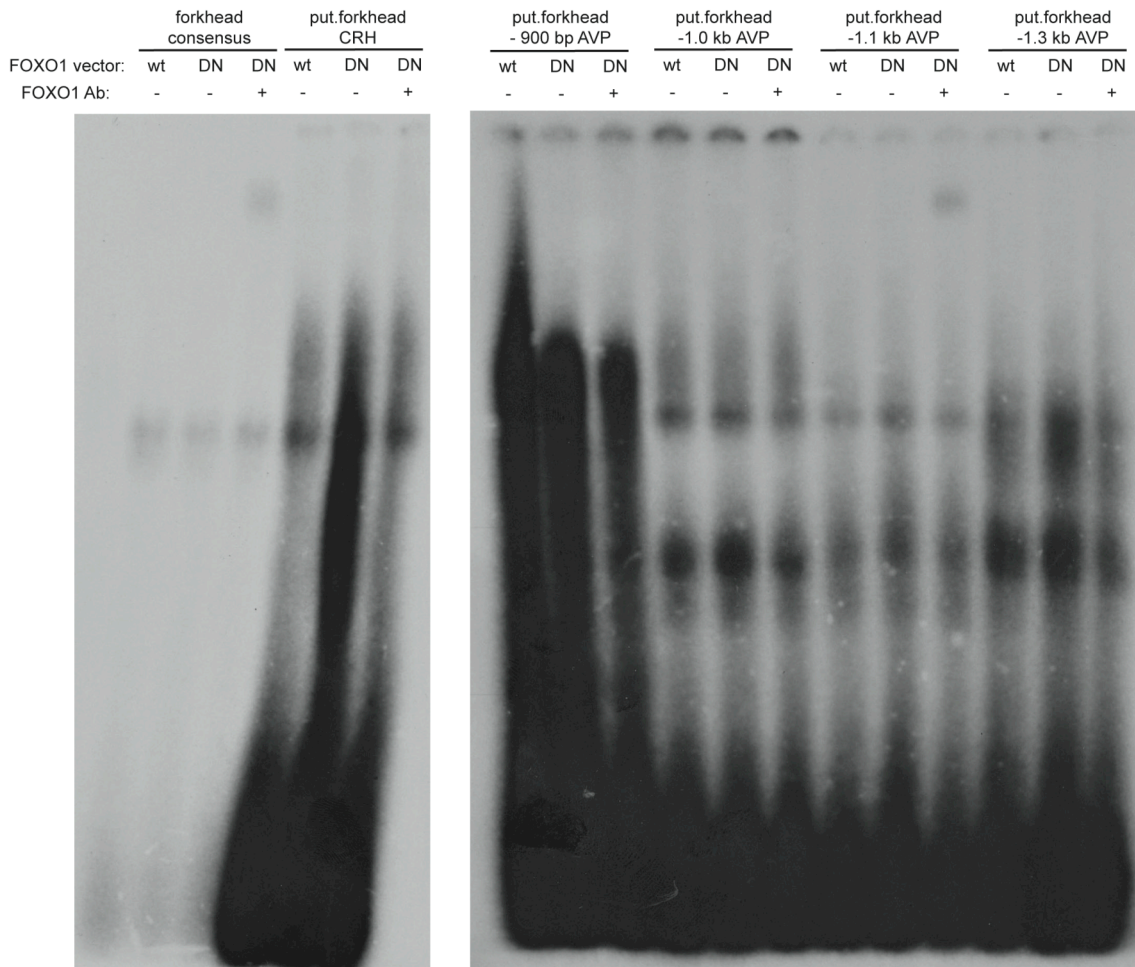


Figure 36: Electro mobility shift assay (EMSA) of FOXO1DN transfected SK-N-SH cells.

SK-N-SH cells were transfected with a FOXO1wildtype (wt) or FOXO1DN (DN) expression vector, as indicated; nuclear extracts were isolated and incubated with the DNA fragments at the indicated position of the promoters; To confirm the specific binding of FOXO1 to the DNA, the samples from the FOXO1DN overexpression were incubated with a FOXO1 specific antibody.

The FOXO1 protein bound specifically to the consensus forkhead response element, as distinct bands are detectable for the three samples. This was supported by a shift in the band arising from the addition of the FOXO1 antibody (fig. 36 for low exposure; fig. 37 for high exposure). Interestingly, proteins from the nuclear extracts bound to all analysed probes of the CRH and AVP promoter. However, a supershift by the FOXO1 antibody could only be detected in one of the analysed probes, indicating that the other probes were

associated with unknown proteins. Importantly, a distinct band was detected for the putative forkhead binding site at -1.1 kb distance to the transcriptional start of the AVP promoter and a specific binding of FOXO1 to this promoter element could be confirmed by the presence of the FOXO1 antibody mediated supershift (fig. 37). Conclusively, FOXO1 seems to bind to the putative forkhead binding site at -1.1 kb distance to the transcriptional start of the AVP promoter, but not to the other putative binding sites of the AVP or the CRH promoter.

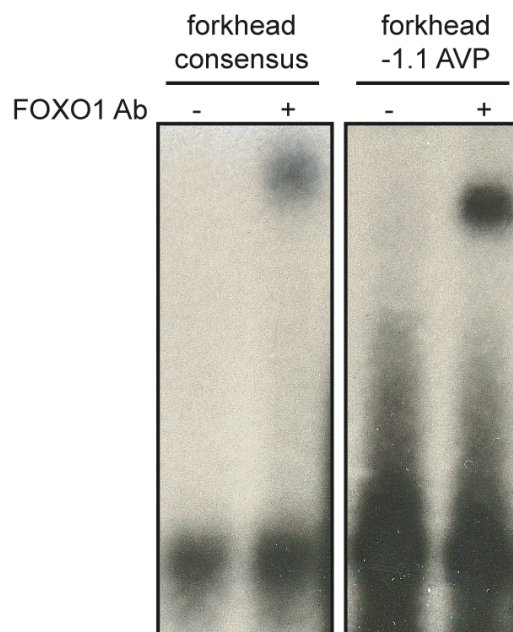


Figure 37: Specific binding of FOXO1DN to the AVP promoter

SK-N-SH cells were transfected with a FOXO1DN expression vector, nuclear extracts were isolated and incubated with the indicated DNA fragments; To confirm the specific binding of FOXO1 to the DNA, the samples were incubated with a FOXO1 specific antibody.

Taken together, FOXO1DN inhibited the cAMP mediated induction of the CRH promoter *in vitro* but this was not dependent on a direct binding to the analysed putative binding site. Additionally, the *in vitro* FOXO1DN overexpression reduced the promoter activity of AVP independent of cAMP signalling. This effect could be mediated by a direct binding of FOXO1DN to the AVP promoter at -1.1 kb distance to the transcriptional start. Finally, the *in vitro* analysis of the CRH and AVP promoter support the *in vivo* evidence of an altered initiation of

the stress response by the overexpression of FOXO1DN in Sim1 neurons in female mice, only.

3.3.3 The estrogen dependent regulation of arginine vasopressin

The *in vivo* data of CRH and AVP levels in the Sim1 neurons did not fully explain the observed blunted corticosterone release in FOXO1DN/DN^{Sim1} females. However, the presence of a newly discovered forkhead binding site on the AVP promoter and a decreased activation of the AVP promoter *in vitro* by FOXO1DN overexpression are strong indicators of an involvement of FOXO1 on the transcriptional control of the AVP gene. Importantly, the gender specific difference supports the evidence that the AVP mediated initiation of the stress response is reduced by FOXO1DN expression in Sim1 neurons through a mechanism that is only present in females. One possibility is an estrogen dependent process, as estrogen reinforces the AVP induction of transcription upon stress, which has been intensively analysed in the past [95, 157]. Interestingly, estrogen response elements (EREs) are located within 1.0 kilobases (kb) of the transcriptional start in the AVP promoter.

To check this possibility, we decided to use SK-N-SH neuroblastoma cells, which are inducible with 17 β -estradiol (E2), the major form of estrogen in humans. First, the modulation of the AVP promoter activity by FOXO1DN was confirmed in these cells. As expected, FOXO1DN transfection in SK-N-SH cells resulted in a reduced promoter activity, that was also independent of forskolin mediated cAMP signalling (fig. 38).

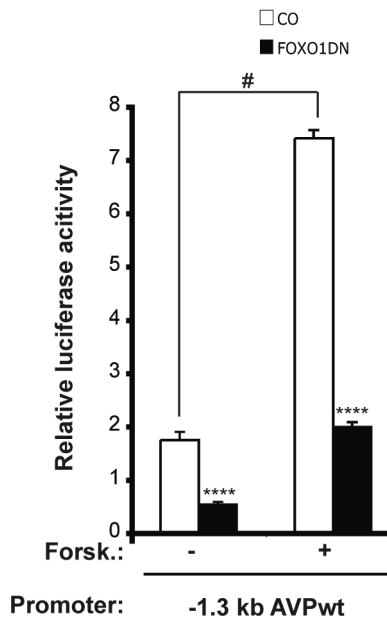


Figure 38: Inhibition of AVP transcription by FOXO1DN overexpression in SK-N-SH cells

SK-N-SH cells were transfected as described with the indicated promoter constructs: the empty pGL4.17 vector with a minimal promoter (control), pGL4.17 with a 1.3kb wildtype AVP promoter fragment upstream of the firefly luciferase (-1,3 kb AVPwt). Co-transfected were the empty pCDNA control vector (open) or the pCDNA FOXO1DN expression vector (solid). Cells were treated with vehicle (-) or forskolin (+) to stimulate cAMP signalling. All transfections were done in triplicates and all assays were repeated 3 times. The pRL-0 vector was co-transfected and all firefly expression levels were standardized by the renilla values. Statistically significant difference between forskolin simulated and unstimulated levels (#, $p < 0.0001$); statistically significant difference between FOXO1DN and control co-transfected luciferase levels (****, $p < 0.0001$)

To evaluate the FOXO1DN effect on the AVP promoter induction by 17β -estradiol (E2), the amount of FOXO1DN overexpression vector cotransfected with the reporter construct in SK-N-SH cells was reduced to the minimal level that still has an effect to minimize indirect effects. The AVP reporter (-1.3 kb AVP) was inducible to a small but statistically significant extent by E2 in a dose dependent manner (fig. 39). However, FOXO1DN overexpression significantly reduced the promoter activity at already 10 nM of E2 in relation to control levels that rise upon E2 treatment. This difference increased with increased E2 concentrations.

Results

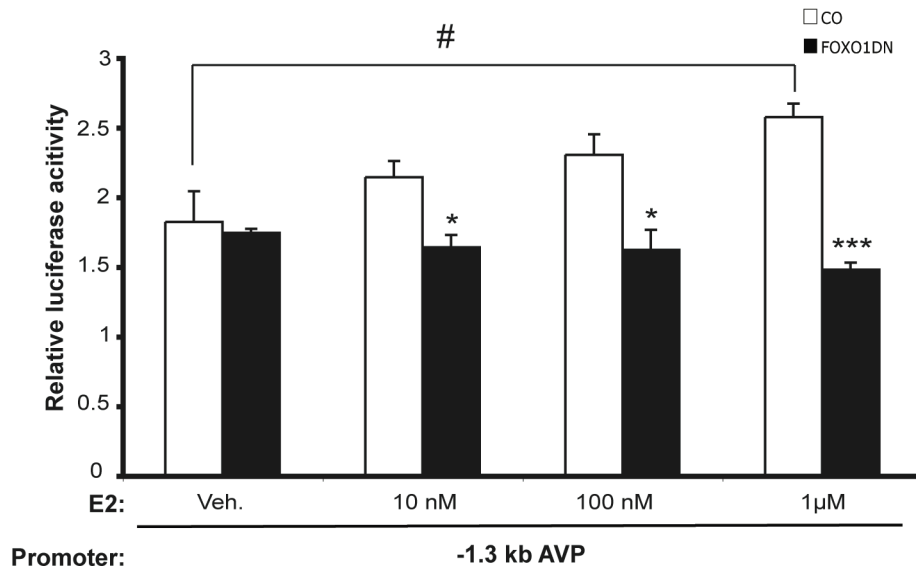


Figure 39: Reduced 17 β -estradiol stimulation of the AVP promoter by FOXO1DN overexpression

SK-N-SH cells were transfected as described with the indicated promoter construct, pGL4.17 with a 1.3kb wildtype AVP promoter fragment upstream of the firefly luciferase (-1,3 kb AVP). Cotransfected were the empty pCDNA control vector (open) or the pCDNA FOXO1DN expression vector (solid). Cells were treated with vehicle (veh.) or 17 β -estradiol (E2) in the indicated concentrations. All transfections were done in triplicates and all assays were repeated 3 times. The pRL-0 vector was co-transfected and all firefly expression levels were standardized by the renilla values. Statistically significant difference between estradiol stimulated and unstimulated levels (#, $p < 0.05$); statistically significant difference between FOXO1DN and control co-transfected luciferase levels (*, $p < 0.05$; **, $p < 0.01$)

Consequently, the estrogen dependent upregulation of the AVP promoter was blunted by FOXO1DN cotransfection and this inhibition could be mediated by an interaction of FOXO1DN with the now confirmed forkhead binding site at -1.1 kb of the AVP promoter.

In summary, the stress dependent AVP induction was altered in FOXO1DN/DN^{Sim1} female mice *in vivo*, which was reflected by a blunted corticosterone release upon stress. This was probably due to reduction of AVP promoter activity by FOXO1DN binding to a forkhead binding site that is located -1.1 kb in relation to the transcriptional start, as shown *in vitro*. However, the gender specificity and the *in vitro* analysis of the estrogen response implicate, that FOXO1DN inhibits specifically the estrogen dependent upregulation of the AVP promoter upon stress.

4 Discussion

The paraventricular nucleus (PVN) of the hypothalamus comprises a distinct subset of neurons regulating a diversity of processes including energy homeostasis and stress response. The pivotal role of the PVN for maintenance of the organism's energy balance is reflected by studies creating lesions selectively in the PVN, which lead to hyperphagia and obesity [58, 60]. Additionally, AgRP and POMC expressing neurons in the arcuate nucleus, which are associated with the regulation of feeding, project to neurons of the PVN [40, 159]. In line with this, both AgRP and α -MSH, a processing product of POMC, bind to the melanocortin receptor 4 (MC4R) on PVN neurons to induce and reduce feeding, respectively [81, 153].

The PVN is not only involved in the regulation of energy metabolism, but is also linked to the stress response. Seen from an evolutionary perspective this link is important in the state of "fight or flight", when the organism has to switch priorities from a situation of regular energy intake and storage, to a state of an energy supply to organs important for its defence, such as muscle, heart and lungs [84]. Especially, CRH and AVP released from the PVN initiate the stress response by the activation of the hypothalamic pituitary adrenal (HPA) axis. Otherwise, CRH expression in the PVN contributes to the anorexigenic effect of leptin, further supporting the link between energy metabolism and stress responses [67]. In addition, pharmacological studies have shown a crucial role for the central melanocortin system in the regulation of both the stress response as well as feeding behaviour [160, 161]. Recently, Lu et al. demonstrated that the administration of the α -MSH agonist, MTII, into the PVN induced CRH transcription in a MC4R dependent manner. In the periphery, MTII administration had an effect on the HPA axis mediated corticosterone release as well as on food intake [68]. Thus, melanocortin signalling seems to connect both energy metabolism and stress response in the PVN.

The transcription factor FOXO1 and the ATP sensitive potassium (K_{ATP}) channel are involved in several important metabolic pathways in different tissues including the arcuate nucleus of the hypothalamus. Thus, the aim of this thesis was to elucidate if these central molecules in the regulation of energy

homeostasis could link energy homeostasis to the stress response in Sim1 expressing neurons of the PVN.

4.1 Unaltered energy homeostasis by the K_{ATP} channel and FOXO1 overexpression in Sim1 neurons

The metabolic parameters of $K_{ATP}\Delta N^{Sim1}$, $K_{ATP}\Delta N/\Delta N^{Sim1}$ and $FOXO1DN/DN^{Sim1}$ mice were fully analysed emphasising the aspects already known to be modulated by the PVN, such as food intake and MC4R signalling. Notably, mice expressing a transgene in a Sim1 dependent way are useful tools to address the role of these neurons in different pathways, as this mouse line recombines loxP flanked DNA mainly in the PVN and supraoptic nucleus (SON) [82] (section 3.1 & 3.2). Not only the PVN as a site of Sim1-cre expression, but also the Sim1 expressing neurons of the SON are of particular interest to study the regulation of energy homeostasis, as neuronal activity of these neurons is altered upon feeding [162].

In spite of the known involvement of Sim1 neurons in energy metabolism, the analysis of metabolic parameters as body weight, food intake and body composition did not reveal a defect in $K_{ATP}\Delta N^{Sim1}$, $K_{ATP}\Delta N/\Delta N^{Sim1}$ and $FOXO1DN/DN^{Sim1}$ transgenic mice. In addition, these mice were sensitive to peripherally administered glucose, insulin and the MC4R agonist, MTII. In this respect it has to be noted that both mouse lines analysed are based on the overexpression of truncated proteins that have to compete with the endogenous ones to mediate the effect. In the case of the K_{ATP} channel, the pore is constituted of 4 subunits, which have to be replaced by the $K_{ATP}\Delta N$ variant expressed in a high dose. This could explain the only mild alteration of the change in membrane resistance and the mean membrane potential seen in $K_{ATP}\Delta N-Z/EG^{Sim1}$ mice. Though both mouse lines were bred to homozygosity to deal with this fact, it can still not be excluded that the dominant negative or constitutive active effect of these transgenes is too weak to result in a clear metabolic phenotype.

Another possible explanation for the absence of any metabolic effects by overexpression of $K_{ATP}\Delta N$ could be a process of compensation. As the Sim1-

cre recombines the DNA in an early stage during the development [163], the central nervous system could compensate potential defects arising from the alteration of the firing frequency. Notably, the ratio of excitatory to inhibitory synapses connected to a neuron determines the cell-autonomous regulation of electrical activity and excitability of the cell. The ability of a synapse to change in strength has been described as synaptic plasticity [164]. Especially in $K_{ATP}\Delta N/\Delta N^{Sim1}$ mice, compensation could be achieved by the modification of synaptic plasticity or other compensatory mechanisms. An expression of the $K_{ATP}\Delta N$ gene in adult mice using a different cre-recombinase approach would circumvent such a potential compensation.

Taken together, FOXO1 signalling or the K_{ATP} channel dependent membrane excitability seem not to play a role in Sim1 neuron mediated control of energy homeostasis, although compensatory mechanisms characteristic for the central nervous system can not be excluded. Thus, our data suggest that the G-protein coupled MC4R in Sim1 neurons mediates its potential effects on transcription and membrane excitability to regulate food intake in a FOXO1 and K_{ATP} channel independent way. Finally, the peripheral insulin or glucose metabolism is not influenced by these genetic modifications in Sim1 expressing neurons.

4.2 Reduced stress response by Foxo1DN overexpression in Sim1 neurons of female mice

The PVN has been shown to initiate the stress response releasing CRH and AVP from nerve terminals into the hypothalamic pituitary portal system, which activates the HPA axis resulting in corticosterone release (reviewed in [86]). In $FOXO1DN/DN^{Sim1}$ female mice, the corticosterone release from the adrenal glands was abolished upon stress, indicating that FOXO1DN overexpression specifically in Sim1 expressing neurons could alter the stress response in these mice. The HPA axis of the stress response is initiated by induction of AVP and CRH expression in the paraventricular nucleus, where FOXO1DN is expressed in $FOXO1DN/DN^{Sim1}$ mice. However, the altered serum concentrations of corticosterone could not be fully explained by a differential expression at the mRNA level of these hypothalamic neuropeptides in FOXO1DN overexpressing

mice compared to control mice: Whereas CRH mRNA expression levels were unaltered, a 40% reduction of AVP expression was observed in the hypothalamus, but this reduction did not reach statistical significance.

A potential alteration of the neuropeptide expression could be masked due to several reasons: First and foremost, the peak of AVP and/or CRH expression could occur earlier after the initiation of the stress response and could be very transient due to activation of negative feedback mechanisms. Notably, the brain was dissected after one hour of stress for the simultaneous determination of hypothalamic neuropeptide expression and serum corticosterone levels, as the HPA axis response is known to be high at this time point. Possibly, the analysis after one hour of stress induction might not be the ideal time point to investigate transcriptional regulation of AVP and CRH. Second, the PVN is a heterogeneous nucleus, which consists of so-called magnocellular and parvocellular PVN neurons, and both subsets contain Sim1 neurons. Although both subsets of neurons were shown to express AVP, the regulation and function of AVP differs markedly in the different subsets of neurons [154]. Thereby, a significant difference in the AVP expression in the parvocellular stress responsive subset could be masked by an unaltered expression in the magnocellular PVN, which is known to regulate the kidney water balance. Finally, since Sim1 neurons only represent a subpopulation of the PVN [82], it is not unlikely that small but significant differences in gene expression in these neurons are masked by the unchanged levels in the surrounding areas that do not express the Sim1-cre and thereby FOXO1DN. A detailed hypothalamic *in situ* analysis on different timepoints after the initiation of stress could therefore further elucidate the regulation of CRH and AVP upon stress. With such an approach subsets of neurons expressing AVP for the regulation of the stress response could possibly be distinguished from neurons that regulate the kidney water balance.

Further support that FOXO1DN overexpression might directly affect neuropeptide expression in Sim1 neurons was collected from *in vitro* experiments. Both predicted promoters of CRH and AVP contain several putative FOXO1 binding sites. A luciferase reporter assay with the CRH promoter revealed that the overexpression of FOXO1DN decreased the

induction of the promoter by forskolin dependent cAMP signalling. However, the predicted forkhead binding site seems not to be a functional promoter element for FOXO1 binding as indicated by the electromobility shift assay (EMSA). Furthermore, CRH levels upon stress were unaltered *in vivo* between the genotypes analysed indicating that the observed *in vitro* reduction of CRH transcription upon FOXO1DN expression might arise from unspecific effects. Thus, further *in vivo* analysis of the CRH expression in FOXO1DN/DN^{Sim1} female mice, for instance at an earlier time point, is necessary to elucidate, if the effect detected *in vitro* could be extrapolated to an *in vivo* context.

In contrast to CRH, the AVP expression had a tendency to be reduced by FOXO1DN overexpression in Sim1 neurons in female mice. In line with this, FOXO1DN overexpression *in vitro*, resulted in a reduction of the promoter activity of AVP and this in a forskolin independent way. Importantly, a predicted binding site for FOXO1, located in 1.1 kb distance from the transcriptional start, was confirmed experimentally in this study by EMSA and a subsequent supershift with a FOXO1 specific antibody. Together, these results suggest a direct binding of FOXO1 (FOXO1DN) to the AVP promoter. However, it cannot be excluded that FOXO1DN mediates its dominant negative effect on FOXO3A or FOXO4 dependent transcription, as the consensus sites for FOXO1, FOXO3A and FOXO4 are identical [123]. Notably, FOXO3A, but not FOXO4, is expressed in the central nervous system [165]. However, a hypothalamic specific expression and function for FOXO3A has not been described, thus far. Conclusively, a direct binding and regulation of the AVP promoter by FOXO proteins is likely, which is supported by the *in vitro* analysis of the AVP promoter, the strong tendency towards reduced AVP levels upon stress observed *in vivo* and indirectly by the abolished corticosterone induction upon stress in FOXO1DN/DN^{Sim1} female mice.

In addition to the expression in the PVN, Sim1-cre also mediates the recombination and thereby FOXO1DN expression in the SON and the amygdala of FOXO1DN/DN^{Sim1} mice. The SON is known to upregulate CRH and AVP upon stress in a similar manner as in the PVN. How this influences the HPA axis, in relation to the PVN, has not been analysed thus far [166, 167] and was not addressed in this study. A detailed hypothalamic *in situ* analysis could also

address a potential effect of FOXO1DN expression on the regulation of CRH and AVP in these two distinct hypothalamic nuclei.

In line with the altered AVP expression in the hypothalamus, the AVP but not the CRH levels in the amygdala are significantly decreased in FOXO1DN/DN^{Sim1} female mice. This reduction in AVP levels could be an indirect effect of the reduced peripheral corticosterone levels in these mice. Notably, CRH and AVP expression are known to be induced in response to corticosterone-glucocorticoid receptor (GR) activation in the central (CeA) and the basolateral (BLA) nucleus of the amygdala, which are the main areas for acquisition and consolidation of fear memory [158, 168]. Alternatively, the altered AVP expression levels in the amygdala of FOXO1DN/DN^{Sim1} female mice could be due to a cell-autonomous effect of FOXO1DN in the amygdala as well. In this respect, it is important to note that indeed Sim1 is expressed in the NLOT region of the amygdala, as shown by us. As both effects could work in an additive or synergistic way, further experiments are needed to analyse to what extent the indirect corticosterone effect or the cell-autonomous effect in the NLOT contributes to the altered expression of AVP in the amygdala of FOXO1DN/DN^{Sim1} mice. To conclude, the altered AVP expression in the amygdala of FOXO1DN/DN^{Sim1} female mice suggests that the anxiety behaviour in response to stress could be altered. Therefore, it would be interesting to further analyse the induction of anxiety in response to stress in FOXO1DN/DN^{Sim1} female mice by extensive behaviour analyses.

4.3 The gender specific effect of FOXO1DN on the HPA axis

The data collected in this study clearly show an effect of FOXO1DN overexpression on AVP expression both *in vitro* and *in vivo*. Importantly, the *in vivo* data clearly indicates a gender specific effect. Selectively in females, Sim1-specific expression of FOXO1DN induced alterations of the HPA axis on different levels, as seen on hypothalamic AVP expression levels, corticosterone release by the adrenal glands and AVP expression levels in the amygdala. As the female hormone estrogen has been shown to reinforce the HPA axis of stress response by the activation of AVP and CRH, the sex-specific effect on

AVP expression in FOXO1DN/DN^{Sim1} mice points to a possible involvement of this hormone [94, 157]. First evidence supporting an involvement of estrogen on the FOXO1DN mediated effect on AVP expression in Sim1 neurons, was gathered by an *in vitro* AVP promoter analysis. This showed an induction of AVP promoter dependent luciferase transcription by estrogen administration, whereas this effect was impaired by the overexpression of FOXO1DN. To date, *in vivo* data supporting the specific role of estrogen in the FOXO1DN dependent downregulation of AVP is still lacking. One way to address the involvement of estrogen, would be by ovariectomising FOXO1DN/DN^{Sim1} and control mice, as ovariectomy leads to the complete loss of estrogen. If FOXO1DN mediates its effect by interfering with the estrogen mediated reinforcement of the HPA axis, ovariectomised FOXO1DN/DN^{Sim1} and control mice should have a similar stress response that is in general lower than the sham operated control mice. If this is the case, estrogen replacement in ovariectomised mice of both genotypes could further support the view of an estrogen specific effect.

An estrogen dependent effect of FOXO1DN in Sim1 neurons would implicate that the FOXO1DN protein might interfere with the estrogen receptor (ER) binding to the promoter and its activation of transcription. In the canonical model of ER signalling, the ERs are primarily located in the cytosol in absence of estrogen. Upon estrogen binding, the receptor dimerizes, migrates into the nucleus, and subsequently binds to specific estrogen response elements (ERE) in the promoter of target genes. Furthermore, the DNA bound ER recruits other proteins that are responsible for the transcriptional control of downstream genes (reviewed in [169]). Importantly, Zhao et al and others have revealed by a yeast two hybrid screening and GST pulldown experiments that FOXO1 can interact with the estrogen receptor α (ER α). Hence, estrogen stimulation in the PVN could result in a complex of FOXO1 and ER α binding to the AVP promoter, although an involvement of FOXO3A or ER β cannot be excluded.

Such a complex could bind to the promoter elements by different mechanisms: First, the FOXO protein could recognize its newly identified binding site and recruit the ER to activate transcription. In this case, FOXO1DN overexpression could inhibit this interaction either by the absence of the transactivation domain in the FOXO1DN protein (fig. 40A) or by the loss of the ability to interact with

the ER (fig. 40B). Second, the FOXO/ER complex could bind to the ERE via the ER to activate transcription. In this case, the loss of the transactivation domain in the FOXO1DN protein could be responsible for the reduced transcription (fig. 40C). Finally, both proteins could bind to their own binding sites and activate transcription by their interaction via a secondary structure of the DNA (fig. 40D).

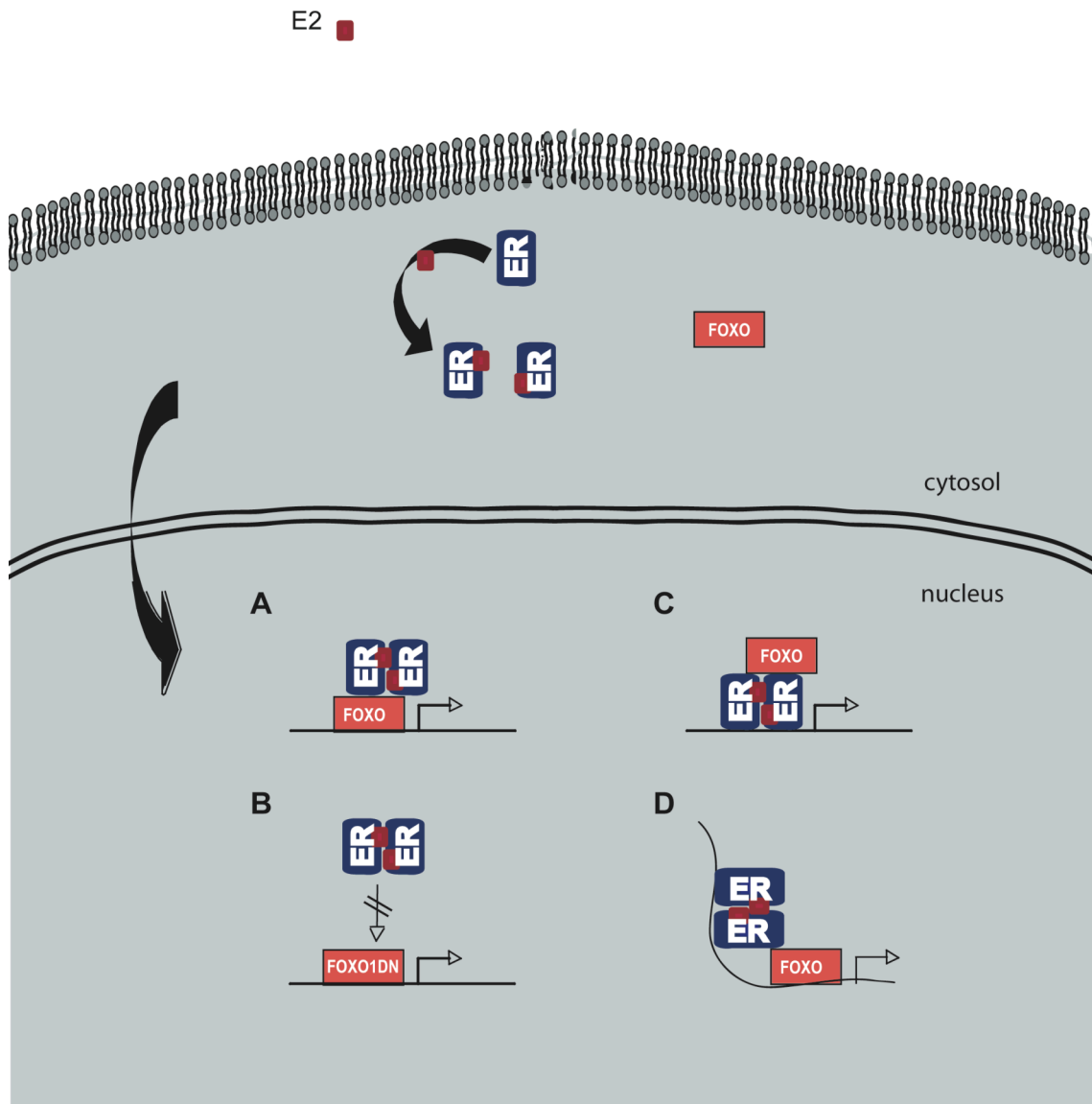


Figure 40: Models of FOXO and ER dependent promoter interaction

A,B: The FOXO/ER complex could bind to the forked binding site via FOXO to activate transcription. FOXO1DN overexpression could inhibit this interaction either by the absence of the transactivation domain in the FOXO1DN protein (A) or by the loss of the ability to interact with the ER (B). C: The FOXO/ER complex could bind to the ERE via the ER to activate transcription. In this case, the truncated FOXO1DN protein could be responsible for the reduced transcription. D: A secondary structure of the DNA could bring both proteins, binding to their own binding sites, into close proximity to form the complex.

These hypotheses are based on the assumption that a FOXO/ER complex leads to the activation of transcription of its target genes such as AVP. However, estrogen has also been shown to induce nuclear export and hence inactivation of FOXO1, in complex with ER α , in breast cancer cell lines [170, 171]. The model of estrogen receptor signalling is based on the ability of the ER to interact with different transcriptional co-activators or co-repressors, which are expressed in a tissue specific manner [172]. Additionally, the same ligand can act as an agonist in one tissue and antagonistic in another one. For instance, tamoxifen is used as a breast cancer treatment acting antagonistic on the ER, but in bone it activates the ER preventing osteoporosis [173]. Conclusively, further experiments are needed to unravel the exact molecular mechanism of ER and FOXO1 mediated effects on AVP transcription as well as on how they interact with each other to mediate their effects. Chromatin immunoprecipitation assays using specific antibodies against FOXO1, FOXO3A and ER α , could already give first hints to solve these questions.

Interestingly, the kinetics and relative expression levels of CRH to AVP vary on the kind and duration of stress. Whereas CRH is more involved in the response to a novel stressor, AVP plays an important role in a state of chronic stress [90, 92, 93]. Strikingly, our data suggested an important role of AVP expression in acute stress of female mice, as acute stress was analysed in this study. However, it cannot be excluded that stress response in female mice is differently regulated than in male mice, on which the model of acute versus chronic stress has been based so far [154]. In female mice, the competition of CRH and AVP in the initiation of the HPA axis could be markedly different and influenced by estrogen. However, further experiments are needed to support this idea. Moreover, it will be interesting to analyse the response of FOXO1DN/DN^{Sim1} females exposed to chronic stress, as AVP is known to be the principal gene involved.

In summary, this coherent set of findings indicates that in female mice the reinforcement of the stress response is dependent on FOXO transcription factor signalling in Sim1 neurons, which might be mediated by an interaction with the estrogen-ER pathway and subsequent activation of the AVP promoter.

4.4 Perspectives

The inhibition of FOXO signalling in Sim1 neurons by the overexpression of FOXO1DN has revealed, for the first time, that a FOXO transcription factor is essential for the effective reinforcement of the HPA axis stress response in females. Further studies will be needed to identify and analyse the endogenous regulation of the AVP promoter in females. Especially, the hypothesized interaction of ER α with FOXO1 on the AVP promoter still has to be confirmed. Interestingly, this study suggests an involvement of FOXO1 in the estrogen dependent reinforcement of the stress response, whereas previously, the stress response has been shown to inhibit the reproductive system (reviewed in [174]). The cross-talk between these two systems can be understood from an evolutionary perspective: In a state of “fight or flight”, reproduction is not a priority. Thus, the female response to stress seems to markedly differ to the male response. Finally, intensifying the research of the female stress response is pivotal for a better understanding and treatment of chronic stress associated diseases such as depression and obesity.

5 Summary

The paraventricular nucleus (PVN) of the hypothalamus comprises a distinct subset of neurons regulating a diversity of processes including energy homeostasis and stress response. The transcription factor FOXO1 and the ATP sensitive potassium (K_{ATP}) channel are involved in several important metabolic pathways in different tissues including the hypothalamus, one of the key brain regions controlling energy homeostasis. In the present study, transgenic knock-in strategies have been designed to address the function of these central players in energy homeostasis and stress response in Sim1 expressing neurons, which are present mainly in the PVN and supraoptic nucleus (SON). Thus, a constitutive active variant of the K_{ATP} channel ($K_{ATP}\Delta N$), resulting in a high potassium outflow of the neuron, or a dominant negative variant of the FOXO1 protein (FOXO1DN), which blocks the transcription of FOXO family target genes, were expressed in a Sim1-cre dependent manner. The analysis of these genetically modified mice revealed no difference in energy and glucose metabolism. Hence, FOXO1 signalling or the K_{ATP} channel dependent membrane excitability seem not to play a role in Sim1 neuron mediated control of energy homeostasis. However, FOXO1DN overexpression inhibited the transcription of arginine vasopressin (AVP), which is one of the initiating neuropeptides of the stress response, both *in vitro* and in a tendency *in vivo*, possibly by decreasing the estrogen dependent regulation of AVP transcription. Importantly, FOXO1DN overexpression could impair the female initiation of the stress response in Sim1 neurons resulting in a blunted corticosterone release from adrenal glands. Hence, this coherent set of findings indicates that transcription factor signalling of the FOXO family in the Sim1 expressing neurons can alter the reinforcement of the stress response in female mice.

6 Zusammenfassung

Der Nucleus paraventricularis (PVN) des Hypothalamus besteht aus einer klar abgegrenzten Gruppe von Neuronen, die an diversen Prozessen beteiligt ist. Zu diesen Prozessen zählen die Regulation der Energiehomöostase und die Stressantwort. Der Transkriptionsfaktor FOXO1 und der ATP sensitive Kalium (K_{ATP}) Kanal regulieren wichtige metabolische Signaltransduktionen in verschiedenen Organen. In der hier vorliegenden Studie wurden transgene „knock-in“ Strategien entwickelt, um die Funktion dieser zentralen Moleküle bezüglich der Energiehomöostase und Stressantwort in Sim1 Neuronen zu untersuchen. Die hierzu verwendete Sim1-cre Maus exprimiert die Cre-Recombinase hauptsächlich im PVN und dem Nucleus supraopticus (SON), was die Expression einer konstitutiv aktiven Variante des K_{ATP} Kanals ($K_{ATP}\Delta N$) und einer dominant negativen Variante des FOXO1 Proteins (FOXO1DN) in diesen Neuronen ermöglicht. Während die $K_{ATP}\Delta N$ Variante zu einem vermehrten Kaliumexport führt, verhindert FOXO1DN die Transkription von Zielgenen der FOXO Familie. Allerdings konnte keine Veränderung im Energie- oder Glucosemetabolismus dieser genetisch modifizierten Mäuse festgestellt werden. Somit scheinen die FOXO1 Signaltransduktion sowie ein K_{ATP} Kanal vermitteltes Membranpotenzial nicht essentiell für die Sim1 Neuronen abhängige Kontrolle der Energiehomöostase zu sein. Andererseits inhibierte die Überexpression von FOXO1DN, *in vitro* und tendenziell *in vivo*, die Transkription von Arginine Vasopressin (AVP), einem die Stressantwort initiierenden Neuropeptid, was möglicherweise durch die Verringerung der Östrogen vermittelten Regulation der AVP Transkription bewerkstelligt wurde. Vor allem die Initiation der Stressantwort in weiblichen Mäusen wurde durch FOXO1DN Überexpression beeinträchtigt, was die Corticosterone Ausschüttung der Nebennieren verhinderte. Diese kohärenten Ergebnisse weisen darauf hin, dass die Verstärkung der Stressantwort in weiblichen Mäusen durch Transkriptionsfaktoren der FOXO Familie in Sim1 Neuronen beeinflusst wird.

7 References

1. Bundesamt, S. *Datenreport 2008-Kapitel 9 Gesundheit und soziale Sicherung 2008* [cited.
2. BRFSS. *Behavioral Risk Factor Surveillance System*. 2008 [cited.
3. CDC, *State-Specific Prevalence of Obesity Among Adults*. 2008, MMWR. p. 36.
4. Mokdad, A.H., et al., *Prevalence of obesity, diabetes, and obesity-related health risk factors, 2001*. JAMA, 2003. **289**(1): p. 76-9.
5. Dixon, J.B., *The effect of obesity on health outcomes*. Mol Cell Endocrinol, 2009.
6. WHO, *Definition and diagnosis of diabetes mellitus and intermediate hyperglycemia*. report of a WHO/IDF consultation, 2006.
7. Lillioja, S., et al., *Insulin resistance and insulin secretory dysfunction as precursors of non-insulin-dependent diabetes mellitus. Prospective studies of Pima Indians*. N Engl J Med, 1993. **329**(27): p. 1988-92.
8. Martin, B.C., et al., *Role of glucose and insulin resistance in development of type 2 diabetes mellitus: results of a 25-year follow-up study*. Lancet, 1992. **340**(8825): p. 925-9.
9. Wild, S., et al., *Global prevalence of diabetes: estimates for the year 2000 and projections for 2030*. Diabetes Care, 2004. **27**(5): p. 1047-53.
10. Edholm, O.G., *Energy balance in man studies carried out by the Division of Human Physiology, National Institute for Medical Research*. J Hum Nutr, 1977. **31**(6): p. 413-31.
11. Schwartz, M.W., *Central nervous system regulation of food intake*. Obesity (Silver Spring), 2006. **14 Suppl 1**: p. 1S-8S.
12. Schwartz, M.W. and D. Porte, Jr., *Diabetes, obesity, and the brain*. Science, 2005. **307**(5708): p. 375-9.
13. Bruning, J.C., et al., *Role of brain insulin receptor in control of body weight and reproduction*. Science, 2000. **289**(5487): p. 2122-5.
14. Bronster, D.J., et al., *Central nervous system complications in liver transplant recipients--incidence, timing, and long-term follow-up*. Clin Transplant, 2000. **14**(1): p. 1-7.
15. Schwartz, M.W., et al., *Central nervous system control of food intake*. Nature, 2000. **404**(6778): p. 661-71.
16. Kahn, C.R., *Banting Lecture. Insulin action, diabetogenes, and the cause of type II diabetes*. Diabetes, 1994. **43**(8): p. 1066-84.
17. Pilkis, S.J. and D.K. Granner, *Molecular physiology of the regulation of hepatic gluconeogenesis and glycolysis*. Annu Rev Physiol, 1992. **54**: p. 885-909.
18. Margolis, R.U. and N. Altszuler, *Insulin in the cerebrospinal fluid*. Nature, 1967. **215**(5108): p. 1375-6.
19. Havrankova, J., J. Roth, and M. Brownstein, *Insulin receptors are widely distributed in the central nervous system of the rat*. Nature, 1978. **272**(5656): p. 827-9.

References

20. Woods, S.C., et al., *Chronic intracerebroventricular infusion of insulin reduces food intake and body weight of baboons*. *Nature*, 1979. **282**(5738): p. 503-5.
21. White, M.F., et al., *A cascade of tyrosine autophosphorylation in the beta-subunit activates the phosphotransferase of the insulin receptor*. *J Biol Chem*, 1988. **263**(6): p. 2969-80.
22. Kahn, C.R., et al., *Direct demonstration that receptor crosslinking or aggregation is important in insulin action*. *Proc Natl Acad Sci U S A*, 1978. **75**(9): p. 4209-13.
23. Jacobs, A.R., D. LeRoith, and S.I. Taylor, *Insulin receptor substrate-1 pleckstrin homology and phosphotyrosine-binding domains are both involved in plasma membrane targeting*. *J Biol Chem*, 2001. **276**(44): p. 40795-802.
24. Lehr, S., et al., *Identification of major tyrosine phosphorylation sites in the human insulin receptor substrate Gab-1 by insulin receptor kinase in vitro*. *Biochemistry*, 2000. **39**(35): p. 10898-907.
25. Myers, M.G., Jr., et al., *IRS-1 is a common element in insulin and insulin-like growth factor-I signaling to the phosphatidylinositol 3'-kinase*. *Endocrinology*, 1993. **132**(4): p. 1421-30.
26. Skolnik, E.Y., et al., *The function of GRB2 in linking the insulin receptor to Ras signaling pathways*. *Science*, 1993. **260**(5116): p. 1953-5.
27. Plum, L., M. Schubert, and J.C. Bruning, *The role of insulin receptor signaling in the brain*. *Trends Endocrinol Metab*, 2005. **16**(2): p. 59-65.
28. Whitman, M., et al., *Type I phosphatidylinositol kinase makes a novel inositol phospholipid, phosphatidylinositol-3-phosphate*. *Nature*, 1988. **332**(6165): p. 644-6.
29. Vanhaesebroeck, B. and D.R. Alessi, *The PI3K-PDK1 connection: more than just a road to PKB*. *Biochem J*, 2000. **346 Pt 3**: p. 561-76.
30. Cheatham, B. and C.R. Kahn, *Insulin action and the insulin signaling network*. *Endocr Rev*, 1995. **16**(2): p. 117-42.
31. Zhang, Y., et al., *Positional cloning of the mouse obese gene and its human homologue*. *Nature*, 1994. **372**(6505): p. 425-32.
32. Montague, C.T., et al., *Congenital leptin deficiency is associated with severe early-onset obesity in humans*. *Nature*, 1997. **387**(6636): p. 903-8.
33. Chen, H., et al., *Evidence that the diabetes gene encodes the leptin receptor: identification of a mutation in the leptin receptor gene in db/db mice*. *Cell*, 1996. **84**(3): p. 491-5.
34. Farooqi, I.S., et al., *Effects of recombinant leptin therapy in a child with congenital leptin deficiency*. *N Engl J Med*, 1999. **341**(12): p. 879-84.
35. Farooqi, I.S., et al., *Beneficial effects of leptin on obesity, T cell hyporesponsiveness, and neuroendocrine/metabolic dysfunction of human congenital leptin deficiency*. *J Clin Invest*, 2002. **110**(8): p. 1093-103.
36. Maffei, M., et al., *Leptin levels in human and rodent: measurement of plasma leptin and ob RNA in obese and weight-reduced subjects*. *Nat Med*, 1995. **1**(11): p. 1155-61.
37. Morton, G.J., et al., *Central nervous system control of food intake and body weight*. *Nature*, 2006. **443**(7109): p. 289-95.

38. Berthoud, H.R., *Multiple neural systems controlling food intake and body weight*. *Neurosci Biobehav Rev*, 2002. **26**(4): p. 393-428.
39. Paxinos, G.F., K.B.J. , *The Mouse Brain in Stereotaxic Coordinates*. 2001: ACADEMIC PRESS.
40. Cowley, M.A., et al., *Leptin activates anorexigenic POMC neurons through a neural network in the arcuate nucleus*. *Nature*, 2001. **411**(6836): p. 480-4.
41. Schwartz, M.W., et al., *Leptin increases hypothalamic pro-opiomelanocortin mRNA expression in the rostral arcuate nucleus*. *Diabetes*, 1997. **46**(12): p. 2119-23.
42. Elmquist, J.K., et al., *Unraveling the central nervous system pathways underlying responses to leptin*. *Nat Neurosci*, 1998. **1**(6): p. 445-50.
43. Chretien, M., et al., *From beta-lipotropin to beta-endorphin and 'pro-opiomelanocortin'*. *Can J Biochem*, 1979. **57**(9): p. 1111-21.
44. Zhou, A., B.T. Bloomquist, and R.E. Mains, *The prohormone convertases PC1 and PC2 mediate distinct endoproteolytic cleavages in a strict temporal order during proopiomelanocortin biosynthetic processing*. *J Biol Chem*, 1993. **268**(3): p. 1763-9.
45. Fan, W., et al., *Role of melanocortinergic neurons in feeding and the agouti obesity syndrome*. *Nature*, 1997. **385**(6612): p. 165-8.
46. Adan, R.A., et al., *Differential effects of melanocortin peptides on neural melanocortin receptors*. *Mol Pharmacol*, 1994. **46**(6): p. 1182-90.
47. Mountjoy, K.G., *The human melanocyte stimulating hormone receptor has evolved to become "super-sensitive" to melanocortin peptides*. *Mol Cell Endocrinol*, 1994. **102**(1-2): p. R7-11.
48. Hahn, T.M., et al., *Coexpression of Agrp and NPY in fasting-activated hypothalamic neurons*. *Nat Neurosci*, 1998. **1**(4): p. 271-2.
49. Haskell-Luevano, C. and E.K. Monck, *Agouti-related protein functions as an inverse agonist at a constitutively active brain melanocortin-4 receptor*. *Regul Pept*, 2001. **99**(1): p. 1-7.
50. Ollmann, M.M., et al., *Antagonism of central melanocortin receptors in vitro and in vivo by agouti-related protein*. *Science*, 1997. **278**(5335): p. 135-8.
51. Swart, I., et al., *Hypothalamic NPY, AGRP, and POMC mRNA responses to leptin and refeeding in mice*. *Am J Physiol Regul Integr Comp Physiol*, 2002. **283**(5): p. R1020-6.
52. Gropp, E., et al., *Agouti-related peptide-expressing neurons are mandatory for feeding*. *Nat Neurosci*, 2005. **8**(10): p. 1289-91.
53. Luquet, S., et al., *NPY/AgRP neurons are essential for feeding in adult mice but can be ablated in neonates*. *Science*, 2005. **310**(5748): p. 683-5.
54. Benoit, S.C., et al., *The catabolic action of insulin in the brain is mediated by melanocortins*. *J Neurosci*, 2002. **22**(20): p. 9048-52.
55. Sipols, A.J., D.G. Baskin, and M.W. Schwartz, *Effect of intracerebroventricular insulin infusion on diabetic hyperphagia and hypothalamic neuropeptide gene expression*. *Diabetes*, 1995. **44**(2): p. 147-51.
56. Schwartz, M.W., et al., *Identification of targets of leptin action in rat hypothalamus*. *J Clin Invest*, 1996. **98**(5): p. 1101-6.

57. Morrison, C.D., et al., *Leptin inhibits hypothalamic Npy and Agrp gene expression via a mechanism that requires phosphatidylinositol 3-OH-kinase signaling*. Am J Physiol Endocrinol Metab, 2005. **289**(6): p. E1051-7.
58. Tokunaga, K., et al., *Comparison of ventromedial and paraventricular lesions in rats that become obese*. Am J Physiol, 1986. **251**(6 Pt 2): p. R1221-7.
59. Baker, R.A. and M. Herkenham, *Arcuate nucleus neurons that project to the hypothalamic paraventricular nucleus: neuropeptidergic identity and consequences of adrenalectomy on mRNA levels in the rat*. J Comp Neurol, 1995. **358**(4): p. 518-30.
60. Sims, J.S. and J.F. Lorden, *Effect of paraventricular nucleus lesions on body weight, food intake and insulin levels*. Behav Brain Res, 1986. **22**(3): p. 265-81.
61. Swanson, L.W. and P.E. Sawchenko, *Hypothalamic integration: organization of the paraventricular and supraoptic nuclei*. Annu Rev Neurosci, 1983. **6**: p. 269-324.
62. Melnick, I., et al., *Developmental switch in neuropeptide Y and melanocortin effects in the paraventricular nucleus of the hypothalamus*. Neuron, 2007. **56**(6): p. 1103-15.
63. Hoffman, N.W., J.G. Tasker, and F.E. Dudek, *Immunohistochemical differentiation of electrophysiologically defined neuronal populations in the region of the rat hypothalamic paraventricular nucleus*. J Comp Neurol, 1991. **307**(3): p. 405-16.
64. Swanson, L.W., et al., *Separate neurons in the paraventricular nucleus project to the median eminence and to the medulla or spinal cord*. Brain Res, 1980. **198**(1): p. 190-5.
65. Fenton, R.A. and H.B. Moeller, *Recent discoveries in vasopressin-regulated aquaporin-2 trafficking*. Prog Brain Res, 2008. **170**: p. 571-9.
66. Lechan, R.M. and C. Fekete, *The TRH neuron: a hypothalamic integrator of energy metabolism*. Prog Brain Res, 2006. **153**: p. 209-35.
67. Uehara, Y., et al., *Hypothalamic corticotropin-releasing hormone is a mediator of the anorexigenic effect of leptin*. Diabetes, 1998. **47**(6): p. 890-3.
68. Lu, X.-Y., et al., *Interaction between {alpha}-Melanocyte-Stimulating Hormone and Corticotropin-Releasing Hormone in the Regulation of Feeding and Hypothalamo-Pituitary-Adrenal Responses*. J. Neurosci., 2003. **23**(21): p. 7863-7872.
69. Holder, J.L., Jr., N.F. Butte, and A.R. Zinn, *Profound obesity associated with a balanced translocation that disrupts the SIM1 gene*. Hum Mol Genet, 2000. **9**(1): p. 101-8.
70. Willer, C.J., et al., *Six new loci associated with body mass index highlight a neuronal influence on body weight regulation*. Nat Genet, 2009. **41**(1): p. 25-34.
71. Farooqi, I.S., et al., *Clinical spectrum of obesity and mutations in the melanocortin 4 receptor gene*. N Engl J Med, 2003. **348**(12): p. 1085-95.
72. Michaud, J.L., et al., *Development of neuroendocrine lineages requires the bHLH-PAS transcription factor SIM1*. Genes Dev, 1998. **12**(20): p. 3264-75.

73. Kublaoui, B.M., et al., *Sim1 haploinsufficiency impairs melanocortin-mediated anorexia and activation of paraventricular nucleus neurons*. Mol Endocrinol, 2006. **20**(10): p. 2483-92.
74. Kublaoui, B.M., et al., *SIM1 overexpression partially rescues agouti yellow and diet-induced obesity by normalizing food intake*. Endocrinology, 2006. **147**(10): p. 4542-9.
75. Yang, C., et al., *Adenoviral-mediated modulation of Sim1 expression in the paraventricular nucleus affects food intake*. J Neurosci, 2006. **26**(26): p. 7116-20.
76. Kublaoui, B.M., et al., *Oxytocin deficiency mediates hyperphagic obesity of Sim1 haploinsufficient mice*. Mol Endocrinol, 2008. **22**(7): p. 1723-34.
77. Mountjoy, K.G., et al., *The cloning of a family of genes that encode the melanocortin receptors*. Science, 1992. **257**(5074): p. 1248-51.
78. Kishi, T., et al., *Expression of melanocortin 4 receptor mRNA in the central nervous system of the rat*. J Comp Neurol, 2003. **457**(3): p. 213-35.
79. Mountjoy, K.G., et al., *Localization of the melanocortin-4 receptor (MC4-R) in neuroendocrine and autonomic control circuits in the brain*. Mol Endocrinol, 1994. **8**(10): p. 1298-308.
80. Huszar, D., et al., *Targeted disruption of the melanocortin-4 receptor results in obesity in mice*. Cell, 1997. **88**(1): p. 131-41.
81. Marsh, D.J., et al., *Response of melanocortin-4 receptor-deficient mice to anorectic and orexigenic peptides*. Nat Genet, 1999. **21**(1): p. 119-22.
82. Balthasar, N., et al., *Divergence of melanocortin pathways in the control of food intake and energy expenditure*. Cell, 2005. **123**(3): p. 493-505.
83. Pardini, A.W., et al., *Distribution of insulin receptor substrate-2 in brain areas involved in energy homeostasis*. Brain Res, 2006. **1112**(1): p. 169-78.
84. Chrousos, G.P., *Stress and disorders of the stress system*. Nat Rev Endocrinol, 2009. **5**(7): p. 374-81.
85. Liu, Y., et al., *Cyclic adenosine 3',5'-monophosphate responsive element binding protein phosphorylation is required but not sufficient for activation of corticotropin-releasing hormone transcription*. Endocrinology, 2008. **149**(7): p. 3512-20.
86. Whitnall, M.H., *Regulation of the hypothalamic corticotropin-releasing hormone neurosecretory system*. Prog Neurobiol, 1993. **40**(5): p. 573-629.
87. Lolait, S.J., et al., *The hypothalamic-pituitary-adrenal axis response to stress in mice lacking functional vasopressin V1b receptors*. Endocrinology, 2007. **148**(2): p. 849-56.
88. Ma, X.M. and G. Aguilera, *Differential regulation of corticotropin-releasing hormone and vasopressin transcription by glucocorticoids*. Endocrinology, 1999. **140**(12): p. 5642-50.
89. Ma, X.M., C. Camacho, and G. Aguilera, *Regulation of corticotropin-releasing hormone (CRH) transcription and CRH mRNA stability by glucocorticoids*. Cell Mol Neurobiol, 2001. **21**(5): p. 465-75.
90. Luo, X., et al., *Stress-specific regulation of corticotropin releasing hormone receptor expression in the paraventricular and supraoptic nuclei of the hypothalamus in the rat*. J Neuroendocrinol, 1994. **6**(6): p. 689-96.

91. Ma, X.M., S.L. Lightman, and G. Aguilera, *Vasopressin and corticotropin-releasing hormone gene responses to novel stress in rats adapted to repeated restraint*. *Endocrinology*, 1999. **140**(8): p. 3623-32.
92. Aguilera, G., *Regulation of pituitary ACTH secretion during chronic stress*. *Front Neuroendocrinol*, 1994. **15**(4): p. 321-50.
93. Kiss, A. and G. Aguilera, *Regulation of the hypothalamic pituitary adrenal axis during chronic stress: responses to repeated intraperitoneal hypertonic saline injection*. *Brain Res*, 1993. **630**(1-2): p. 262-70.
94. Lalmansingh, A.S. and R.M. Uht, *Estradiol regulates corticotropin-releasing hormone gene (*crh*) expression in a rapid and phasic manner that parallels estrogen receptor-alpha and -beta recruitment to a 3',5'-cyclic adenosine 5'-monophosphate regulatory region of the proximal *crh* promoter*. *Endocrinology*, 2008. **149**(1): p. 346-57.
95. Pak, T.R., et al., *Estrogen receptor-beta mediates dihydrotestosterone-induced stimulation of the arginine vasopressin promoter in neuronal cells*. *Endocrinology*, 2007. **148**(7): p. 3371-82.
96. Patchev, V.K., et al., *Implications of estrogen-dependent brain organization for gender differences in hypothalamo-pituitary-adrenal regulation*. *FASEB J*, 1995. **9**(5): p. 419-23.
97. Weiser, M.J. and R.J. Handa, *Estrogen impairs glucocorticoid dependent negative feedback on the hypothalamic-pituitary-adrenal axis via estrogen receptor alpha within the hypothalamus*. *Neuroscience*, 2009. **159**(2): p. 883-95.
98. Ochedalski, T., et al., *Interaction between oestrogen and oxytocin on hypothalamic-pituitary-adrenal axis activity*. *J Neuroendocrinol*, 2007. **19**(3): p. 189-97.
99. Mirshamsi, S., et al., *Leptin and insulin stimulation of signalling pathways in arcuate nucleus neurones: PI3K dependent actin reorganization and KATP channel activation*. *BMC Neurosci*, 2004. **5**: p. 54.
100. Miki, T., et al., *ATP-sensitive K⁺ channels in the hypothalamus are essential for the maintenance of glucose homeostasis*. *Nat Neurosci*, 2001. **4**(5): p. 507-12.
101. Inagaki, N., et al., *Reconstitution of IKATP: an inward rectifier subunit plus the sulfonylurea receptor*. *Science*, 1995. **270**(5239): p. 1166-70.
102. Belgardt, B.F., T. Okamura, and J.C. Bruning, *Hormone and glucose signalling in POMC and AgRP neurons*. *J Physiol*, 2009. **587**(Pt 22): p. 5305-14.
103. Plum, L., et al., *Enhanced PIP3 signaling in POMC neurons causes KATP channel activation and leads to diet-sensitive obesity*. *J Clin Invest*, 2006. **116**(7): p. 1886-901.
104. Koster, J.C., et al., *Targeted overactivity of beta cell K(ATP) channels induces profound neonatal diabetes*. *Cell*, 2000. **100**(6): p. 645-54.
105. Reimann, F., et al., *Involvement of the n-terminus of Kir6.2 in coupling to the sulphonylurea receptor*. *J Physiol*, 1999. **518** (Pt 2): p. 325-36.
106. Koster, J.C., et al., *ATP inhibition of KATP channels: control of nucleotide sensitivity by the N-terminal domain of the Kir6.2 subunit*. *J Physiol*, 1999. **515** (Pt 1): p. 19-30.
107. Spanswick, D., et al., *Insulin activates ATP-sensitive K⁺ channels in hypothalamic neurons of lean, but not obese rats*. *Nat Neurosci*, 2000. **3**(8): p. 757-8.

108. Gross, D.N., A.P. van den Heuvel, and M.J. Birnbaum, *The role of FoxO in the regulation of metabolism*. *Oncogene*, 2008. **27**(16): p. 2320-36.
109. Arden, K.C., *FOXO animal models reveal a variety of diverse roles for FOXO transcription factors*. *Oncogene*, 2008. **27**(16): p. 2345-50.
110. Nakae, J., M. Oki, and Y. Cao, *The FoxO transcription factors and metabolic regulation*. *FEBS Lett*, 2008. **582**(1): p. 54-67.
111. Wang, M.C., D. Bohmann, and H. Jasper, *JNK extends life span and limits growth by antagonizing cellular and organism-wide responses to insulin signaling*. *Cell*, 2005. **121**(1): p. 115-25.
112. Nakae, J., et al., *The LXXLL motif of murine forkhead transcription factor FoxO1 mediates Sirt1-dependent transcriptional activity*. *J Clin Invest*, 2006. **116**(9): p. 2473-83.
113. Nakae, J., et al., *Regulation of insulin action and pancreatic beta-cell function by mutated alleles of the gene encoding forkhead transcription factor Foxo1*. *Nat Genet*, 2002. **32**(2): p. 245-53.
114. Castrillon, D.H., et al., *Suppression of ovarian follicle activation in mice by the transcription factor Foxo3a*. *Science*, 2003. **301**(5630): p. 215-8.
115. Paik, J.H., et al., *FoxOs are lineage-restricted redundant tumor suppressors and regulate endothelial cell homeostasis*. *Cell*, 2007. **128**(2): p. 309-23.
116. Tothova, Z., et al., *FoxOs are critical mediators of hematopoietic stem cell resistance to physiologic oxidative stress*. *Cell*, 2007. **128**(2): p. 325-39.
117. O'Brien, R.M. and D.K. Granner, *Regulation of gene expression by insulin*. *Physiol Rev*, 1996. **76**(4): p. 1109-61.
118. O'Brien, R.M., et al., *Insulin-regulated gene expression*. *Biochem Soc Trans*, 2001. **29**(Pt 4): p. 552-8.
119. Zhang, W., et al., *FoxO1 regulates multiple metabolic pathways in the liver: effects on gluconeogenic, glycolytic, and lipogenic gene expression*. *J Biol Chem*, 2006. **281**(15): p. 10105-17.
120. Kim, M.S., et al., *Role of hypothalamic Foxo1 in the regulation of food intake and energy homeostasis*. *Nat Neurosci*, 2006. **9**(7): p. 901-6.
121. Nakae, J., et al., *Insulin regulation of gene expression through the forkhead transcription factor Foxo1 (Fkhr) requires kinases distinct from Akt*. *Biochemistry*, 2001. **40**(39): p. 11768-76.
122. Nakae, J., et al., *The forkhead transcription factor Foxo1 (Fkhr) confers insulin sensitivity onto glucose-6-phosphatase expression*. *J Clin Invest*, 2001. **108**(9): p. 1359-67.
123. Maiese, K., Z.Z. Chong, and Y.C. Shang, *"Sly as a FOXO": new paths with Forkhead signaling in the brain*. *Curr Neurovasc Res*, 2007. **4**(4): p. 295-302.
124. Kitamura, T., et al., *Forkhead protein FoxO1 mediates Agrp-dependent effects of leptin on food intake*. *Nat Med*, 2006. **12**(5): p. 534-40.
125. Nakae, J., et al., *The forkhead transcription factor Foxo1 regulates adipocyte differentiation*. *Dev Cell*, 2003. **4**(1): p. 119-29.
126. Fu, Z. and D.J. Tindall, *FOXOs, cancer and regulation of apoptosis*. *Oncogene*, 2008. **27**(16): p. 2312-9.
127. Plum, L., et al., *The obesity susceptibility gene Cpe links FoxO1 signaling in hypothalamic pro-opiomelanocortin neurons with regulation of food intake*. *Nat Med*, 2009. **15**(10): p. 1195-201.

128. Accili, D. and K.C. Arden, *FoxOs at the crossroads of cellular metabolism, differentiation, and transformation*. Cell, 2004. **117**(4): p. 421-6.
129. Belgardt, B.F., et al., *PDK1 deficiency in POMC-expressing cells reveals FOXO1-dependent and -independent pathways in control of energy homeostasis and stress response*. Cell Metab, 2008. **7**(4): p. 291-301.
130. Remedi, M.S., et al., *Secondary consequences of beta cell inexcitability: identification and prevention in a murine model of K(ATP)-induced neonatal diabetes mellitus*. Cell Metab, 2009. **9**(2): p. 140-51.
131. Novak, A., et al., *Z/EG, a double reporter mouse line that expresses enhanced green fluorescent protein upon Cre-mediated excision*. Genesis, 2000. **28**(3-4): p. 147-55.
132. Vintersten, K., et al., *Mouse in red: red fluorescent protein expression in mouse ES cells, embryos, and adult animals*. Genesis, 2004. **40**(4): p. 241-6.
133. Lawlor, M.A., et al., *Essential role of PDK1 in regulating cell size and development in mice*. Embo J, 2002. **21**(14): p. 3728-38.
134. Saiki, R.K., et al., *Analysis of enzymatically amplified beta-globin and HLA-DQ alpha DNA with allele-specific oligonucleotide probes*. Nature, 1986. **324**(6093): p. 163-6.
135. Saiki, R.K., et al., *Enzymatic amplification of beta-globin genomic sequences and restriction site analysis for diagnosis of sickle cell anemia*. Science, 1985. **230**(4732): p. 1350-4.
136. Hogan, B.C., F. and Lacy, I., *Manipulating the mouse embryo*. Cold Spring harbor Laboratory Press, 1987.
137. Silver, L.M., *Mouse genetics: concepts and practice*. Oxford University Press, 1995.
138. Isken, F., et al., *Deficiency of glucose-dependent insulinotropic polypeptide receptor prevents ovariectomy-induced obesity in mice*. Am J Physiol Endocrinol Metab, 2008. **295**(2): p. E350-5.
139. Janoschek, R., et al., *gp130 signaling in proopiomelanocortin neurons mediates the acute anorectic response to centrally applied ciliary neurotrophic factor*. Proc Natl Acad Sci U S A, 2006. **103**(28): p. 10707-12.
140. Konner, A.C., et al., *Insulin action in AgRP-expressing neurons is required for suppression of hepatic glucose production*. Cell Metab, 2007. **5**(6): p. 438-49.
141. Seibler, J., et al., *Rapid generation of inducible mouse mutants*. Nucleic Acids Res, 2003. **31**(4): p. e12.
142. Sambrook, J.a.M., T., *Molecular Cloning*. Cold Spring harbor Laboratory Press, 1989.
143. Mesaros, A., et al., *Activation of Stat3 signaling in AgRP neurons promotes locomotor activity*. Cell Metab, 2008. **7**(3): p. 236-48.
144. Sandri, M., et al., *Foxo Transcription Factors Induce the Atrophy-Related Ubiquitin Ligase Atrogin-1 and Cause Skeletal Muscle Atrophy*. Cell, 2004. **117**(3): p. 399-412.
145. Dunn-Meynell, A.A., N.E. Rawson, and B.E. Levin, *Distribution and phenotype of neurons containing the ATP-sensitive K⁺ channel in rat brain*. Brain Res, 1998. **814**(1-2): p. 41-54.

146. Karschin, C., et al., *Overlapping distribution of K(ATP) channel-forming Kir6.2 subunit and the sulfonylurea receptor SUR1 in rodent brain*. FEBS Lett, 1997. **401**(1): p. 59-64.
147. Miki, T., et al., *Abnormalities of pancreatic islets by targeted expression of a dominant-negative KATP channel*. Proc Natl Acad Sci U S A, 1997. **94**(22): p. 11969-73.
148. Butler, A.A. and R.D. Cone, *Knockout studies defining different roles for melanocortin receptors in energy homeostasis*. Ann N Y Acad Sci, 2003. **994**: p. 240-5.
149. Wang, J., et al., *Effects of ghrelin, corticotrophin-releasing hormone, and melanotan-II on food intake in rats with paraventricular nucleus lesions*. Exp Clin Endocrinol Diabetes, 2007. **115**(10): p. 669-73.
150. Leloup, C., et al., *Glucose transporter 2 (GLUT 2): expression in specific brain nuclei*. Brain Res, 1994. **638**(1-2): p. 221-6.
151. Parton, L.E., et al., *Glucose sensing by POMC neurons regulates glucose homeostasis and is impaired in obesity*. Nature, 2007. **449**(7159): p. 228-32.
152. Altomonte, J., et al., *Inhibition of Foxo1 function is associated with improved fasting glycemia in diabetic mice*. Am J Physiol Endocrinol Metab, 2003. **285**(4): p. E718-28.
153. Pierroz, D.D., et al., *Effects of acute and chronic administration of the melanocortin agonist MTII in mice with diet-induced obesity*. Diabetes, 2002. **51**(5): p. 1337-45.
154. Aguilera, G., et al., *The parvocellular vasopressinergic system and responsiveness of the hypothalamic-pituitary-adrenal axis during chronic stress*. Prog Brain Res, 2008. **170**: p. 29-39.
155. Schilling, K., et al., *Regulation of vasopressin expression in cultured diencephalic neurons by glucocorticoids*. Neuroendocrinology, 1991. **53**(5): p. 528-35.
156. Chen, Y., et al., *Rapid phosphorylation of the CRE binding protein precedes stress-induced activation of the corticotropin releasing hormone gene in medial parvocellular hypothalamic neurons of the immature rat*. Brain Res Mol Brain Res, 2001. **96**(1-2): p. 39-49.
157. Shapiro, R.A., C. Xu, and D.M. Dorsa, *Differential transcriptional regulation of rat vasopressin gene expression by estrogen receptor alpha and beta*. Endocrinology, 2000. **141**(11): p. 4056-64.
158. Kolber, B.J., et al., *Central amygdala glucocorticoid receptor action promotes fear-associated CRH activation and conditioning*. Proc Natl Acad Sci U S A, 2008. **105**(33): p. 12004-9.
159. Kalra, S.P., et al., *Interacting appetite-regulating pathways in the hypothalamic regulation of body weight*. Endocr Rev, 1999. **20**(1): p. 68-100.
160. Dhillon, W.S., et al., *The hypothalamic melanocortin system stimulates the hypothalamo-pituitary-adrenal axis in vitro and in vivo in male rats*. Neuroendocrinology, 2002. **75**(4): p. 209-16.
161. Calogero, A.E., et al., *Multiple feedback regulatory loops upon rat hypothalamic corticotropin-releasing hormone secretion. Potential clinical implications*. J Clin Invest, 1988. **82**(3): p. 767-74.

References

162. Johnstone, L.E., T.M. Fong, and G. Leng, *Neuronal activation in the hypothalamus and brainstem during feeding in rats*. Cell Metabolism, 2006. **4**(4): p. 313-321.
163. Holder, J.L., Jr., et al., *Sim1 gene dosage modulates the homeostatic feeding response to increased dietary fat in mice*. Am J Physiol Endocrinol Metab, 2004. **287**(1): p. E105-13.
164. Horvath, T.L., *Synaptic plasticity in energy balance regulation*. Obesity (Silver Spring), 2006. **14 Suppl 5**: p. 228S-233S.
165. Furuyama, T., et al., *Identification of the differential distribution patterns of mRNAs and consensus binding sequences for mouse DAF-16 homologues*. Biochem J, 2000. **349**(Pt 2): p. 629-34.
166. Suzuki, H., et al., *Regulatory mechanism of the arginine vasopressin-enhanced green fluorescent protein fusion gene expression in acute and chronic stress*. Peptides, 2009. **30**(9): p. 1763-70.
167. Zhang, Y.Y., et al., *c-Fos expression in the supraoptic nucleus is the most intense during different durations of restraint water-immersion stress in the rat*. J Physiol Sci, 2009. **59**(5): p. 367-75.
168. Roozendaal, B., et al., *Involvement of stress-released corticotropin-releasing hormone in the basolateral amygdala in regulating memory consolidation*. Proc Natl Acad Sci U S A, 2002. **99**(21): p. 13908-13.
169. Ordonez-Moran, P. and A. Munoz, *Nuclear receptors: genomic and non-genomic effects converge*. Cell Cycle, 2009. **8**(11): p. 1675-80.
170. Lombardi, M., et al., *Hormone-dependent nuclear export of estradiol receptor and DNA synthesis in breast cancer cells*. J Cell Biol, 2008. **182**(2): p. 327-40.
171. Mazumdar, A. and R. Kumar, *Estrogen regulation of Pak1 and FKHR pathways in breast cancer cells*. FEBS Lett, 2003. **535**(1-3): p. 6-10.
172. Shang, Y. and M. Brown, *Molecular determinants for the tissue specificity of SERMs*. Science, 2002. **295**(5564): p. 2465-8.
173. Deroo, B.J. and K.S. Korach, *Estrogen receptors and human disease*. J Clin Invest, 2006. **116**(3): p. 561-70.
174. Chrousos, G.P., D.J. Torpy, and P.W. Gold, *Interactions between the hypothalamic-pituitary-adrenal axis and the female reproductive system: clinical implications*. Ann Intern Med, 1998. **129**(3): p. 229-40.

8 Acknowledgements

I am sincerely grateful to Prof. Dr. Jens C. Brüning for the opportunity to work in his lab on this interesting project. I appreciate his support and tremendous optimism.

I would like to thank Prof. Dr. Mats Paulsson, Prof. Dr. Siegfried Roth and Dr. Ursula Lichtenberg for agreeing to form my thesis committee.

I am especially grateful to Dr. Beatrice Coornaert and Dr. Carmen Sánchez for critically reading my thesis, discussing the results and giving the moral support, when it was most required. Furthermore, I would like to thank Diana Willmes, Nina Leuschen, Dr. Claire Pujol, Tim Klöckener, Sulay Tovar and Bengt Belgardt for all the support in the last weeks and years.

I would like to thank all members of the Brüning Lab for stimulating discussions, help with experiments and advice. Special thanks go to my labmates and friends Marianne Ernst, Bruno Klisch, Jens Alber and Sandra Jäckel for all those years together and also to Sigrid Irenbusch, Sonja Becker, Pia Scholl and Brigitte Hampel for the technical support and all those little things.

Finally, I am endlessly grateful for the love and encouragement of my parents Marieluisse and Norbert Redemann and my brother Björn Redemann.

9 Erklärung

Ich versichere, dass ich die von mir vorgelegte Dissertation selbständig angefertigt, die benutzten Quellen und Hilfsmittel vollständig angegeben und die Stellen der Arbeit - einschließlich Tabellen, Karten und Abbildungen -, die anderen Werken im Wortlaut oder dem Sinn nach entnommen sind, in jedem Einzelfall als Entlehnung kenntlich gemacht habe; dass diese Dissertation noch keiner anderen Fakultät oder Universität zur Prüfung vorgelegen hat; dass sie - abgesehen von unten angegebenen Teilpublikationen - noch nicht veröffentlicht worden ist sowie, dass ich eine solche Veröffentlichung vor Abschluß des Promotionsverfahrens nicht vornehmen werde. Die Bestimmungen dieser Promotionsordnung sind mir bekannt. Die von mir vorgelegte Dissertation ist von Prof. Dr. Jens C. Brüning betreut worden.

Köln, Dezember 2009

Nora Redemann

Teilpublikationen im Rahmen dieser Arbeit:

10 Lebenslauf

Nora Redemann

Arnulfstr.24

50937 Köln

Telefon: 0221 / 7160894

E-Mail: nora.redemann@uni-koeln.de

Persönliche Angaben

Name: Nora Redemann
Geburtsdatum: 4.7.1980
Staatsangehörigkeit: deutsch
Geburtsort: Frechen
Familienstand: ledig

Schulbildung

1986 – 1990 Albert-Schweizer-Schule in Köln-Weiden
1990 – 1999 Georg-Büchner-Gymnasium in Köln-Weiden
Schulabschluss: Abitur

Berufsausbildung

1999-2005 Universität zu Köln – Biologiestudium (Diplom)
Abschluss: Diplom Biologie
Seit Sept / 2005 Universität zu Köln – International Graduate School
for Genetics and Functional Genomics
Seit April / 2006 Promotion am Institut für Genetik
Betreuer: Prof. Dr. Jens Brüning

Praktische Erfahrungen

Mai / 1999 Boehringer Ingelheim Pharma KG (Onkologie)
August / 2002 Institut für Hygiene und öffentl. Gesundheit Bonn

Juli - August / 2003 Microbiologisches Labor für Wasseranalytik der
Rheinenergie AG

Sprachkenntnisse

Am Gymnasium: 9 Jahre Englisch, 4 Jahre Latein (mit Latinum),
4 Jahre Französisch

2002 Certificate in Advanced English of
the University of Cambridge

2002/2003 ERASMUS Austausch für 2 Semester:
University of Manchester